Relativistic thermal plasmas

by

Susan Stepney

Institute of Astronomy and Newnham College

University of Cambridge

Submitted as a dissertation for the degree of

Doctor of Philosophy

September 1983

Preface

I would like to express my thanks to my supervisor, Professor Martin Rees, for proposing this subject, and for many helpful suggestions. My thanks also to Dr. Paul Guilbert for many stimulating discussions, and for permission to use his computer program, without which the work described in the later chapters would not have been possible. The facilities provided by the Cambridge Computer Service were indispensable. Dr. R. J. Gould made helpful comments on § 2.3.3.

I am grateful to S.E.R.C. and to Newnham College for financial support.

My thanks to GCAL and to Diablo for their accurate and rapid typing. Except where explicit reference is made to the work of others, this dissertation is the result of my own work. It includes nothing which is the outcome of work done in collaboration. It contains < 60 000 words.

Summary

The study of relativistic thermal plasmas, where $kT_e \gtrsim m_e c^2$, is of growing importance in the field of high energy astrophysics. Models of the observed γ-ray burst sources require the existence of such high temperatures, as do some of the models of active galactic nuclei.

The question of self-consistency arises; can the particles maintain a Maxwellian distribution, or is the cooling too great? The timescale for two body relaxation via Coulomb collisions is well-known in the nonrelativistic limit (Spitzer, 1956), but is invalid at the temperatures being considered here. No relativistic generalization existed, although some approximate expressions have been given (Gould, 1982a; Lightman & Band, 1981).

In the first half of this thesis I derive an exact expression for the fully relativistic energy exchange rate in terms of an integral over the scattering cross section, and evaluate it for the cases of electron-proton, electron-electron and proton-proton relaxation. I compare the resulting timescales with the major energy-loss timescales - those of bremsstrahlung, pair-production, pion production and synchrotron cooling - to find in what temperature ranges it is possible to consider the particle distribution to be Maxwellian.

In the presence of an equipartition magnetic field synchrotron cooling dominates, and the electron distribution is only Maxwellian for temperatures $kT_e \lesssim m_e c^2$. When there is no magnetic field bremsstrahlung is the dominant cooling process and the electron distribution can be Maxwellian for $kT_e \lesssim 10 m_e c^2$. Protons cool much more slowly, and their distribution can remain Maxwellian at all temperatures of interest.

So it is reasonable to investigate thermal relativistic plasmas, and to build more detailed models of such systems. Since the problem is highly non-linear, detailed modelling requires computer simulation. In the second half of this thesis I describe the development of a computer program to model a thermal plasma slab at mildly relativistic temperatures. I present the results for the equilibrium structure of constant temperature slabs and for time dependent, cooling models.

Contents

1 Introduction

The recent X-ray and γ-ray satellites have provided data which indicate that there are places in the universe with temperatures higher than 10^{10} K (1 MeV). In particular, the KONUS experiment on board the Venera 11 and 12 space probes detected 143 γ-ray burst sources in the period between September 1978 and February 1980 (Mazets *et al*., 1981b). If the spectra are fitted with a thermal bremsstrahlung model, the emission temperatures range from 50 keV to 1 MeV. In addition, several of the sources show what may be cyclotron lines, and electron-positron annihilation lines (Mazets *et al*., 1981a). An annihilation line from the centre of the galaxy has been observed (Leventhal, MacCullam & Stang, 1978), and Cygnus X-1 may also show an annihilation line (Nolan & Matteson, 1983). Active galactic nuclei also emit at energies of a few hundred keV, although no lines have been observed. Guilbert, Fabian & Rees (1983) have argued that much of the γ-ray and hard X-ray emission from compact sources has been reprocessed by mildly relativistic electron-positron pairs.

Modelling a thermal plasma with a temperature of $kT \sim m_e c^2$ requires the consideration of new physical processes – electron-positron pair production and annihilation, and electron-electron bremsstrahlung. Also familiar processes, such as synchrotron radiation and electron-proton relaxation, have different temperature dependences from the non-relativistic limits.

Mildly relativistic plasmas, those with $kT_e \lesssim m_e c^2$, corresponding to X-ray emission temperatures, have been studied by, for example, Felten & Rees (1972), Illarionov & Syunyaev (1972) and Stoeger (1977). In this region the relativistic effects can be treated as small perturbations (Gould, 1980). When $kT_e \gg m_e c^2$ the ultrarelativistic cross sections can be used. However, the case we are interested in is $kT \sim m_e c^2$, where neither limit is applicable. The full relativistic cross sections must be used. Bisnovatyi-Kogan, Zel'dovich & Syunyaev (1971) were the first to treat this problem. More recently Gould (1981a,b), Lightman (1982) and Lightman & Band (1981) have considered general properties of relativistic thermal plasmas. Svensson (1982b) has considered electron-positron pair production in some detail.

In this thesis I calculate the timescales of the various processes occurring in the plasma, for a range of temperatures $10^{-3} \lesssim kT/m_e c^2 \lesssim 10^3$. The relative timescales are of crucial importance in determining both the plasma's equilibrium state and its time evolution.

Energy can be fed into the plasma by a variety of routes. The case of a sudden input of high energy photons, a 'fireball', has been discussed by Cavallo & Rees (1978). The plasma can also be heated mechanically; impulsively, by a shock, or continuously, by turbulence. This would mainly heat the protons, which in turn heat the electrons. As it is the electrons which radiate, cooling the plasma, the rate of energy exchange between electrons and protons is a crucial factor.

In the case of continuous heating, the relative rates of energy exchange and radiation will determine the electron and proton temperatures. Such a two-temperature plasma is required in some accretion disk models (Shapiro, Lightman & Eardley, 1976). For impulsive heating the protons will be shocked up to a much higher temperature than the electrons. Then, if the heating rate is high enough, the electron temperature will start to rise. Otherwise the electrons radiate too quickly, and may never reach relativistic temperatures.

Here the only electron heating considered is that from electron-proton Coulomb collisions. For an electron-positron corona with no protons, required in other accretion disk models (e.g. Bisnovatyi-Kogan & Blinnikov, 1977; Liang & Price, 1977) some turbulent heating mechanism is required.

An important cooling mechanism in relativistic plasmas is electron-positron pair production (chapter 3). In the optically thin case pairs are produced by particle-particle collisions. In the optically thick case particle-photon and photon-photon collisions must also be included. Since no incoherent process can radiate faster than the corresponding black-body, this sets a lower limit on any radiation timescale (§ 4.1). This is a very important constraint in the case of cyclotron radiation, which has a very high emissivity at low frequencies (§ 4.4). The protons can also be cooled by pion production (§ 4.3).

In the absence of magnetic fields, bremsstrahlung is the dominant radiation mechanism (§ 4.2), and at relativistic temperatures electron-electron bremsstrahlung is comparable to electron-proton bremsstrahlung. However, when a magnetic field is present, synchrotron radiation dominates. In an accretion disk around a $1M_{\odot}$ black hole, for example, an equipartition field of a few teslas would be expected. Around a supermassive black hole the density is lower, and so the equipartition field strength will be lower. But near a magnetic neutron star the field will be superstrong, $10^6 - 10^8$ T, since it is comparable to the quantum critical field, $B_{\rm o} \simeq 4\times10^9\,{\rm T}$.

After the discussion of the various timescales, the next simplest question one can ask is: what is the equilibrium structure of a mildly relativistic plasma? To answer this question, radiative transfer of photons above the pair-production threshold has to be considered. This is a highly non-linear process, and all but the most simple problems have to be solved with the aid of a computer. In chapter 7 I describe the development of a computer program to model a slab of high temperature plasma, incorporating most of the processes discussed in the previous chapters. In chapter 8 the constant temperature (equilibrium) models are discussed. Once we have a handle on the structure of such slabs, we can consider more complicated cases. Cooling slabs are treated in chapter 9.

Since the study of relativistic thermal plasmas is in its infancy, and since even simple models require a large expenditure of effort in writing computer programs, the results presented here do not pretend to model real astrophysical objects. Rather, they are the first

step, intended to give a feel for the physical processes involved. Hopefully they will point the way to future research and more realistic models.

1.1 Notation

The word "electron" is used to refer to both the negative particles, e^- (called negatrons by some authors),[1] and to electrons in general (e^- and e^+) when they have the same properties. This usually does not lead to confusion. In cases of ambiguity, a subscript "–" is used in the former case, and a subscript "*e*" in the latter. Subscripts "+", "*p*" and "γ" refer to positrons, protons and photons respectively.

To simplify the results I have found it convenient to work with dimensionless quantities. In future the physical quantities will be indicated by a subscript asterisk. The notation used is

$$\begin{array}{lllll} T = kT_* / m_e c^2 & T = 1 & \Rightarrow & T_* & = 5.9 \times 10^9 \text{ K} \\ \theta = kT_* / Mc^2 = Tm_e / M & \theta_p = 1 & \Rightarrow & T_{*p} & = 1.1 \times 10^{13} \text{ K} \\ \omega = \hbar\omega_* / m_e c^2 & \omega = 1 & \Rightarrow & \omega_* & = 0.511 \text{ MeV} \\ x = \hbar\omega_* / kT_* & & & & \\ \sigma = \sigma_* / \sigma_T & \sigma = 1 & \Rightarrow & \sigma_* & = 4.65 \times 10^{-29} \text{ m}^2 \\ B = B_* e\hbar\omega_* / (m_e c)^2 & B = 1 & \Rightarrow & B_* & = 4.4 \times 10^9 \text{ T} \end{array} \qquad (1.1)$$

There are two dimensionless temperatures here; T_A is the temperature of species A in units of the electron rest mass, and θ_A is the temperature in units of the species rest mass, M_A. So $T_e = \theta_e$ and $T_p = 1836\,\theta_p$. Species A and B have the same physical temperature if $T_A = T_B$. The temperature is non-relativistic if $\theta \ll 1$, and ultrarelativistic if $\theta \gg 1$.

The dimensionless photon energy ω is also in units of the electron rest mass. Hence photons of energy $\omega > 1$ are 'relativistic' in the sense that they can create electron-positron pairs, and that Klein-Nishina corrections need to be made to the Thomson scattering cross section. The other dimensionless photon energy, x, is in units of the electron thermal energy. So photons are hotter than the electrons if $x > 1$, cooler if $x < 1$. Bremsstrahlung photons are produced with energies $x \lesssim 1$, $\omega \lesssim T$, whilst annihilation photons have energies $\omega \sim 1 + T$. Comptonization is important if x is very different from 1.

All particle densities are normalized to 'per proton'; $N_A = n_A N_p$. In particular, z is the number of pairs per proton. Hence, for an electrically neutral plasma, $N_+ = zN_p$, $N_- = (1+z)N_p$ and $N_e = (1+2z)N_p$. $z \gg 1$ represents a pair dominated plasma.

Times are expressed in units of the 'proton Thomson time', $t_p = 1/N_p\sigma_T c$; $t = t_*/t_p$. This is chosen rather than the more usual electron time, $1/N_e\sigma_T c$, since the electron density is not constant but depends on the pair density. This gives the time between successive collisions of a photon with the electrons in a cold plasma containing no pairs. In hot plasmas ($T > 1$)

[1] Though Jauch & Rohrlich (1980) consistently refer to "negatons" and "positons" throughout.

Klein-Nishina corrections decrease scattering cross section and so increase the scattering time. The presence of pairs effectively increases the electron number density and so decreases the time by a factor $1/(1+2z)$. Since most of the processes described in the following chapters are two body interactions, the dimensionless timescales are independent of the density (though they often depend on *z*).

Throughout this thesis the electrons are assumed to have a thermal distribution, as are the protons when their temperature cannot be taken as zero. (The validity of this assumption is discussed in chapter 5). The relativistic Maxwell distribution is

$$N(\gamma) = N\gamma^2\beta\, e^{-\gamma/\theta} \big/ \theta\, K_2(1/\theta) \tag{1.2}$$

where β is the velocity in units of *c*, γ is the usual relativistic factor, $\gamma = \sqrt{1-\beta^2}$ and K_2 is a modified Bessel function. Since averaging over relativistic Maxwellians often involves the manipulation of these Bessel functions, some of their more important properties are summarized in Appendix 2.

1.2 Numerical Values

Since most of the quantities derived in the next chapters are expressed in dimensionless units, the discussion can seem a little abstract at times. It is useful to have a feel for the numerical values of the physical quantities. Two regions where relativistic thermal plasmas may exist are around compact objects, in which case $M \sim M_\odot$, and in active galactic nuclei, with $M \sim 10^8 M_\odot$.

We can estimate typical values for soma of the plasma parameters – e.g. temperature, density, magnetic field – quite straightforwardly. For example, the black body temperature corresponding to a source of radius R emitting a luminosity L is found by putting $L/4\pi R^2 = \sigma T_*^4$. This gives

$$T^4 = \left[\frac{L}{L_{Edd}}\right]\left[\frac{R}{R_S}\right]^{-2}\left[\frac{M}{M_\odot}\right]^{-1}\frac{45}{4\pi^3\alpha_f^3}\frac{m_p}{m_e}\frac{r_e}{R_{S\odot}} \tag{1.3}$$

where the Eddington luminosity $L_{Edd} \simeq 10^8\, M/M_\odot$ watts, and the Schwarzschild radius $R_S \simeq 3\times10^3\, M/M_\odot$ metres. This gives the temperature

$$T_*^{bb} = 4\times10^7\left[\frac{L}{L_{Edd}}\right]^{1/4}\left[\frac{R}{R_S}\right]^{-1/2}\left[\frac{M}{M_\odot}\right]^{-1/4}\ \mathrm{K} \tag{1.4}$$

An estimate of the particle number density, *N*, can be made by putting $L = \eta N m_p c^2 4\pi R^2 v_{in}$, where η is the efficiency, and v_{in} is the infall velocity. v_{in} will equal the free fall velocity, $v_{ff} = c\sqrt{R_S/R}$, for radial motion, and it will be lower if any disk-like structure forms. For the approximately $1/R$ potential of a black hole, most of the energy is liberated within a few gravitational radii of the centre. Putting $R \sim 3R_S$ (and $\eta \sim 0.1$) gives the number density

$$N = 5\times10^{24}\left[\frac{L}{L_{Edd}}\right]\left[\frac{v_{in}}{v_{ff}}\right]^{-1}\left[\frac{M}{M_\odot}\right]^{-1} \text{ m}^{-3} \tag{1.5}$$

The Thomson time corresponding to this density, $t_p = 1/N\sigma_T c$, is therefore

$$t_p = 10^{-5}\left[\frac{L}{L_{Edd}}\right]^{-1}\left[\frac{v_{in}}{v_{ff}}\right]\left[\frac{M}{M_\odot}\right] \text{ seconds} \tag{1.6}$$

The equipartition field strength is then obtained from $B^2/2\mu_0 = 3NkT_*/2$, which gives, at $R \sim 3R_S$,

$$B_* = 50\ \left[\frac{L}{L_{Edd}}\right]^{5/8}\left[\frac{v_{in}}{v_{ff}}\right]^{-1/2}\left[\frac{M}{M_\odot}\right]^{-5/8} \text{ Tesla} \tag{1.7}$$

This is the sort of field strength that might be expected in an accretion disk around a compact object. If the central object were a magnetic neutron star, it could have a field $10^6 - 10^8$ T.

2 Thermalization of a Relativistic Gas

Before discussing the properties of relativistic thermal plasmas, we must first find the thermalization timescale. If this is much longer than those of the relevant cooling processes (in particular bremsstrahlung, see § 4.2) then it is not self-consistent to consider such plasmas. Thermalization gets more difficult at higher temperatures – the timescale increases – due to the decrease of the scattering cross section at high energies. (e.g. the Rutherford cross section goes like $1/v^4$). Spitzer (1956) found the non-relativistic timescale for Rutherford scattering; it goes like $T^{3/2}$. The non-relativistic bremsstrahlung timescale also increases with temperature, but only as $T^{1/2}$. If these timescales are extrapolated to relativistic temperatures, they cross when the temperature is a few hundred $m_e c^2$. This extrapolation is not valid, however, since relativistic corrections change the energy dependence of these processes. To find the correct answer, we need, among other things, a relativistic generalization of Spitzer's formula. This requires an excursion into relativistic kinematics.

2.1 Energy Exchange in a Relativistic Collision

To simplify the expressions in the following discussion, c is set equal to unity. Let the four-vector x^μ have components (x^o, **x**). Then, using the metric (+ – – –), the scalar product becomes $x^\mu y_\mu \equiv x \cdot y = x^o y^o - \mathbf{x} \cdot \mathbf{y}$. Quantities in the centre-of-momentum (CM) frame are indicated by a prime.

Consider two species, *A* and *B*, with masses *m* and *M* respectively. Let their distribution functions be isotropic in the plasma frame. Before the collision their 4-momenta (in the plasma frame) are

$$\begin{aligned} p_A^\mu &= m\gamma_A(1, \boldsymbol{\beta}_A) \\ p_B^\mu &= m\gamma_B(1, \boldsymbol{\beta}_B) \end{aligned} \tag{2.1}$$

After the collision $p_{A2}^\mu = m\gamma_{A2}(1, \boldsymbol{\beta}_{A2})$ and so the energy exchange is $m\Delta\gamma_A = m(\gamma_{A2} - \gamma_A)$. The velocity of the CM of the two body system relative to the plasma frame is

$$\mathbf{V} = \frac{m\gamma_A \boldsymbol{\beta}_A + M\gamma_B \boldsymbol{\beta}_B}{m\gamma_A + M\gamma_B} \tag{2.2}$$

Let this direction define the *x*-axis, i.e. **V** = *V*(1,0,0). Then $V\beta_{Ax} = \mathbf{V} \cdot \boldsymbol{\beta}$. Lorentz transforming p_A^μ to the CM frame gives

$$p_A'^\mu = m\gamma_A \left[\Gamma(1 - V\beta_{Ax}), \Gamma(\beta_{Ax} - V), \beta_{Ay}, \beta_{Az} \right] \tag{2.3}$$

where Γ is the γ-factor of the CM relative to the plasma frame; $\Gamma^2 = 1/(1 - V^2)$. So the CM energy and *x*-velocity before the collision are

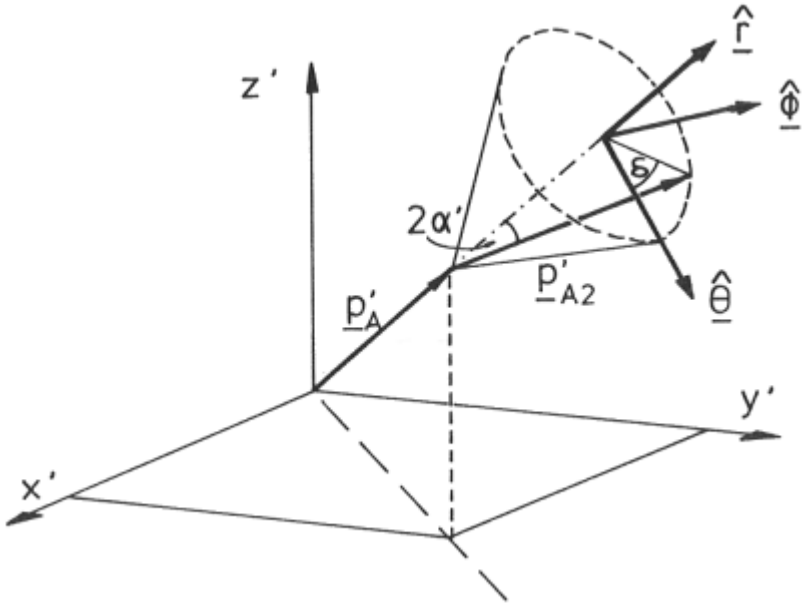

Figure (2.1)

Scattering in the centre of momentum (CM) frame. The scattering angle is $2\alpha'$. δ is an angle related to the orientation of the orbital plane. There is no energy exchange in this frame, hence $|\mathbf{p}'_A| = |\mathbf{p}'_{A2}|$.

$$\gamma'_A = \Gamma\gamma_A(1 - V\beta_{Ax}) \tag{2.4a}$$

$$\beta'_{Ax} = \beta_{Ax}/(1 - V\beta_{Ax}) \tag{2.4b}$$

Let particle A be scattered through an angle $2\alpha'$ in the CM frame, as shown in figure (2.1). Since there is no energy exchange in this frame the magnitude of $\mathbf{p}'_A$ is unaltered – only its direction changes. Hence

$$p'_{A2} = |p_A|\left[\hat{\mathbf{r}}\cos 2\alpha' + (\hat{\boldsymbol{\theta}}\cos\delta + \hat{\boldsymbol{\varphi}}\sin\delta)\sin 2\alpha'\right] \tag{2.5}$$

Here δ is an (unknown) angle related to the orientations of the orbital plane. The actual value of δ depends on the details of the particular scattering, but it will disappear in the averaging process. $\hat{\mathbf{r}}$, $\hat{\boldsymbol{\theta}}$ and $\hat{\boldsymbol{\varphi}}$ are the usual spherical polar unit vectors. Their x components are

$$r_x = x/r \tag{2.6a}$$

$$\theta_x = xz/\rho r \tag{2.6b}$$

$$\phi_x = -y/\rho \tag{2.6c}$$

where $\rho^2 = x^2 + y^2$ and $r^2 = \rho^2 + z^2$. We now average over the distribution function. Because the distributions are isotropic in the plasma frame, $\langle p_{Ay}\rangle = \langle p_{Az}\rangle = 0$. Since the Lorentz transformation parallel to the x-axis leaves the y and z components of p unchanged, (i.e. $p'_{Ay} = p_{Ay}$ and $p'_{Az} = p_{Az}$) these components average to zero in the CM frame as well. It is not the case that the x component averages to zero in the CM frame, however, since the

direction of the Lorentz transformation relative to this frame depends on $\boldsymbol{\beta}_A$. In fact, since $\langle \theta_x \rangle = \langle \phi_x \rangle = 0$, equation (2.5) becomes

$$\langle p'_{A2x} \rangle = p'_{Ax} \cos 2\alpha \tag{2.7}$$

Thus the dependence on δ has disappeared. Lorentz transforming the averaged p'^{μ}_{A2} back to the plasma frame gives the average energy after the collision as

$$\langle \gamma_{A2} \rangle = \Gamma \gamma'_{A2}(1 + V\beta'_{A2x}) = \Gamma \gamma'_A (1 + V\beta'_{Ax} \cos 2\alpha) \tag{2.8}$$

Hence the average energy exchange is

$$\langle \Delta E_A \rangle = -2mM \sin^2 \alpha' \frac{M\gamma_A - m\gamma_B + \gamma(m\gamma_A - M\gamma_B)}{m^2 + M^2 + 2\gamma mM} \tag{2.9}$$

where $\gamma = \gamma_A \gamma_B (1 - \boldsymbol{\beta}_A \cdot \boldsymbol{\beta}_B)$ is the γ-factor of relative motion.

Frankel, Hines & Dewar (1979) have calculated the energy loss in a single relativistic two body collision, but have not performed the averaging necessary to get equation (2.9). This averaging needs to be done carefully, since the distribution functions are isotropic only in the rest frame of the plasma, not in the CM frame.

The non-relativistic limit of equation (2.9) is

$$\langle \Delta E_A^{NR} \rangle = -mM \sin^2 \alpha' \frac{(\beta_A^2 - \beta_B^2)(M + m) + \beta^2 (m - M)}{(m + M)^2} \tag{2.10}$$

where now β is the non-relativistic relative velocity, $\beta^2 = (\boldsymbol{\beta}_A - \boldsymbol{\beta}_B)^2$.

2.2 Energy Exchange Rate Between Maxwellian Distributions

Now that we know the average energy exchange in a single collision, we can average it over Maxwellian particle distributions to find the relaxation time. The relativistically invariant differential reaction rate for a distribution of particles scattering with differential cross section dσ is (Landau & Lifshitz, 1975, Chapter 12)

$$dR_{12} = d\sigma \, \beta \frac{p_1 \cdot p_2}{\gamma_1 \gamma_2} \frac{dn_1 \, dn_2}{1 + \delta_{12}} \tag{2.11}$$

where β is the relative velocity, p is the 4-momentum and the dn are the distribution functions. δ_{12} is the Kronecker delta, which takes care of double counting when the particles are identical. Integrating equation (2.11) for general distribution functions results in an at least 7-dimensional integral, more if the cross section is angle dependent. However, on taking do to be the isotropic relativistic Maxwell distribution of equation (1.2) and changing the order of integration, all but one of the integrals can be performed. This gives the reaction rate

$$R_{12} = \frac{n_1 n_2}{1 + \delta_{12}} \langle \sigma_{12} \rangle \tag{2.12}$$

where $\langle \sigma_{12} \rangle$ is the cross section suitably averaged over the Maxwellian distributions. After a few pages of algebra (Weaver, 1976) it is found to be:

$$\langle \sigma_{12} \rangle = \int_1^\infty \sigma(\gamma)\gamma^2\beta^2 \frac{K_1(z)}{z} d\gamma \Big/ \theta_1\theta_2 K_2(1/\theta_1)\, K_2(1/\theta_2) \tag{2.13}$$

where $z^2 = (\theta_1^2 + \theta_2^2 + 2\gamma\theta_1\theta_2)/\theta_1^2\theta_2^2$. Hence the scattering rate can be expressed as a *single* integral over the scattering cross section. Equation (2.13) reduces to the correct non-relativistic limit:

$$\langle \sigma_{12}^{NR} \rangle = \sqrt{\frac{2}{\pi}} \frac{n_1 n_2}{1+\delta_{12}} \int_0^\infty \sigma(\beta)\beta^3 \exp\left[\frac{-\beta^2}{2(\theta_1+\theta_2)}\right] d\beta \Big/ (\theta_1+\theta_2)^{3/2} \tag{2.14}$$

To calculate the relaxation timescale, the reaction rate must be weighted by the average energy per collision. Thus we wish to evaluate

$$\frac{dE_1}{dt} = \int \langle \Delta E_1 \rangle dR_{12} = \int \langle \Delta E_1 \rangle d\sigma(\gamma,\alpha')\beta \frac{p_1 \cdot p_2}{\gamma_1\gamma_2} \frac{dn_1\, dn_2}{1+\delta_{12}} \tag{2.15}$$

Here the cross section depends not only on the relative velocity, but also on the (centre of momentum) scattering angle, $2\alpha'$. $\langle \Delta E_1 \rangle$ is given by equation (2.9). Then, on integrating over Maxwellian distribution functions, we get (after several pages of algebra)

$$\begin{aligned} \frac{dE_1}{dt} = -2Mm \frac{n_1 n_2}{1+\delta_{12}} & \frac{T_1 - T_2}{\theta_1^2\theta_2^2 K_2(1/\theta_1) K_2(1/\theta_2)} \\ & \times \int_1^\infty \int_{\alpha_1}^{\alpha_2} \frac{(\gamma^2-1)^2 \sigma(\gamma,\alpha') \sin^2\alpha'}{M^2 + m^2 + 2\gamma mM} \frac{K_2(z)}{z^2} d\Omega' d\gamma \end{aligned} \tag{2.16}$$

Hence the relaxation rate can also be expressed as an integral over the relevant CM scattering cross section. Note that the integration is over the *CM* angles and the *relative* γ-factor. Some care must be taken when evaluating timescales since particle-particle scattering cross sections are usually expressed in the rest frame of one (target) particle. The angular part must be transformed to the CM. See Appendix 1.

In equation (2.16), $\alpha_1 = 1/\Lambda$ is the minimum scattering half-angle. For divergent (Coulomb) cross sections it is determined by the minimum momentum transfer, that of the excitation of a single plasmon in the forward direction. Hence $\alpha_1 \sim \omega_p/2\gamma$ and so $\Lambda \sim T/\omega_p$. Strictly, α_1 is a function of γ, but since the Ω' integral results in a term like ln α_1, a typical value of γ (i.e. T) can be substituted. For relativistic plasmas, the plasma frequency is $\omega_p^2 = r_e N_e \sigma_T / 2T\alpha_f^2$ (Gould, 1981). (r_e is the classical electron radius, σ_T is the Thomson cross section and α_f is the fine structure constant.) Taking T = 1 and N_e = 10^{20} m^{-3} gives $\ln\Lambda \simeq 20$. It is essentially a Coulomb logarithm. For convergent cross sections α_1 = 0.

α_2 is the maximum scattering half-angle. For distinguishable particles $\alpha_2 = \pi/2$. For identical particles scattering with a symmetrized cross section $\alpha_2 = \pi/4$.

The non-relativistic limit of equation (2.16) is

$$\frac{dE_1}{dt} = -2\sqrt{\frac{2}{\pi}}\frac{Mm}{(M+m)^2}\frac{n_1 n_2}{1+\delta_{12}}\frac{T_1 - T_2}{(\theta_1+\theta_2)^{5/2}} \times \int_0^\infty \int_{\alpha_1}^{\alpha_2} \sigma(\alpha', \beta)\beta^5 \sin^2\alpha' \exp\left[\frac{-\beta^2}{2(\theta_1+\theta_2)}\right] d\Omega' d\beta \tag{2.17}$$

2.3 Relaxation Timescales

In a plasma heated by shocks or turbulence the protons will gain more energy than will the electrons. It is, however, mainly the electrons which radiate (except for some pion production at very high temperatures, see § 4.3). Hence the energy exchange rate from protons to electrons is a crucial factor in determining the temperature structure of the plasma. If the separate electron-electron and proton-proton thermalization timescales are shorter than the electron heating timescale, the electrons and protons will be able to achieve Maxwellian distributions with different temperatures, such that $T_e < T_p < m_p T_e / m_e$.

We are now in a position to evaluate these timescales by substituting the relevant cross sections into equation (2.16). The cross sections for electron-proton, electron-electron and electron-positron scattering are well known, so these relaxation rates can be easily evaluated. Proton-proton relaxation is more difficult to calculate. Above energies of a few MeV elastic nuclear scattering becomes important, and a numerical fit must be made to the experimental cross section.

2.3.1 Electron-Proton Relaxation

The relaxation timescale is defined (by, analogy with Spitzer, 1956) as

$$t^{ep} = \left| \frac{\varepsilon n_e (T_e - T_p)}{dE_e/dt} \right| \tag{2.18}$$

where $\varepsilon T_e = \langle \gamma_e \rangle - 1$ is the average kinetic energy of the electrons:

$$\varepsilon = \frac{1}{T}\left[\frac{K_1(1/T)}{K_2(1/T)} + 3T - 1\right] \tag{2.19a}$$

$$= \tfrac{3}{2} + \tfrac{15}{8}T - \tfrac{15}{8}T^2 + O(T^3) \quad ; \quad T \ll 1 \tag{2.19b}$$

$$= 3 - 1/T + 1/2T^2 + O(T^{-3}) \quad ; \quad 1 \ll T \tag{2.19c}$$

The Rutherford formula for the cross section assumes that both particles are pointlike and spinless, which is a good approximation for low energy and small angle (large impact parameter) scattering. Including the effects of electron and proton spin, proton recoil, magnetic scattering and a non-pointlike proton results in the Rosenbluth cross section (Perkins, 1972). It is less than the Rutherford cross section for all scattering angles, but this difference is smallest at small scattering angles, those which dominate in Coulomb scattering. It turns out that for scattering angles (in the proton's rest frame) $\alpha_o < m_p / \gamma m_e$, the

Rutherford formula is sufficiently accurate. If $\alpha_o \gg \alpha_{min} = 1/2\Lambda$ the total rate will be unaffected by replacing $\alpha_{max} = \pi/2$ by α_o. So if $\gamma \ll 2m_p\Lambda/m_e$ ($\gamma \ll 10^{-12}$ for ln Λ = 20) the Rutherford formula may be used. This easily holds for the energies being considered here, and so the cross section is simply

$$d\sigma = \frac{3}{32\pi\gamma^2\beta^4}\frac{d\Omega}{\sin^4\alpha} = \frac{3}{32\pi\gamma^2\beta^4}\left[\frac{2\gamma m_e}{m_p}+1\right]\frac{d\Omega'}{\sin^4\alpha'} \tag{2.20}$$

See Appendix 1 for the transformation of angles from the (unprimed) rest frame to the (primed) CM frame. Substituting this cross section into equation (2.16) gives the general expression for the electron heating rate as

$$\frac{dE_e}{dt} = \frac{-3m_e}{2m_p}\frac{(1+2z)(T_e-T_p)\ln\Lambda}{K_2(1/\theta_e)K_2(1/\theta_p)} \times\left[\frac{2(\theta_e+\theta_p)^2+1}{\theta_e+\theta_p}K_1\left(\frac{\theta_e+\theta_p}{\theta_e\theta_p}\right)+2K_0\left(\frac{\theta_e+\theta_p}{\theta_e\theta_p}\right)\right] \tag{2.21}$$

In most cases of interest the protons are non-relativistic, $\theta_p \ll 1$, and then equation (2.21) reduces to

$$\frac{dE_e}{dt} = \frac{-3m_e}{2m_p}(1+2z)(T_e-T_p)\ln\Lambda\frac{\exp(-1/\theta_e)}{K_2(1/\theta_e)} \times\sqrt{\frac{\theta_e}{(\theta_e+\theta_p)^3}}\left[2(\theta_e+\theta_p)^2+2(\theta_e+\theta_p)+1\right] \tag{2.22}$$

If both species are non-relativistic ($\theta_e, \theta_p \ll 1$) this in turn reduces to

$$\frac{dE_e^{NR}}{dt} = \frac{-3}{\sqrt{2\pi}}\frac{m_e}{m_p}\frac{(1+2z)(T_e-T_p)\ln\Lambda}{(\theta_e+\theta_p)^{3/2}} \tag{2.23a}$$

$$t^{ep,NR} = \sqrt{\frac{\pi}{2}}\frac{m_p}{m_e}\left[T_e+T_p\frac{m_e}{m_p}\right]^{3/2}\Big/\ln\Lambda \tag{2.23b}$$

This non-relativistic limit reproduces Spitzer's (1956) result. For the case when $T_p \lesssim T_e$, the timescale is simply proportional to $T_e^{3/2}$. If, however, the electrons are relativistic (but the protons still non-relativistic, i.e. $\theta_e \gg 1$, $\theta_p \ll 1$) then

$$\frac{dE_e}{dt} = \frac{-3m_e}{2m_pT_e}(1+2z)(T_e-T_p)\ln\Lambda \tag{2.24a}$$

$$t^{ep} = 2T_em_p/m_e\ln\Lambda \tag{2.24b}$$

Thus, for T_e > 1, the timescale increases more slowly than in the non-relativistic case, since now $t_e \propto T_e$. If both species are relativistic ($\theta_e, \theta_p \gg 1$), then

$$\frac{dE_e}{dt} = \frac{-3}{4T_eT_p}(1+2z)(T_e - T_p)\ln\Lambda \tag{2.25a}$$

$$t^{ep,UR} = 4T_eT_p \Big/ \ln\Lambda \tag{2.25b}$$

However, this is probably not relevant physically, since in this case both species will cool much more quickly by either bremsstrahlung (in the case of the electrons) or pion production (by the protons), as will be shown in chapter 4. So the particles will be unable to maintain (by two body interactions) the Maxwellian distributions assumed to derive this result.

2.3.2 Electron-Electron Relaxation

The electron-electron interaction takes place via Møller scattering (Jauch & Rohrlich, 1980, § 12.1). The cross section in the relevant notation is

$$\frac{d\sigma}{d\Omega'} = \frac{3}{8\pi}\frac{8}{(\gamma^2-1)(\gamma-1)}\left[\frac{\gamma^2}{\sin^4\alpha'} - \frac{2\gamma^2+\gamma-1}{4\sin^2\alpha'} + \frac{(\gamma-1)^2}{8}\right] \tag{2.26a}$$

Small angle scattering dominates, since this cross section diverges as α tends to zero. So taking the small angle limit (neglecting all but the first term and putting cos $\alpha' = 1$) gives

$$\frac{d\sigma}{d\Omega'} = \frac{3}{8\pi}\frac{\gamma^2}{(\gamma^2-1)(\gamma-1)}\frac{1}{2\sin^4\alpha'} \tag{2.26b}$$

This gives the timescale

$$t^{ee} = \frac{4\varepsilon K_2^2(1/T)}{3(1+z)\ln\Lambda}\Big/\left[\left(4T+1/2T\right)K_1(2/T) + 2K_0(2/T)\right] \tag{2.27a}$$

with high and low temperature limits

$$t^{ee} = \frac{4\sqrt{\pi}T^{3/2}}{(1+2z)\ln\Lambda} \quad ; \quad T \ll 1 \tag{2.27b}$$

$$t^{ee} = \frac{8T^2}{(1+2z)\ln\Lambda} \quad ; \quad 1 \ll T \tag{2.27c}$$

The factor of $1 + 2z$ occurs in the equations since the dimensionless timescale is normalized to the 'proton Thomson time', not the electron time. In fact, the principal terms of the Møller cross section (that proportional to $1/\sin^4\alpha'$) in the non-relativistic and ultrarelativistic limits is the same as the Rutherford cross section, although the transformation from rest frame to CM angles is not so simple as for electron-proton scattering, equation (2.20). So this timescale could be obtained directly from the electron-proton timescale by putting $T_p = T_e$, and including a factor of two for identical particle effects.

This result disagrees with that of Gould (1982a) in that equation (2.27) includes a Coulomb logarithm. However, Gould's (1981) approximation to the energy exchange is invalid at small scattering angles – those which dominate to produce the ln Λ term.

Electron-positron scattering occurs via the Bhaba cross section (Jauch & Rohrlich, 1980, § 12.2). The cross section is

$$\frac{d\sigma}{d\Omega'} = \frac{3}{8\pi}\frac{1}{8(\gamma+1)}\left\{\frac{2\left[2+4(\gamma-1)\cos^2\alpha'+(\gamma-1)^2(1+\cos^4\alpha')\right]}{(\gamma-1)^2\sin^4\alpha'}\right.$$
$$-\frac{4\left[3+4(\gamma-1)\cos^2\alpha'+(\gamma-1)^2\cos^4\alpha'\right]}{(\gamma^2-1)\sin^2\alpha'} \qquad (2.28a)$$
$$\left.+\frac{\left[12+8(\gamma-1)+(\gamma-1)^2(1+\cos^2\alpha')\right]}{(\gamma+1)^2}\right\}$$

Again, just including the dominant term proportional to $1/\sin^4\alpha'$ and putting $\cos\alpha' = 1$ gives

$$\frac{d\sigma}{d\Omega'} = \frac{3}{8\pi}\frac{\gamma^2}{(\gamma^2-1)(\gamma-1)}\frac{1}{2\sin^4\alpha'} \qquad (2.28b)$$

which is identical to the principal Møller term. Hence the electron-positron timescale is just one-half the electron-electron timescale, as there are no identical particle effects.

2.3.3 Proton-Proton Relaxation

The result for pure Coulomb scattering in the non-relativistic case can be obtained directly from the electron-electron timescale, equation (2.27b), by the following argument. Since in the non-relativistic case the cross section in both electron-electron and proton-proton scattering is essentially the Rutherford cross section, the form of the energy exchange rate and relaxation timescales will differ only in the subscript *e*'s or *p*'s. Writing equation (2.27b) in physical (starred) quantities gives

$$t_*^{ee} N_p \sigma_T c = \frac{4\sqrt{\pi}}{\ln\Lambda}\left[\frac{kT_{*e}}{m_e c^2}\right]^{3/2} \qquad (2.29)$$

Replacing all *e*'s by *p*'s, remembering the implicit $1/m_e^2$ in σ_T gives

$$t_*^{pp} N_p \sigma_T c\left[\frac{m_e}{m_p}\right]^2 = \frac{4\sqrt{\pi}}{\ln\Lambda}\left[\frac{kT_{*p}}{m_p c^2}\right]^{3/2} \qquad (2.30)$$

Then rewriting this in dimensionless quantities gives the timescale as

$$t^{pp} = \frac{4\sqrt{\pi}}{\ln\Lambda}\left[\frac{m_p}{m_e}\right]^{1/2} T_p^{\,3/2} \qquad (2.31)$$

This holds for temperatures $T_p < 1$. At higher energies the modification of the cross section due to nuclear scattering must be included. For relative kinetic energies below a few MeV only the $l = 0$ (*s* wave) nuclear scattering term need be included (Schiff, 1968, § 50). The modified scattering amplitude is

$$f(\theta) = f_C(\theta) + \frac{\sin\delta_0}{k}\exp i(\eta_0 + \delta_0) \tag{2.32}$$

where the wavenumber $k = m\beta c/2\hbar$, δ_0 is the l = 0 phase shift and $f_C(\theta)$ is the Coulomb scattering amplitude

$$f_C(\theta) = \frac{\alpha_f}{2k\beta\sin^2\alpha}\exp i\left[-\tfrac{\alpha_f}{\beta}\ln\sin^2\alpha + \pi + 2\eta_0\right] \tag{2.33}$$

(Schiff, 1968, § 21). α_f = 1/137 is the fine structure constant. The Born approximation corresponds to velocities $\beta/\alpha_f \gg 1$. The appropriate antisymmetrized cross section for scattering identical spin-half particles is

$$\frac{d\sigma}{d\Omega} = \left|f(\theta)\right|^2 + \left|f(\pi-\theta)\right|^2 - \Re\left[f(\theta)f^*(\pi-\theta)\right] \tag{2.34}$$

Substituting equations (2.32) and (2.33) into equation (2.34) gives the cross section

$$\begin{aligned}\frac{d\sigma_{\text{tot}}}{d\Omega} &= \frac{d\sigma_C}{d\Omega} + \frac{\sin^2\delta_0}{k} \\ &\quad -\frac{\alpha_f\sin\delta_0}{2\beta k^2}\left[\frac{\cos\left(\tfrac{\alpha_f}{\beta}\ln\sin^2\alpha + \delta_0\right)}{\sin^2\alpha} + \frac{\cos\left(\tfrac{\alpha_f}{\beta}\ln\cos^2\alpha + \delta_0\right)}{\cos^2\alpha}\right]\end{aligned} \tag{2.35}$$

The last term in equation (2.35) represents the interference between the nuclear and Coulomb scattering. The Coulomb cross section is

$$\frac{d\sigma_C}{d\Omega} = \left(\frac{\alpha_f}{2k\beta}\right)^2\left[\frac{1}{\sin^4\alpha} + \frac{1}{\cos^4\alpha} - \frac{\cos\left(\tfrac{\alpha_f}{\beta}\ln\tan^2\alpha_0\right)}{\sin^2\alpha\cos^2\alpha}\right] \tag{2.36}$$

This is the Mott scattering formula for identical particles. The last term in equation (2.36) represents the interference due to identical particle effects.

Defining the total cross section to be (c.f. equation 2.16)

$$\sigma = 4\int\frac{d\sigma}{d\Omega}\sin^2\alpha\, d\Omega = 32\pi\int\frac{d\sigma}{d\Omega}\sin^3\alpha\cos\alpha\, d\alpha \tag{2.37}$$

and substituting for $d\sigma/d\Omega$ gives

$$\begin{aligned}\sigma &= \frac{4\pi\alpha_f^2}{k^2\beta^2}\left[2\ln\Lambda - \tfrac{1}{2} - \int_{1/4\Lambda^2}^1\cos\left(\tfrac{\alpha_f}{\beta}\ln y\right)\frac{dy}{1+y}\right] + 2\pi\frac{\sin^2\delta_0}{k^2} \\ &\quad -8\pi\frac{\alpha_f\sin\delta_0}{\beta k^2}\left[\int_0^{1/2}\cos\left(\tfrac{\alpha_f}{\beta}\ln y + \delta_0\right)dy + \int_{1/2}^1\cos\left(\tfrac{\alpha_f}{\beta}\ln y + \delta_0\right)\frac{1-y}{y}dy\right]\end{aligned} \tag{2.38}$$

$$\sigma = \sigma_C + \sigma_N - \sigma_I$$

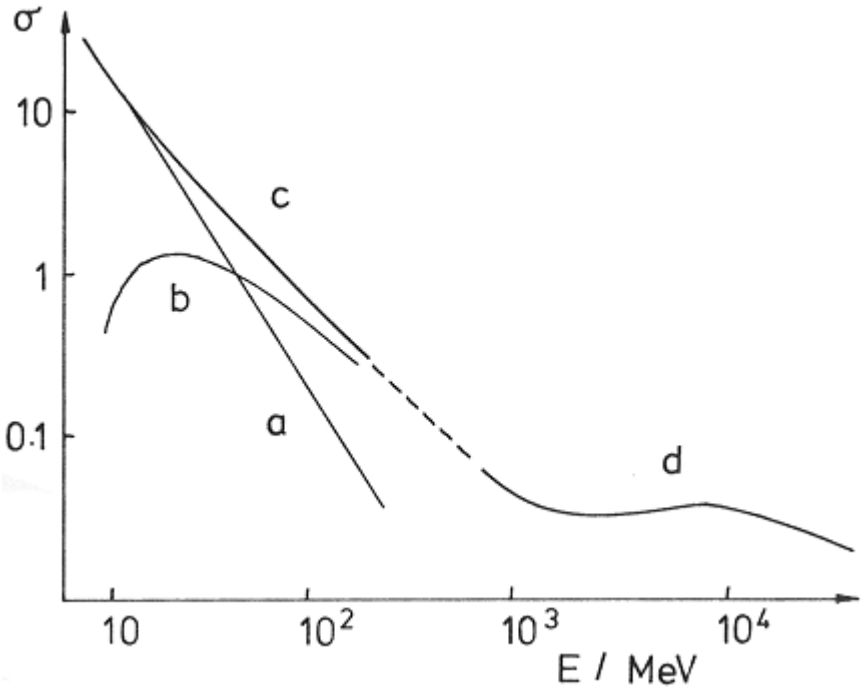

Figure (2.2)

The proton-proton elastic scattering cross section as a function of proton kinetic energy. **(a)** pure Coulomb scattering cross section, ln Λ = 20 **(b)** nuclear and interference terms (Gould, 1982 b) **(c)** total cross section, equation (2.40) **(d)** experimentally determined elastic scattering cross section, Particle Data Group (1980).

For $\beta/\alpha_f \ll 1$ ($E \ll 0.025$ MeV) the integrands oscillate rapidly and their contributions tend to zero. (i.e. the interference terms disappear in the classical limit). This leaves

$$\sigma = \sigma_C + \sigma_N = \frac{2\pi}{k^2}\left[\frac{4\alpha_f^2}{\beta^2}\ln\Lambda + \sin^2\delta_0\right] \tag{2.39}$$

However, since $\sin^2\delta_0 \ll 1$ and $(\alpha_f/\beta)^2 \ln\Lambda \gg 1$ the nuclear contribution is negligible at these energies.

More interesting is the case where $\beta/\alpha_f \gg 1$. The integrands in (2.38) are now slowly varying, and can be approximated by setting $\cos\left[\frac{\alpha_f}{\beta}\ln y\right] = 1$ and $\sin\left[\frac{\alpha_f}{\beta}\ln y\right] = 0$. This gives

$$\sigma = \frac{8\pi\alpha_f^2}{k^2\beta^2}\ln\Lambda + 2\pi\frac{\sin^2\delta_0}{k^2} - 4\pi\ln 2\,\frac{\alpha_f}{\beta}\frac{\sin\delta_0}{k^2} \tag{2.40}$$

The phase shift δ_0 can be calculated using effective range theory (Blatt & Weisskopf, 1952, § 4.2). The interference and nuclear terms are equal (and hence cancel) when E ~ 0.8 MeV. I used Gould's (1982b) calculated values of δ_0 for E < 20 MeV and the experimentally determined cross sections (Particle Data Group, 1980) for higher energies to get the modified relaxation timescale. See figure (2.2).

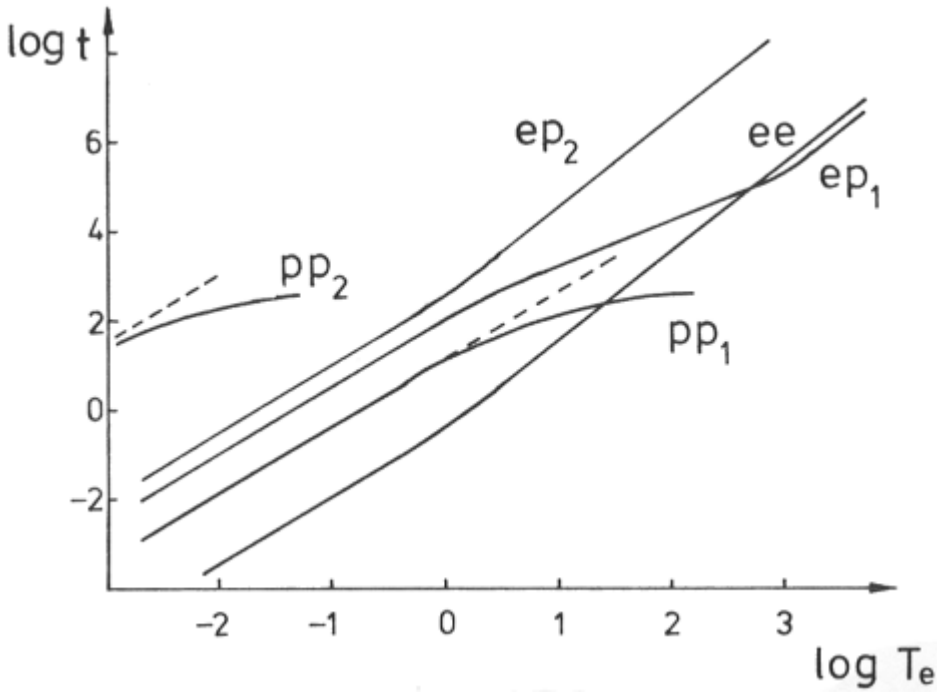

Figure (2.3)

Relaxation timescales. **(ee)** electron-electron **(ep_1)** electron-proton, $T_p = T_e$ **(ep_2)** electron-proton, $\theta_p = \theta_e$ **(pp_1)** proton-proton, $T_p = T_e$ (the dashed line is pure Coulomb) **(pp_2)** proton-proton, $\theta_p = \theta_e$

2.3.4 Comparison of Relaxation Timescales

The various timescales derived above are plotted in figure (2.3) as a function of electron temperature. Processes involving protons are plotted for the two extreme proton temperatures, $T_p = T_e$ and $\theta_p = \theta_e$.

At non-relativistic temperatures, all the timescales go like $T^{3/2}$, since they are all basically the same process – Rutherford scattering. The electron-electron relaxation time is the shortest. Then, if the protons and electrons have the same temperature, the proton-proton is the next shortest, with $t^{pp} = t^{ee}(m_p / m_e)^{1/2} \simeq 43 t^{ee}$. Finally comes the electron-proton energy exchange timescale, $t^{ep} \simeq t^{ee}(m_p / 4\sqrt{2} m_e) \simeq 325 t^{ee}$. So if the electron and proton temperatures are not too different, they could separately thermalize to form a two temperature plasma before the protons significantly heat the electrons. However, if the protons are much hotter than the electrons, their thermalization timescale becomes longer than the energy exchange timescale.

The situation is different at relativistic temperatures. Since for electron-electron scattering both particles are relativistic, the relativistic beaming factor $p_1 \cdot p_2 / \gamma_1 \gamma_2 = m_1 m_2 (1 - \boldsymbol{\beta}_1 \cdot \boldsymbol{\beta}_2)$ in equation (2.11), which suppresses all but head-on collisions, serves to increase the temperature dependence of the timescale to T_e^2. However, for electron-proton scattering

(when the temperatures are the same) only one species is relativistic, and the beaming factor is negligible. Instead the timescale becomes proportional to T_e. [2]

Proton-proton scattering is dominated by nuclear scattering even while the protons are still non-relativistic. This increase in the cross section reduces the timescale considerably. So much so, in fact, that for the case when $T_e = T_p$, the individual timescales are equal (and less than t^{ep}) when $T \simeq 10$.

So even in the relativistic regime the protons and electrons can maintain Maxwellians at different temperatures. Again, the difference in temperature cannot be too great, but now for a different reason. We shall see in Chapter 4 that the protons cannot maintain a Maxwellian at a very high temperature, since they cool too fast by pion production.

[2] In the case where the protons are very much hotter than the electrons, so both species are relativistic, the beaming effect dominates and so the timescale is proportional to T^2. However, as was noted earlier, this is probably not a physically relevant regime.

3 Pair Production and Annihilation

Relativistic plasmas are qualitatively different from the lower temperature cases because of electron-positron pair effects. The electrons are relativistic – their kinetic energy is of the same order as their rest mass. Hence they are able to pair-produce in collisions. Typical energies of the internally produced bremsstrahlung photons ($\hbar\omega_* \sim kT_*$) are also high enough to pair-produce. The problem becomes extremely non-linear, as pairs annihilate into hard photons which in turn create more pairs, and so on.

Anything more than the most simple calculations requires numerical modelling, as is described in later chapters. For now, however, we still have to show that the cooling due to pair effects is not so great as to preclude the formation of a Maxwellian electron distribution.

3.1 Annihilation

3.1.1 Timescale

The cross section for electron-positron annihilation is (Landau & Lifshitz, 1971, equation 88.10)

$$\sigma_{+-} = \frac{3}{8(\gamma+1)}\left[\frac{\gamma^2+4\gamma+1}{\gamma^2-1}\ln\left(\gamma+\sqrt{\gamma^2-1}\right)-\frac{\gamma+3}{\sqrt{\gamma^2-1}}\right] \tag{3.1}$$

Note that this is a monotonically *decreasing* function of the relative energy. The consequences of this are interesting constraints on the parameters of an equilibrium plasma, which will be discussed in § 3.2.2 and chapter 8.

For distinguishable particles with the same temperature, the reaction rate (equation 2.13) becomes

$$R_{ann} = z(1+z)\langle\sigma_{ann}\rangle \tag{3.2a}$$

$$\langle\sigma_{ann}\rangle = \frac{1}{T^2K_2^2(1/T)}\int_1^\infty \sigma_{+-}(\gamma)(\gamma^2-1)\frac{K_1(z)}{z}d\gamma \tag{3.2b}$$

where $z^2 = 2(1+\gamma)/T^2$. The high and low temperature limits of the rate are

$$\langle\sigma_{ann}\rangle = \tfrac{3}{8} \quad ; \quad T \ll 1 \tag{3.3a}$$

$$3(\ln 2T - \gamma_E)/16T^2 \quad ; \quad 1 \ll T \tag{3.3b}$$

Svensson (1982b) has fitted a function over the whole temperature range with an accuracy of better than 2%

$$\langle\sigma_{ann}\rangle = \tfrac{3}{16}\left[\tfrac{1}{2}+T^2/\ln(2Te^{-\gamma_E}+1.3)\right] \tag{3.3c}$$

The annihilation timescale can be defined as

$$t^{ann} = \left| n_+ / R_{ann} \right| = 1/(1+z)\left\langle \sigma_{ann} \right\rangle \tag{3.4}$$

So the timescale is independent of the temperature when $T < 1$, and increases like T^2 when $T > 1$. This increase is due to the cross section decreasing at high energies.

Ramaty & Mészáros (1981) have calculated t^{ann} in the region $T \sim 1$ using a Monte Carlo technique.

3.1.2 Spectrum

By considering detailed balance, Svensson (1982c) has given the annihilation spectrum from Maxwellian electrons and positrons in the form of a single integral over the pair *production* cross section, $\sigma_{\gamma\gamma}(x)$: (see § 3.2.5)

$$\frac{dn(\omega)}{dt} = \frac{z(1+z)}{TK_2(1/T)} 2e^{-\omega/T} I(\omega T) \tag{3.5}$$

where

$$I(\omega T) = \int_1^\infty 2x^3 \sigma_{\gamma\gamma}(x) \exp(-x^2/\omega T) dx \tag{3.6}$$

is a function of ωT only.[3] The average energy of the annihilation photons can be calculated using equation (3.6) since

$$\left\langle \omega \right\rangle = \int \omega \dot{n}(\omega) d\omega \Big/ \int \dot{n}(\omega) d\omega \tag{3.7}$$

After changing the order of integration, the ω integral can be done analytically, and gives, using equation (7.12.23) of Erdélyi *et al.* (1953)

$$\left\langle \omega \right\rangle = \frac{\int_1^\infty x^5 \sigma_{\gamma\gamma}(x) K_2(2x/T) dx}{\int_1^\infty x^4 \sigma_{\gamma\gamma}(x) K_1(2x/T) dx} \tag{3.8}$$

This has high and low temperature limits

$$\left\langle \omega \right\rangle = 2T \left[\frac{\ln T - \gamma_E + \frac{3}{4}}{\ln T - \gamma_E + \frac{1}{2}} \right] \quad ; \quad 1 \ll T \tag{3.9a}$$

$$1 + \tfrac{3}{2}T + \tfrac{15}{8}T^2 - \tfrac{87}{8}T^3 + O(T^4) \quad ; \quad T \ll 1 \tag{3.9b}$$

Hence $\left\langle \omega \right\rangle$ is always less than $\left\langle \gamma \right\rangle$, the average energy of the annihilating electrons (equation 2.19). This is a consequence of the cross section decreasing at high energies – the lower energy electrons preferentially annihilate. Hence annihilation actually *heats* the electrons.

[3] Since this is a single integral it is relatively straightforward to get accurate numerical expressions for the annihilation spectrum.

3.2 Pair Production

Pairs can be produced in particle-particle (*e-e* and *e-p*), particle-photon and photon-photon collisions. To calculate the timescales for processes involving photons, it is necessary to assume a distribution function (the electrons and protons are assumed Maxwellian throughout). Here I assume a Wien spectrum since then it is possible to get analytic results showing the temperature dependence. But in the computer model described later the photon distribution is calculated self-consistently. So here

$$n_\gamma(\omega) = n_\gamma \omega^2 e^{-\omega/T} \Big/ 2T^3 \tag{3.10}$$

Other possible spectra are bremsstrahlung (§ 4.2) and annihilation (§ 3.1). The bremsstrahlung spectrum will give similar timescales to a Wien spectrum, since its main difference is the presence of more soft photons. It is, however, the hard photons which dominate pair production. The annihilation spectrum will also give similar timescales for $T \gg 1$, since it peaks at ωT. For $T \ll 1$ it peaks at $1+3T/4$, and so provides a source of very hard photons. Svensson (1982b) shows that annihilation photons dominate pair production for $T \lesssim 1$.

3.2.1 Particle-particle pair production

In an optically thin plasma, electron-positron pairs are produced only in particle-particle collisions. The cross section is not well known near threshold, but for $\gamma > 100$, Budnev *et al.* (1975) give

$$\sigma_{PP} = \frac{7\alpha_f^2}{18\pi^2}\left(\ln^3 2\gamma - A\ln^2 2\gamma + B\ln 2\gamma + C\right) \tag{3.11}$$

where γ is the γ-factor of relative motion and the coefficients *A*, *B* and *C* are

	$ep \rightarrow e^+e^-ep$	$ee \rightarrow e^+e^-ee$
A	178/28	178/28
B	2.6	–11
C	~40	~100
threshold γ	3	7

This cross section holds for lower temperatures in the case of electron-electron collisions, where $\gamma \sim 2\gamma_e^2 \sim T^2$, than for electron-proton collisions, where $\gamma \sim \gamma_e \sim T$. In electron-proton collisions, when the protons are non-relativistic ($\theta_p \ll 1$) they can be taken as stationary, and so the pair production rate is

$$\frac{dn_+}{dt} = (1+2z)\left\langle \sigma_{pp} \right\rangle \tag{3.12a}$$

$$\left\langle \sigma_{pp} \right\rangle = \int_1^\infty \sigma_{pp}(\gamma)\beta\, n_e(\gamma)\, d\gamma \tag{3.12b}$$

If the electron temperature is high ($\theta_e \gg 1$) then the lower limit of (3.12) can be taken as zero. On substituting the cross section (3.11), we need to evaluate

$$I_1(n) \equiv \int_0^\infty x^2 \ln^n x\, e^{-x}\, dx \tag{3.13}$$

This is done in appendix 3. For electron-electron collisions (and for electron-proton collisions with $\theta_p \gg 1$) the pair production rate is [4]

$$\frac{dn_+}{dt} = \frac{n_1 n_2}{1+\delta_{12}} \left\langle \sigma_{PP} \right\rangle \tag{3.14a}$$

$$\left\langle \sigma_{PP} \right\rangle = \frac{1}{2\theta_1^2\theta_2^2} \int_1^\infty \gamma^2 \sigma_{PP}(\gamma) \frac{K_1(z)}{z} d\gamma \tag{3.14 b}$$

$$= \tfrac{1}{16} \int_0^\infty z^4 \sigma_{PP}(z) K_1(z)\, dz \tag{3.14 c}$$

where $z^2 = 2\gamma/\theta_1\theta_2$. This requires the evaluation of (appendix 3)

$$I_2(n) \equiv \int_0^\infty z^4 \ln^n z\, K_1(z)\, dz \tag{3.14}$$

Combining these rates gives the total pair production rate (putting $T_e = T_p \equiv T$) as

$$\frac{dn_+}{dt} = \left\langle \sigma_{ee} \right\rangle \frac{(1+2z)^2}{2} + \left\langle \sigma_{ep} \right\rangle (1+2z) \tag{3.16a}$$

$$\left\langle \sigma \right\rangle = \frac{7\alpha_f^2}{18\pi^2} f(T) \tag{3.16b}$$

where

$$\begin{aligned} f_{ee}(T) = &\quad 8(\ln^3 T + 0.92\ln^2 T - 5.1\ln T + 5.5) \\ f_{ep}(T) = &\quad \ln^3 T - 1.5\ln^2 T - 8.93\ln T + 31 \quad ; \quad 1 \ll T \ll m_p/m_e \\ &\quad 8(\ln^3 T - 10.4\ln^2 T + 34\ln T - 31) \quad ; \quad m_p/m_e \ll T \end{aligned} \tag{3.16c}$$

Defining the timescale by

$$t^{pair} = \left| \frac{1+2z}{dn/dt} \right| \tag{3.17}$$

gives the high temperature pair-production timescale

$$t^{pair} = \frac{36\pi^2}{7\alpha_f^2} \frac{1}{f_1(T) + 2(1+2z)\, f_2(T)} \tag{3.18}$$

---

[4] I am here simply calculating the rates *assuming* the particle distributions are Maxwellian, even though later I will show this in fact cannot be the case for $\theta_p > 1$.

So the timescale decreases slowly (logarithmically) with increasing temperature, at high temperatures.

Since the cross sections are unknown near threshold, $\gamma = \gamma_t$, the precise form of the timescales for $T < 1$ cannot be found. However, let us assume that the cross section goes like a power law near threshold, i.e.

$$\sigma_{PP}(\gamma) = A(\gamma - \gamma_t)^s \quad ; \quad \gamma - \gamma_t << 1 \tag{3.19}$$

This is not implausible, since the cross sections for photon-particle and photon-photon pair production are power laws near threshold. They all have different indices, *s*, due to identical particle effects and different numbers of particles in the final state. Then

$$t^{ep} \propto e^{2/T} T^{-s-1/2} \tag{3.20 a}$$

$$t^{ee} \propto e^{2/T} T^{-s-3/2} \tag{3.20 b}$$

So near threshold the timescale goes like

$$t^{PP} \sim \exp(2/T) \tag{3.20 b}$$

3.2.2 Maximum temperature

For an optically thin plasma the equilibrium pair density can be found by equating the annihilation rate and the pair production rate in particle-particle collisions. Since the annihilation rate is a decreasing function of temperature while the production rate increases, the pair density also increases. Bisnovatyi-Kogan, Zel'dovich & Syunyaev (1971) showed that there is a maximum temperature above which annihilation can no longer balance pair production, and the pair density diverges.

The equilibrium condition is

$$z(1+z)\langle\sigma_{ann}\rangle = (1+2z)\langle\sigma_{ep}\rangle + \tfrac{1}{2}(1+2z)^2\langle\sigma_{ee}\rangle \tag{3.21}$$

where $\langle\sigma_{ann}\rangle$ is given by equation (3.2) and $\langle\sigma_{ep}\rangle$, $\langle\sigma_{ee}\rangle$ are given by equation (3.16). The expression is quadratic in *z*, with coefficients that are functions of *T*. So there are two or no roots. Below T_{max} there are two roots, one of which is always negative. Above T_{max} there are either two negative roots or no roots. The equilibrium pair density is plotted in figure (3.1).

The maximum temperature occurs when the coefficient of z^2 is zero, when the pair density tends to infinity. This occurs when

$$\langle\sigma_{ann}\rangle = 2\langle\sigma_{ee}\rangle \tag{3.22}$$

Taking the high temperature limit of $\langle\sigma_{ann}\rangle$, this gives the maximum temperature $T_{max} = 24$. This is lower than the value found by Bisnovatyi-Kogan *et al*. ($T \simeq 40$) because of the more accurate form of the pair production cross sections used here.

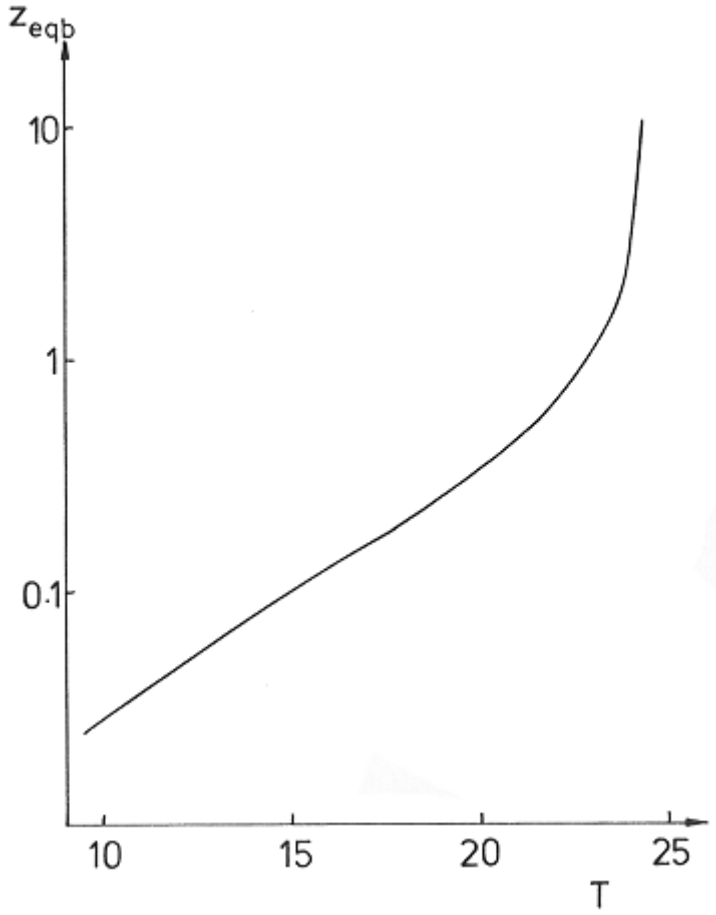

Figure (3.1)

Equilibrium pair density for an optically thin plasma (i.e. only particle-particle pair production included). $T_{max} = 24$

Note that the condition for T_{max}, equation (3.22), does not involve the electron-proton rate, $\langle \sigma_{ep} \rangle$. Near T_{max} z is very large, and hence electron-electron collisions dominate. This is fortunate since T_{max} is well away from the region where $\langle \sigma_{ee} \rangle$ is uncertain, though close to where $\langle \sigma_{ep} \rangle$ is unknown. See figure (3.2).

Physically, the maximum temperature means that any extra energy goes into increasing the number of pairs rather than into increasing the mean energy of the existing particles. Before this temperature is reached, the pair concentration will have made the plasma optically thick, and photon-particle and photon-photon collisions must also be considered. These serve to increase the pair production rate, and hence to decrease the timescale and maximum temperature. Svensson (1982b) has considered these processes in some detail for optically thin plasmas. In chapter 8 I discuss the results for plasmas with optical depths $\gtrsim 1$.

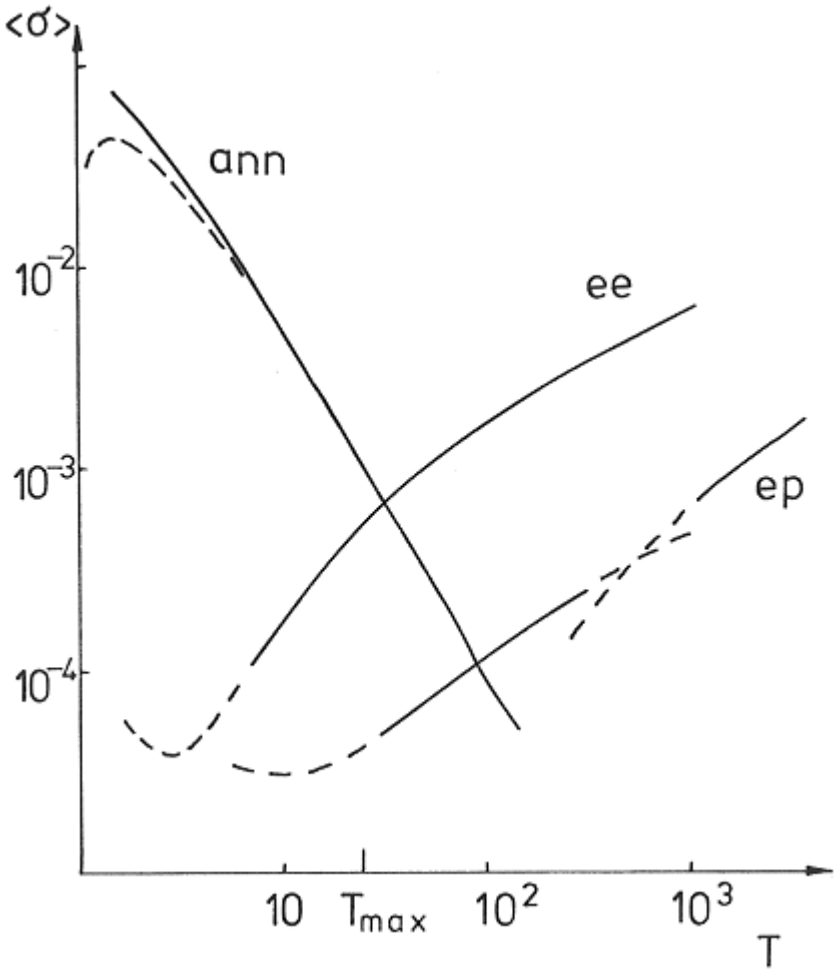

Figure (3.2)

Annihilation and particle-particle pair production cross sections, averaged over Maxwellian distributions. $Rate = \langle \sigma \rangle n_1 n_2 / (1+\delta_{12})$

3.2.3 Photon-Proton

The threshold photon energy in the proton's rest frame is $\omega = 2$. The cross section can be expressed as a function of $\eta = 2/\omega$ in terms of elliptic integrals (Jost, Luttinger & Slotnick, 1950).[5]

$$\sigma_{\gamma p} = \frac{3\alpha_f}{4\pi}\left\{\eta^2\left[2\int_1^{1/\eta}\frac{F_1(x)}{x}dx - F_1\left(\tfrac{1}{\eta}\right)\right] + \tfrac{1}{27}\left[-(109+64\eta^2)E(\varepsilon) + (42+125\eta^2+6\eta^4)F(\varepsilon)\right]\right\} \tag{3.23}$$

where [6]

[5] This is different from the cross section quoted in Jauch & Rohrlich (1980), equation (15.108), which does not reduce to the correct limit.

$$E(m) = \int_0^{\pi/2} (1 - m^2 \sin^2\phi)^{1/2} d\phi$$

$$F(m) = \int_0^{\pi/2} d\phi \Big/ (1 - m^2 \sin^2\phi)^{1/2}$$

$$F_1(x) = \int_1^x F\left(\sqrt{1 - 1/y^2}\right) dy \Big/ y$$

$$\varepsilon = \sqrt{1 - \eta^2}$$

The threshold and high energy limits of the cross section are

$$\begin{aligned} \sigma_{\gamma p}(\omega) = \quad & \alpha_f (\omega - 2)^3 \big/ 32 && ; \quad \omega - 2 \ll 1 \\ & 7\alpha_f (\ln 2\omega - 109/42) \big/ 6\pi && ; \quad 1 \ll \omega \end{aligned} \tag{3.24}$$

The pair production rate by cold protons and Wien photons is

$$\frac{dn}{dt} = n_\gamma \int_2^\infty \sigma_{\gamma p}(\omega) \omega^2 e^{-\omega/T} d\omega \big/ 2T^3 \tag{3.25}$$

Substituting the cross section (3.24) into (3.25) gives the timescales

$$\begin{aligned} t^{\gamma p} = \quad & 8(1+2z) e^{2/T} \big/ 3\alpha_f n_\gamma T && ; \quad T \ll 1 \\ & 6\pi (1+2z) \big/ 7\alpha_f n_\gamma \ln(0.38T) && ; \quad 1 \ll T \end{aligned} \tag{3.26}$$

The timescale decreases exponentially at low temperatures and logarithmically at high temperatures.

3.2.4 Photon-Electron

The threshold photon energy in the electron's rest frame is $\omega = 4$. This cross section has been calculated by Haug (1975). The threshold and high energy limits are

$$\begin{aligned} \sigma_{\gamma e}(\omega) = \quad & \sqrt{3}\alpha_f (\omega - 4)^2 \big/ 2^5 \cdot 3^4 && ; \quad \omega - 4 \ll 1 \\ & 7\alpha_f (\ln 2\omega - \tfrac{109}{42}) \big/ 6\pi && ; \quad 1 \ll \omega \end{aligned} \tag{3.27}$$

This has the same high energy limit as photon-proton pair production, equation (3.24). The threshold limit has a different dependence on $(\omega - \omega_{th})$, due to identical particle effects in this case and not in the former.

The pair production rate by Wien photons and Maxwellian electrons is

$$\frac{dn}{dt} = \frac{n_e n_\gamma}{2T^3 K_2(1/T)} \int_4^\infty \frac{\omega^2}{\sqrt{1+2\omega}} K_1\left(\frac{\sqrt{1+2\omega}}{T}\right) \sigma_{\gamma e}(\omega)\, d\sigma \tag{3.28}$$

This gives the timescales

---

[6] Note: the definition of the elliptic integrals given in Abramowitz & Stegun (1964), chapter 17, is different from that used here and by other authors, e g. Erdélyi *et al* (1953) chapter 13.

$$t^{\gamma e} = \begin{array}{ll} 2^{10} T^2 e^{2/T} \big/ \alpha_f n_\gamma & ; \quad T \ll 1 \\ 3\pi \big/ 7\alpha_f n_\gamma \ln(1.07T) & ; \quad 1 \ll T \end{array}$$

So again there is an exponential decrease at low temperatures and a logarithmic decrease at high temperatures.

3.2.5 Photon-photon

The threshold photon energy in the CM frame is $\omega = 1$. The cross section in this frame is (Jauch & Rohrlich,1980, § 13.3)

$$\sigma_{\gamma\gamma}(\omega) = 3\left[(2\omega^4 + 2\omega^2 - 1)\cosh^{-1}\omega - \omega(\omega^2+1)\sqrt{\omega^2 - 1} \right] \Big/ 8\omega^6 \tag{3.29}$$

The threshold and high energy limits are

$$\sigma_{\gamma\gamma}(\omega) = \begin{array}{ll} 3(\omega^2-1)^{1/2} \big/ 8\omega & ; \quad \omega - 1 \ll 1 \\ 3(2\ln 2\omega - 1) \big/ 8\omega^2 & ; \quad 1 \ll \omega \end{array} \tag{3.30}$$

On substituting for Wien photon distributions, Weaver's (1976) photon-photon reaction rate becomes

$$\frac{dn}{dt} = \frac{n_\gamma^2}{T^5} \int_1^\infty \omega^4 \sigma_{\gamma\gamma}(\omega) K_1(2\omega/T)\, d\omega \tag{3.31}$$

Substitution of the cross section gives the timescale

$$t^{\gamma\gamma} = \begin{array}{ll} (1+2z)64T^3 e^{2/T} \big/ 3\pi n_\gamma^2 & ; \quad T \ll 1 \\ (1+2z)16T^2 \big/ 3n_\gamma^2 \ln(1.12T) & ; \quad 1 \ll T \end{array} \tag{3.32}$$

which has the same qualitative temperature dependence as the other pair production timescales.

3.3 Comparison of Pair Timescales

The pair production and annihilation timescales are plotted in figure (3.3), putting $z = 0$ and $n_\gamma = 1$.

The sharp increase in production timescales for $T < 1$ reflects the exponential cut-off of particles with energies above threshold at these temperatures. The increase in the photon-photon timescale, $t^{\gamma\gamma}$, at high temperatures is a feature of using a Wien photon spectrum, i.e. hard photons, since the relevant pair production cross section is a decreasing function of energy. A bremsstrahlung spectrum, with more soft photons, does not give such a steeply rising timescale. Pair production rates from photons with bremsstrahlung and annihilation spectra are shown in figures (3.4) and (3.5). Note how the annihilation photons dominate at low temperatures, and the bremsstrahlung photons dominate at high temperatures.

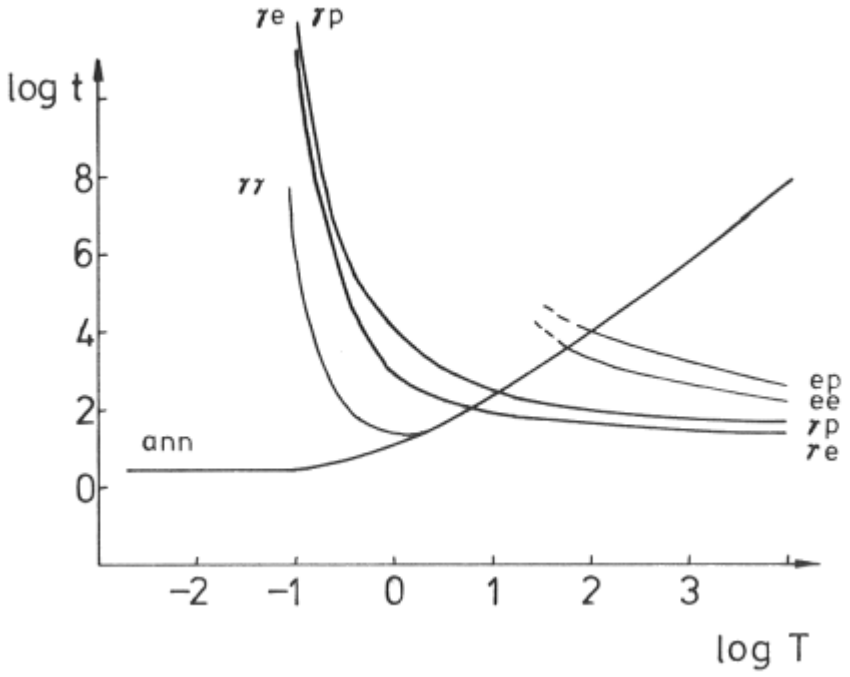

Figure (3.3)

Annihilation and pair production timescales for Maxwellian electron distributions and Wien photon distributions.

$t^{\gamma e}$ is always less than $t^{\gamma p}$, even though the threshold is higher. (In fact, the plotted $t^{\gamma e}$ is an upper limit, since $z = 0$). This is because the *apparent* threshold is lower, since the electrons are moving while the protons are essentially stationary. This is also the reason why $t^{ee} < t^{ep}$.

Bisnovatyi-Kogan *et al*. (1971) argued that all the pair production mechanisms will have the same importance, for although $\sigma^{PP} = O(\alpha_f^2)$, $\sigma^{\gamma P} = O(\alpha_f)$ and $\sigma^{\gamma\gamma} = O(1)$, there are also factors of α_f involved in the production of bremsstrahlung photons, and so $n_\gamma = O(\alpha_f)$. Since $t^{\gamma P} \propto 1/n_\gamma$ and $t^{\gamma\gamma} \propto 1/n_\gamma^2$, this means that all the timescales are of order $1/\alpha_f^2$. This argument holds for $T \gg 1$. However, for $T \sim 1$, the dominance of the harder annihilation photons and the proximity to threshold changes the picture. The combination of the low threshold in photon-photon pair production ($\omega = 1$) and the higher numbers of hard annihilation photons results in this mechanism dominating in all but the most optically thin media.

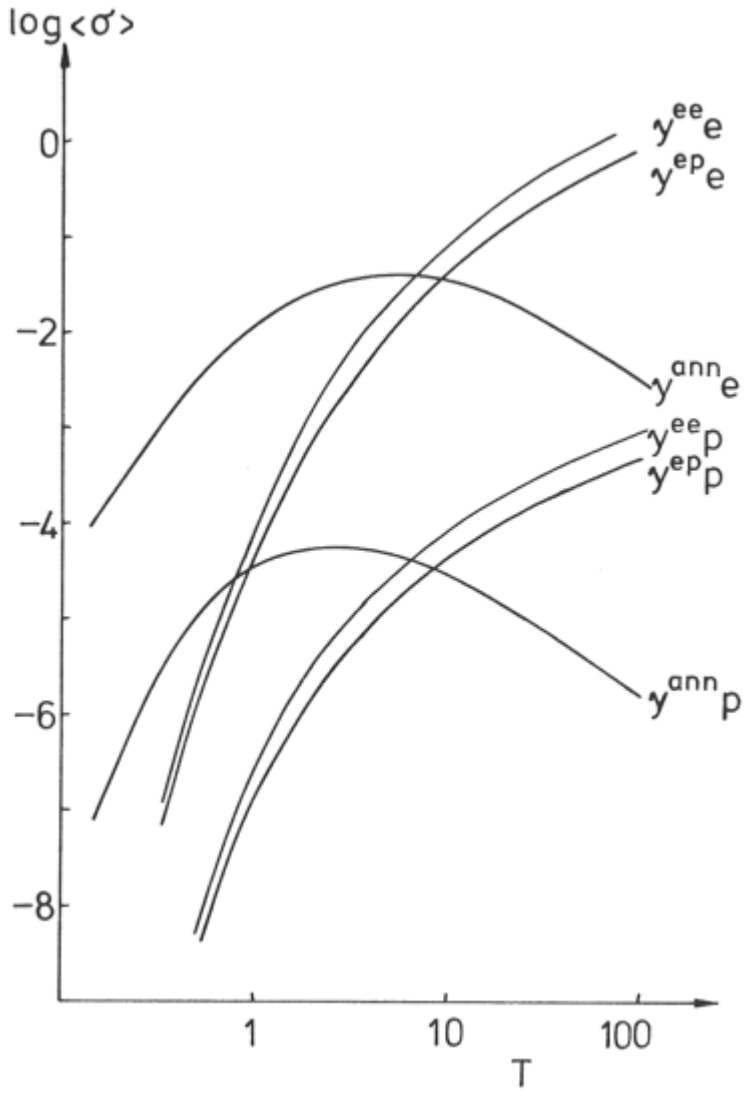

Figure (3.4)

Particle-photon pair production cross sections, averaged over Maxwellian electron distributions and various photon distributions: **(ann)** annihilation photons **(ee)** electron-electron bremsstrahlung photons **(ep)** electron-proton bremsstrahlung photons.

$Rate = \langle \sigma \rangle n_1 n_2 n_3 / (1+\delta_{12})$ where n_1, n_2 are the densities of the particles producing the photons initially (e.g. for annihilation photons $n_1 n_2 / (1+\delta_{12}) = z(1+z)$) and n_3 is the number density of the target particles (n_3 = 1 for protons, = 1+2z for electrons)

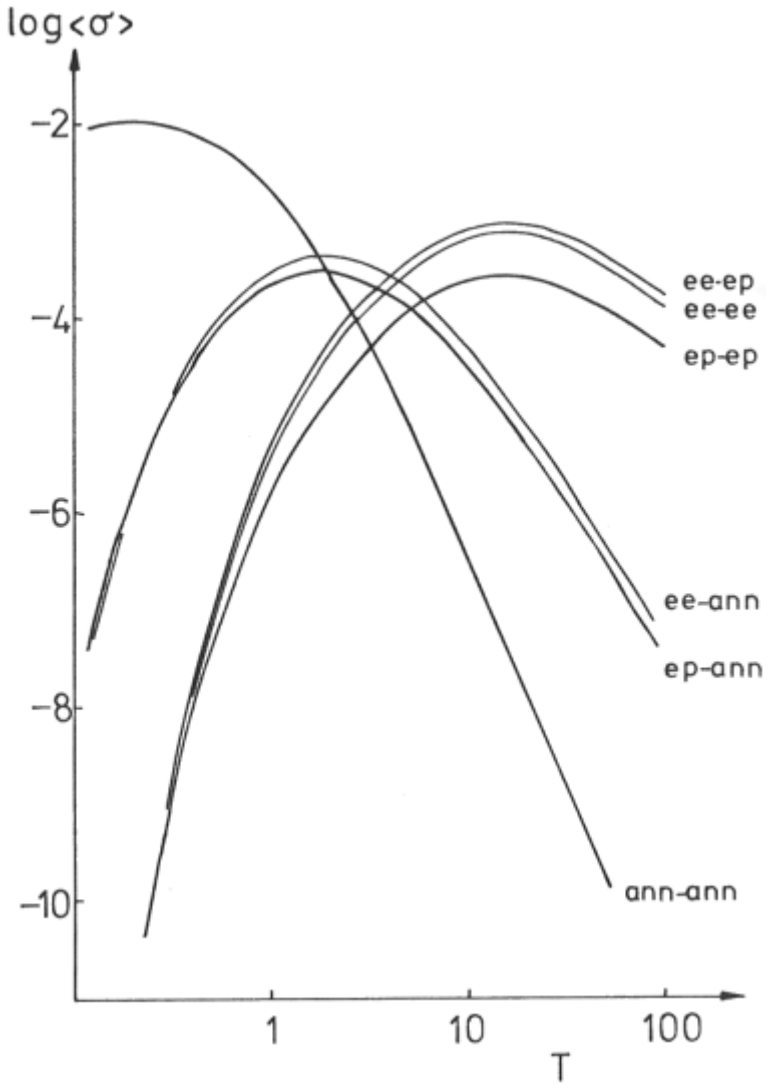

Figure (3.5)

Photon-photon pair production cross sections, averaged over various photon distributions. See previous diagram for key.

$Rate = \langle\sigma\rangle n_1 n_2 /(1+\delta_{12})$ where the number density of photon 1 is $n_1 = n_3 n_4 /(1+\delta_{12})$; n_3 and n_4 being the number densities of the particles producing the photons. E.g. for the annihilation photons the rate is $\langle\sigma_{ann-ann}\rangle [z(1+z)]^2/2$

4 Other Timescales

Other timescales that need to be calculated also occur in the non-relativistic case. However, they have different temperature dependences, and different relative importances.

4.1 Black Body Limits

The fundamental black body emission timescale defines a minimum radiation timescale for a given density, temperature and geometry. Since it is the electrons which radiate (by bremsstrahlung, cyclotron and annihilation radiation) it is their temperature and density which are important.

The black body flux from an isotropically emitting surface is given by the Stefan-Boltzmann law (remembering that a subscript asterisk indicates the physical, rather than dimensionless, quantity):

$$F_* = \sigma T_{*e}^4 = \pi^2 (kT_{*e})^4 / 60c^2 \hbar^3 \quad \mathrm{W\,m^{-2}} \tag{4.1}$$

Consider slab geometry. The electron kinetic energy surface density of a slab with thickness R is

$$E_{*e} = RN_e \varepsilon\, kT_{*e} \quad \mathrm{J\,m^{-2}} \tag{4.2}$$

Hence the timescale is $t_*^{bb} = E_{*e}/2F_*$ (since the slab has two sides) and so, back in dimensionless units

$$\begin{aligned} t^{bb} &= 30\varepsilon(1+2z)\frac{\tau_p}{\pi^2 T_e^3} N_p \left[\frac{r_e}{\alpha_f}\right]^3 \\ &\simeq \tau_p / \alpha_f \Lambda^2 \end{aligned} \tag{4.3}$$

where ln Λ is the Coulomb logarithm, defined in chapter 2. $\tau_p = N_p \sigma_T R$ is the 'proton optical depth'. It is equal to the true electron scattering optical depth when z = 0, and for low energy photons (no Klein-Nishina corrections to the cross section).

This limiting timescale differs in an important respect from those of two body interactions (e.g. relaxation, bremsstrahlung) in that it explicitly involves the optical depth. Since the timescale goes like T^{-3}, its importance decreases in the relativistic regime. It applies not only to the total emission, however, but also at each frequency. This places a severe limit on cyclotron radiation in particular, which has a high emissivity at low frequencies. This will be discussed in more detail later.

4.2 Bremsstrahlung

In the absence of a magnetic field or external flux of soft photons, bremsstrahlung is the dominant electron cooling mechanism.

In the non-relativistic case only electron-proton bremsstrahlung need be considered. The electron-electron (e^-e^-) system has no dipole moment, and its quadrupole radiation is negligible. In the equilibrium case there are too few positrons for significant electron-positron bremsstrahlung.

It is customary to calculate bremsstrahlung emission classically, and then include quantum mechanical corrections in the form of a Gaunt factor. The non-relativistic electron-proton bremsstrahlung from a Maxwellian electron distribution is then

$$\frac{dn(\omega)}{dt} \propto T^{-1/2}\omega^{-1}e^{-\omega/T}\bar{g}(\omega,T) \tag{4.4}$$

The Gaunt factor $\bar{g}$ is a slowly varying (logarithmic) function of T and ω for $T \ll \alpha_f$ and $\omega < T$ (see, e.g., Rybicki & Lightman, 1979, chapter 5). It can be taken as unity to a fairly good approximation. Hence the non-relativistic bremsstrahlung photon spectrum is the product of an exponential and a power law with spectral index 1.

In the relativistic regime the Gaunt factor approach is no longer appropriate. Relativistic and quantum effects are no longer small corrections, easily included in a factor not much different from unity, especially since we are interested in the hard, pair producing photons, with $\omega \gtrsim 1$. In addition the electron-electron emission is comparable with the electron-proton emission, but is harder.

The total bremsstrahlung emission also changes in the relativistic case. It is no longer proportional to $T^{1/2}$. By T = 0.28 (140 keV) the total emission is twice that of the non-relativistic extrapolation, partly due to relativistic corrections to the electron-proton rate, and partly due to the contribution of electron-electron emission.

Gould (1980) gives, for a plasma of electrons and protons

$$\frac{dE}{dt} = 4\alpha_f\left[\frac{2T}{\pi^3}\right]^{1/2}\left[1+6.8T+\frac{5.6\times10^{-3}}{T^{1/2}}\right] \tag{4.5}$$

for the bremsstrahlung cooling rate (energy loss in m_ec^2 per proton per Thomson time, z = 0). This expression is valid for $T \ll 1$, and includes relativistic corrections and electron-electron bremsstrahlung. See also figure (4.1).

4.2.1 Electron-proton bremsstrahlung

In the ultrarelativistic limit the electron-proton cross section is (Jauch & Rohrlich, 1980, chapter 15)

$$\omega\frac{d\sigma}{d\omega} = \frac{3\alpha_f}{2\pi}\left[1-\frac{2\gamma'}{3\gamma}+\frac{\gamma'^2}{\gamma^2}\right]\left[\ln\frac{2\gamma\gamma'}{\omega}-\frac{1}{2}\right] \tag{4.6}$$

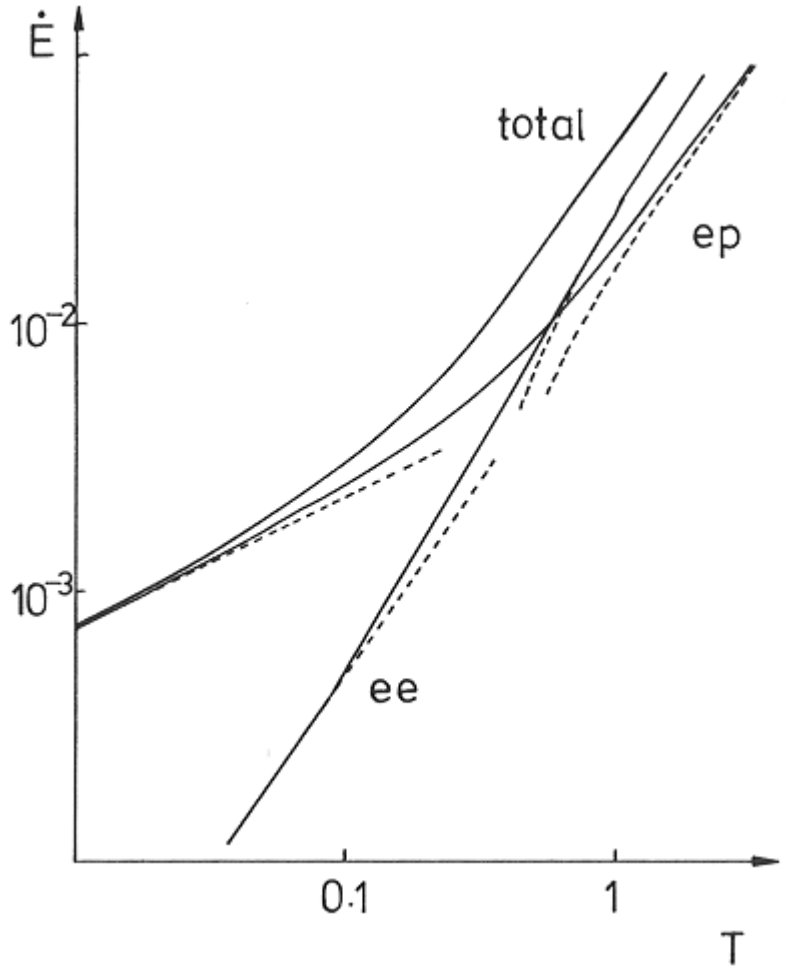

Figure (4.1)

Total bremsstrahlung emission from a $z = 0$ plasma, showing the individual contributions of electron-proton and electron-electron bremsstrahlung. The dotted lines show the various non-relativistic and ultrarelativistic approximations.

where γ is the γ-factor of relative motion prior to the emission (i.e. the initial γ-factor of the electron in the plasma frame, since the protons can be taken to be at rest). γ' is the final γ-factor of the electron after the emission of a photon with energy ω: $\gamma' = \gamma - \omega$.

The ultrarelativistic limit of equation (2.13) gives the energy loss rate as

$$\frac{dE}{dt} = \frac{1+2z}{2T^3}\int_1^\infty \int_0^{\omega_{\max}} \omega \frac{d\sigma}{d\omega} \gamma^2 e^{-\gamma/T} d\omega\, d\gamma \tag{4.7}$$

where $\omega_{max} = \gamma - 1$. So the electron-proton bremsstrahlung cooling rate is

$$\frac{dE^{ep}}{dt} = (1+2z)\frac{9\alpha_f T}{2\pi}\left(\ln 2T - \gamma_E + \tfrac{3}{2}\right) \tag{4.8}$$

This is the result obtained by Stickforth (1961). The timescale is

$$t = 2\pi(1+2z)/3\alpha_f \ln(5.03T) \quad ; \quad 1 \ll T \tag{4.9}$$

4.2.2 Electron-electron bremsstrahlung

Various authors have considered electron-electron bremsstrahlung. Baier, Fadin & Khoze (1967, 1968) have calculated the cross sections for electron-electron ($e^{\pm}e^{(\pm)}$) bremsstrahlung in various reference frames. Haug (1975a,b) gives the multiply differential $e^{\pm}e^{\pm}$ cross section, and discusses thermal electron-electron bremsstrahlung. Alexanian (1968) gives the electron-electron ($e^{-}e^{-}$) energy loss rate from a Maxwellian distribution in the extreme relativistic limit.

The problem here is that the transformation of photon energy to the plasma frame in electron-electron bremsstrahlung is non-trivial. Haug (1975a) has derived the cross section, differential in photon momentum, for a given electron-electron collision. The expression is extremely long and complicated, and needs to be integrated over the particle distributions and photon angles, to yield the thermally averaged cross section differential in photon energy. This (probably) cannot be done analytically. See chapter 6 for a numerical fit to the spectrum.

The extreme relativistic limit of the cooling rate, Alexanian (1968), is

$$\frac{dE^{--}}{dt} = (1+z)^2 \frac{9\alpha_f T}{\pi}\left(\ln 2T - \gamma_E + \tfrac{5}{4}\right) \tag{4.10}$$

Apart from a slightly different logarithmic factor, this is just twice the electron-proton bremsstrahlung rate (4.8). Svensson (1982a) explained why this is so:

In the ultrarelativistic limit the cross sections for electron-electron and electron-proton bremsstrahlung are the same. However, in the electron-electron case both particles radiate, giving a factor of two in the energy loss rate. Another factor of two comes from the leading term, proportional to ln γ in the cross section. γ is the γ-factor of relative motion, and so $\gamma \sim \gamma_e$ in the electron-proton case, and $\gamma \sim \gamma_e^2$ in the electron-electron case. Finally, there is a factor of one half, due to identical particle effects.

Now, the cross section for electron-positron bremsstrahlung is the same as for electron-electron ($e^{\pm}e^{\pm}$) bremsstrahlung in this limit, except for some small differences at the hard photon end of the spectrum (Baier, Fadin & Khoze, 1968). So using the above argument, the electron-positron rate will be twice the electron-electron rate (as there are no identical particle effects) and four times the electron-proton rate.

So, combining these, the total electron-electron bremsstrahlung cooling rate in the ultrarelativistic limit is

$$\frac{dE^{ee}}{dt} = (1+2z)^2 \frac{9\alpha_f T}{\pi} \ln 3.92T \quad ; \quad 1 \ll T \tag{4.11}$$

4.2.3 Timescale

The total bremsstrahlung timescale is given by equation (4.5) for $T \ll 1$, and for $T \gg 1$

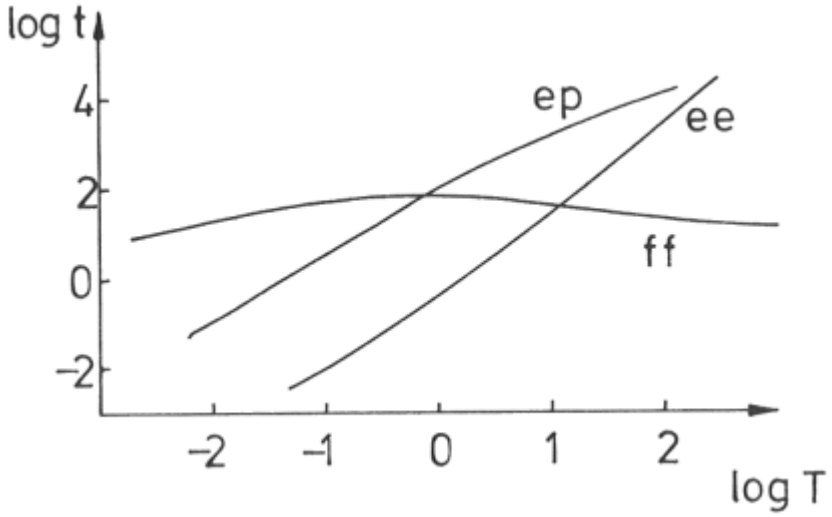

Figure (4.2)

Bremsstrahlung cooling timescale, $z = 0$: **(ff)** bremsstrahlung **(ee)** electron-electron relaxation **(ep)** electron-proton relaxation , $T_p = T_e$.

$$\frac{dE^{tot}}{dt} = \frac{9\alpha_f T}{2\pi}\left[(1+2z)\ln 5.03T + 2(1+2z)^2 \ln(3.92T)\right] \tag{4.12a}$$

$$t = 2\pi/3\alpha_f \left[2(1+2z)\ln(3.92T) + \ln(5.03T)\right] \tag{4.12b}$$

This is plotted in figure (4.2), along with the thermal relaxation timescales. Since the ultrarelativistic bremsstrahlung timescale goes like $1/\ln T$ (rather than like $T^{1/2}$ in the non-relativistic case) and the ultrarelativistic thermalization time like T^2 (rather than $T^{3/2}$) the two curves cross at a temperature significantly lower than the few hundred $m_e c^2$ obtained by extrapolation of the non-relativistic results. In fact they cross when $T \simeq 10$. So any discussion of *thermal* plasmas must necessarily have an electron temperature less than 10 $m_e c^2$ (5 MeV). However, this is sufficiently greater than 1 to be worth discussing.

4.3 Pion and Neutrino Production

Proton bremsstrahlung is negligible, but protons do have a cooling mechanism which cannot be avoided. Pions can be produced in inelastic nuclear proton-proton collisions. The threshold energy is ~ 290 MeV, so for moderate temperatures (T_p ~ 50) the protons in the high energy Maxwell tail can produce pions. This cools the protons without directly heating the electrons.

The important reactions are

$$
p + p \rightarrow \begin{cases}
p + n + \pi^+ & \text{threshold } 292 \text{ MeV} \\
\quad \downarrow \quad\quad \downarrow & \\
\quad p + e^- + \bar{\nu}_e \quad \nu_\mu + \mu^+ & \\
\qquad\qquad\quad \downarrow & \\
\qquad\qquad\quad e^+ + \nu_e + \bar{\nu}_\mu & \\
 & \\
p + p + \pi^0 & \text{threshold } 280 \text{ MeV} \\
\quad \downarrow & \\
\quad 2\gamma & \\
 & \\
d + \pi^+ & \text{threshold } 287 \text{ MeV}
\end{cases}
$$

The neutrinos produced in the π^+ decay will escape the plasma without further interaction, and so their energy is lost. Some of the very hard photons produced in π^o decay will be degraded in energy before escaping, and hence heat the electrons.

If the pions are assumed to be produced at rest by non-relativistic protons, then

$$\frac{dE}{dT} = \frac{-m_\pi \langle \sigma\beta \rangle}{2m_e} \tag{4.13}$$

$$t^\pi = 3T_p m_e \big/ m_\pi \langle \sigma\beta \rangle \tag{4.14}$$

I have used Kolykhalov & Syunyaev's (1979) graph of $\langle \sigma\beta \rangle$ against temperature to get the timescale. Eilek & Kafatos (1983) discuss pion production and decay in more detail.

Inclusion of the non-zero pion momentum reduces the timescale, but inclusion of the fully relativistic proton distribution function increases it. Hence equation (4.14) is a good approximation to the cooling timescale for moderate temperatures. t^π is plotted in figure (4.3) for the two extreme cases: zero pion momentum and maximum pion momentum. The proton-proton relaxation timescale is much less than the pion production timescale when $T_p < 100$, so the proton distribution can maintain a Maxwellian distribution for temperatures less than 50 MeV.

For $T_p \gtrsim 30$ ($kT_{*p} \gtrsim 15$ MeV) the protons actually cool faster by pion production than they do by Coulomb collisions with the electrons. However, only slight deviations from a true Maxwellian in the tail of the distribution will have a dramatic effect on the pion production rate, since the bulk of the protons are well below threshold.

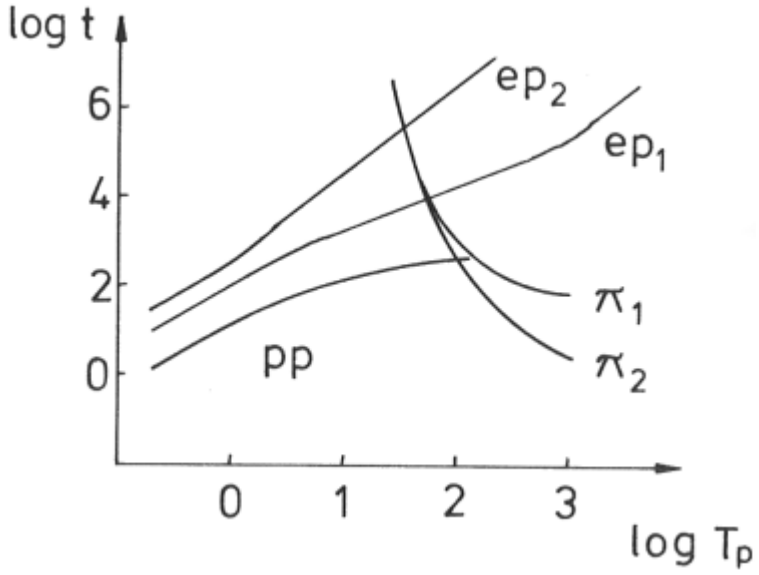

Figure (4.3)

Proton cooling timescale due to pion production: **(π_1)** pions produced with zero momentum **(π_2)** pions produced with maximum momentum **(ep_1)** electron-proton relaxation time, $T_p = T_e$ **(ep_2)** electron-proton relaxation time, $\theta_p = \theta_e$ **(pp)** proton-proton relaxation time

4.4 Magnetobremsstrahlung Cooling

The presence of a magnetic field can cause the electrons to cool by two different processes. The emission of predominantly soft cyclotron (or synchrotron) photons cools the electrons directly. They are then further cooled when they upscatter (Comptonize) these soft photons. Here I will just summarize the timescales due directly to the radiation, which gives an upper limit to the true timescale. Comptonization timescales are discussed by Guilbert (1981b) and Guilbert, Fabian & Ross (1982).

4.4.1 Optically thin case

The power emitted by an isotropic distribution of electrons in a magnetic field of energy density $U_B = B_*^2/2\mu_o m_e c^2$ is (Rybicki & Lightman, 1979)

$$P = \tfrac{4}{3}(1+2z)\gamma^2\beta^2 U_B \qquad (4.15)$$

This emission can be averaged over a thermal electron distribution, using $\langle\gamma^2\beta^2\rangle = 3T\,K_3(1/T)/K_2(1/T)$. So in the non-relativistic (cyclotron) limit, where $T_e \ll 1$, $\langle\gamma^2\beta^2\rangle = 3\,T_e$. In the ultrarelativistic (synchrotron) limit, $1 \ll T_e$ and so $\langle\gamma^2\beta^2\rangle = 12\,T_e^2$. Hence the timescale, defined by $t^B \equiv E_e/P$, is

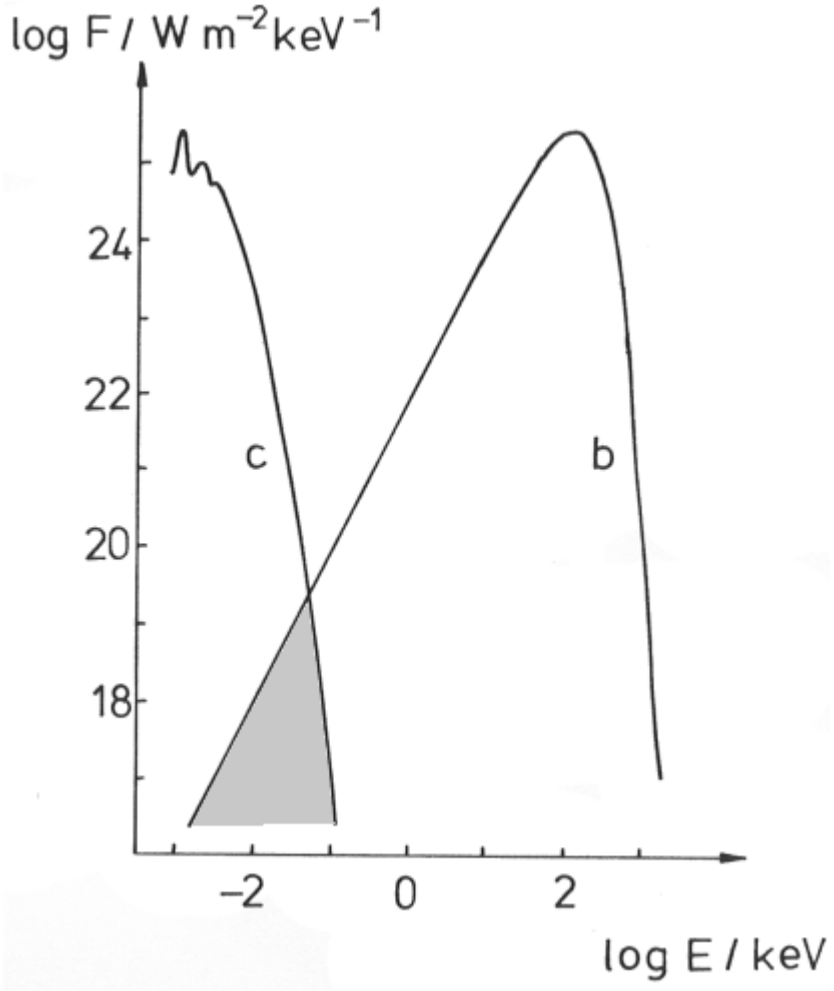

Figure (4.4a)

Cyclotron emissivity (Masters, 1980) for a plasma with T = 0.1, B_* = 104 T, τ = 11: **(b)** black body **(c)** cyclotron. The shaded region represents the flux actually emitted, as given by equation (4.18).

$$t^B = \begin{cases} 3/8U_B & ; \quad T_e \ll 1 \\ 3/16U_B T_e & ; \quad 1 \ll T_e \end{cases} \tag{4.16}$$

This timescale contains a free parameter, the magnetic field. However, in a magnetic field that is in equipartition with the (non-relativistic) protons ($U_B = 3T_p/2$) this becomes

$$t^B = \begin{cases} 1/4T_p & ; \quad T_e \ll 1 \\ 1/8T_e T_p & ; \quad 1 \ll T_e \end{cases} \tag{4.16}$$

4.4.2 Self-absorbed case

As Masters (1978) has pointed out, the emission will be heavily self-absorbed at low frequencies. He considered cyclotron emission (the non-relativistic case, $T \ll 1$), where the effect is more important, since most of the emission is in the Rayleigh-Jeans region, figure (4.4). However, the cooling time is significantly modified up to temperatures $T \lesssim 10$.

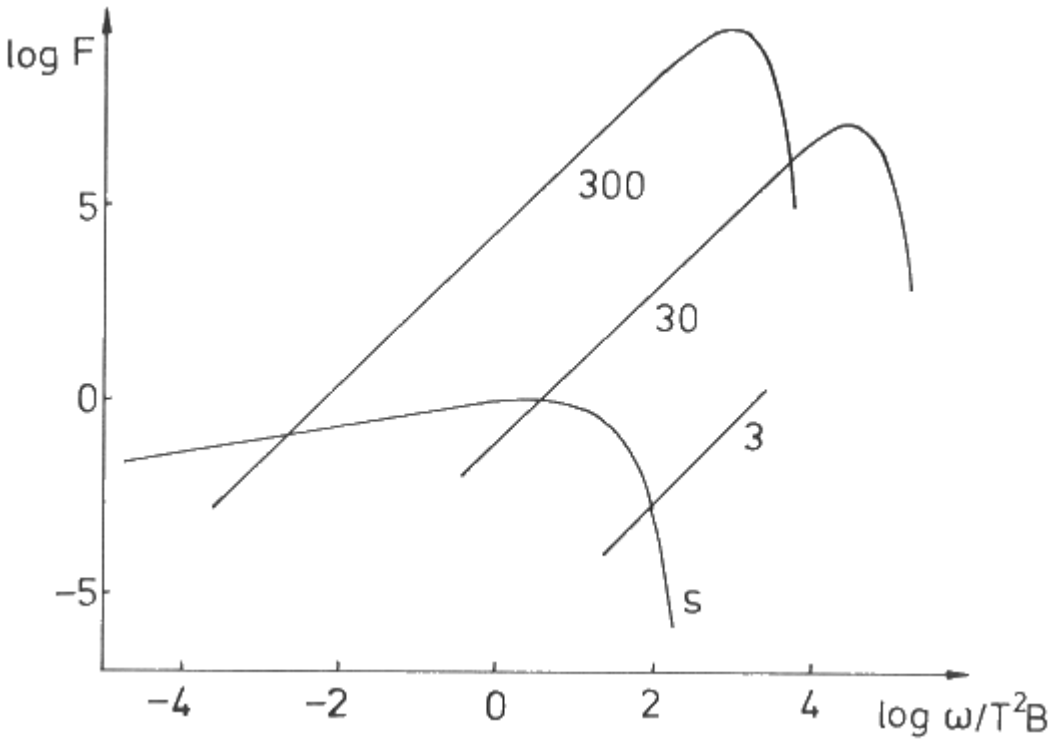

Figure (4.4b)

Synchrotron emissivity at various temperatures. The black body spectra are labelled by *T*. **(s)** synchrotron emissivity. As the temperature increases, less and less of the synchrotron emission will be self-absorbed at low frequencies.

To take self-absorption into account, the emitted spectral power must be averaged over a Maxwellian distribution of electron velocities (see figure 4.5). Then, following the treatment of Masters, the critical frequency ω_o is defined to be where the emitted flux F_ω equals the black body flux F_ω^{bb}. The total emission is then calculated by assuming that the flux is black body for $\omega < \omega_o$, and cyclotron or synchrotron beyond.

$$F = \int_1^{\omega_o} F_\omega^{bb} d\omega + \int_{\omega_o}^{\infty} F_\omega d\omega \tag{4.18}$$

The increased timescales are shown in figure (4.6), along with the electron thermalization timescale. If the protons are hotter than the electrons the equipartition field will be higher, and so the cooling timescale will be even shorter. From the figure, the electrons will only be able to maintain a Maxwellian distribution for $T_e \lesssim 1$.

4.4.3 Superstrong Fields

The critical magnetic field strength, found by equating the cyclotron frequency and the rest mass of the electron, where quantum mechanical effects cannot be neglected, is $B_o = (m_e c)^2 / e\hbar = 4.4 \times 10^9$ T. For the very strong magnetic fields, $B_* \sim B_o$ ($B \sim 1$), which might be experienced near a magnetic neutron star, one-photon pair production becomes significant.

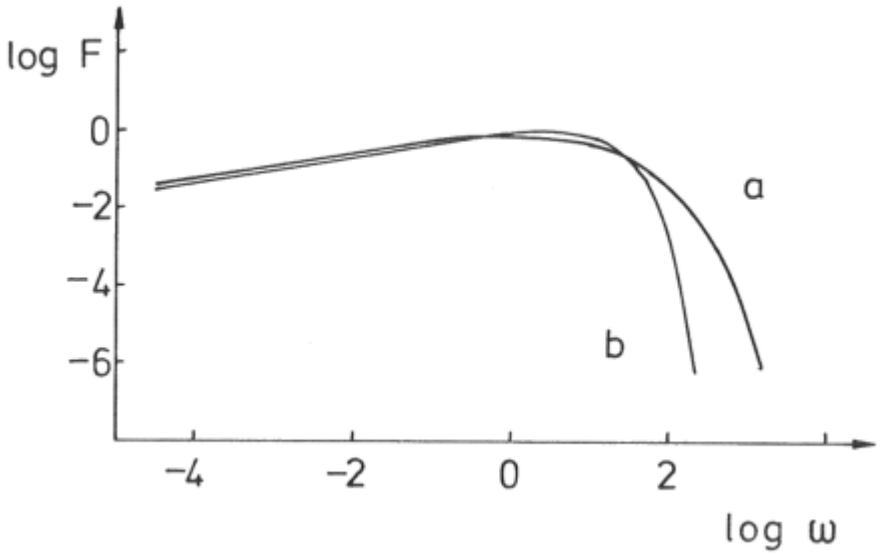

Figure (4.5)

Synchrotron from different electron distributions. **(a)** Maxwellian electrons with temperature T **(b)** monoenergetic electrons with $\gamma^2 = 12\ T^2$ (i.e. the same total emission).

See Daugherty & Harding (1983). Also, the classical synchrotron formulae break down, for three reasons:

(a) The classical radiation reaction (damping force) dominates the Lorentz force on the electron. The radiation reaction is given by

$$f_r \simeq \gamma^2 (B_* c)^2 \frac{e^2}{m^2 c^3} \frac{e^2}{4\pi\varepsilon_o} = \alpha_f \gamma^2 B^2 \frac{m^2 c^3}{h} \tag{4.19a}$$

(Landau & Lifshitz, 1975, equation 76.4) and the Lorentz force is

$$f_L \simeq B_* ec = B \frac{m^2 c^3}{h} \tag{4.19b}$$

Hence the condition for validity becomes

$$f_r \ll f_L \Rightarrow \alpha_f \gamma^2 B \ll 1 \tag{4.19c}$$

(b) The individual quanta emitted are so energetic that electron recoil cannot be neglected. Typical photon energies are $\hbar\omega_{*_c}$, where $\omega_{*_c} = eB_*\gamma^2 / m$, $\omega_c = B\gamma^2$. So the formulae are valid if

$$\omega_c \ll \gamma \Rightarrow \gamma B \ll 1 \tag{4.20}$$

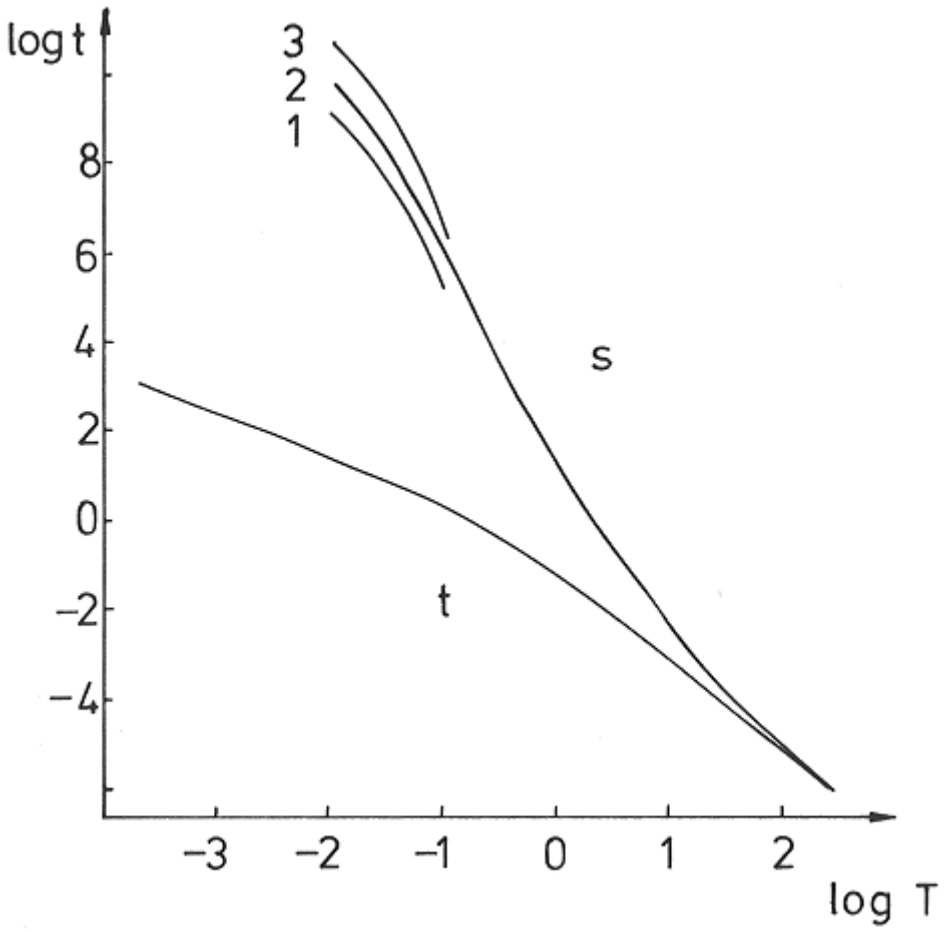

Figure (4.6)

Magnetobremsstrahlung timescales. **(t)** timescale in an equipartition field with $T_p = T_e$, equation (4.17), neglecting self-absorption **(s)** self absorbed case for slabs with thickness (1) 10^4 m (2) 10^5 m (3) 10^6 m.

(c) To be able to treat the electron as a classical particle its de Broglie wavelength ($\lambda = h/p = h/\gamma mv$) must be small compared with the Larmor radius ($r_L = v/\omega_{*B}$)

$$h/p \ll r_L \Rightarrow \gamma^2 \gg B \tag{4.21}$$

The formulae have already broken down due to (a) and (b) before this effect becomes important, figure (4.7).

Consideration of these effects will change the shape of the power spectrum averaged over a Maxwellian since the high energy electrons do not radiate as much as in the classical case. This effect will increase the timescale given in equation (4.16), as will self-absorption. Even so, this timescale is still very much less than the electron thermalization time, and so the electrons will not be able to achieve a Maxwellian distribution by two body interactions.

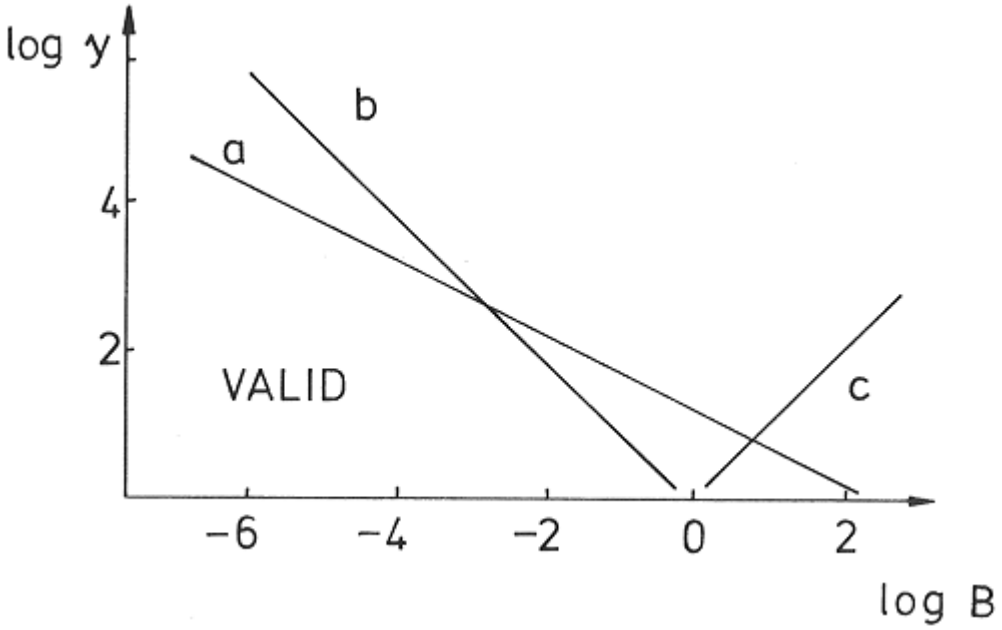

Figure (4.7)

Region of validity of the classical synchrotron formulae (see § 4.4.3) The formulae break down in the indicated regions due to: **(a)** radiation reaction **(b)** recoil of emitting electron **(c)** wave properties of electron

Recently attempts have been made to explain the emission from γ-ray bursters as thermal synchrotron radiation from hot electrons in superstrong magnetic fields around neutron stars. (Ramaty, Lingenfelter & Bussard, 1981; Liang, 1982; Liang *et al.*, 1983). One reason for this is that synchrotron radiation is much more efficient than bremsstrahlung. Previous attempts to put constraints on the distance to γ-ray burst sources on the assumption that the radiation was thermal bremsstrahlung resulted in estimates of a few tens of parsecs. The sources do not have to be so close if the emission is assumed to be thermal synchrotron.

Obviously some thermalization process other than two body interactions is needed for these models. Liang has suggested that some (not well understood) collective plasma process might be able to maintain the required Maxwellian electron distribution. If this is indeed the case, the limits set by the other radiation processes will also be less restrictive. However, in this thesis I will continue to compare the cooling timescales with the better understood Coulomb thermalization timescale.

5 Comparison of Timescales

The more important timescales discussed in the previous chapters are summarized in figure (5.1), with $T_p = T_e$ and $z = 0$.

The purpose of this work on timescales is to decide which processes dominate at which temperatures. In particular, it is necessary to find out if two-body relaxation can maintain a Maxwellian distribution for the particles, or if they cool too fast. Being able to assume a thermal particle distribution considerably simplifies further analysis.

The main processes which cool the protons are energy transfer to the electrons in Coulomb collisions, and pion production. The electrons cool by pair production, bremsstrahlung and synchrotron radiation. These processes have cross sections which are increasing functions of energy. Thus in a Maxwellian distribution it is the particles in the high energy tail which cool fastest. If the thermalization timescale is too long, the tail will not be repopulated and the distribution function will no longer be Maxwellian. This in turn will increase the cooling timescale.

Pion production was discussed in § 4.3. The protons can maintain a Maxwellian distribution, provided $T_p \lesssim 100$. However, as long as the protons are not too much hotter than the electrons, their detailed distribution is not important in the case of electron-proton bremsstrahlung and pair production, and photon-proton pair production. The incident particles are travelling so much faster that they see the protons as essentially stationary.

The presence of an equipartition magnetic field makes it impossible for the electrons to maintain a Maxwellian distribution at relativistic temperatures – the high energy tail cools much too quickly. However, in the case of zero magnetic field the electron cooling mechanism is the less efficient bremsstrahlung, and the electrons will be able to maintain a Maxwellian distribution for $T_e \lesssim 10$. Above this the bremsstrahlung timescale will be increased. The effect will not be large, however. The timescale depends only weakly on γ; $t \sim 1/\ln\gamma$.

Pair production itself would not start to modify the electron distribution until $T_e \sim 60$. By then, however, it will already have been modified by bremsstrahlung. This increases the pair production timescale, though again only weakly; $t \sim 1/\ln^3\gamma$.

Since the separate electron-electron and proton-proton relaxation timescales are less than the energy exchange timescale, it is possible for the electrons and protons to maintain Maxwellians at different temperatures, provided $T_e \lesssim 10$.

If the particles do not have Maxwellian distributions the concept of temperature becomes less well defined. However, the distribution functions will still have a spread of energies about the mean, and will be isotropic, and so are still, in some sense, ‘thermal’.

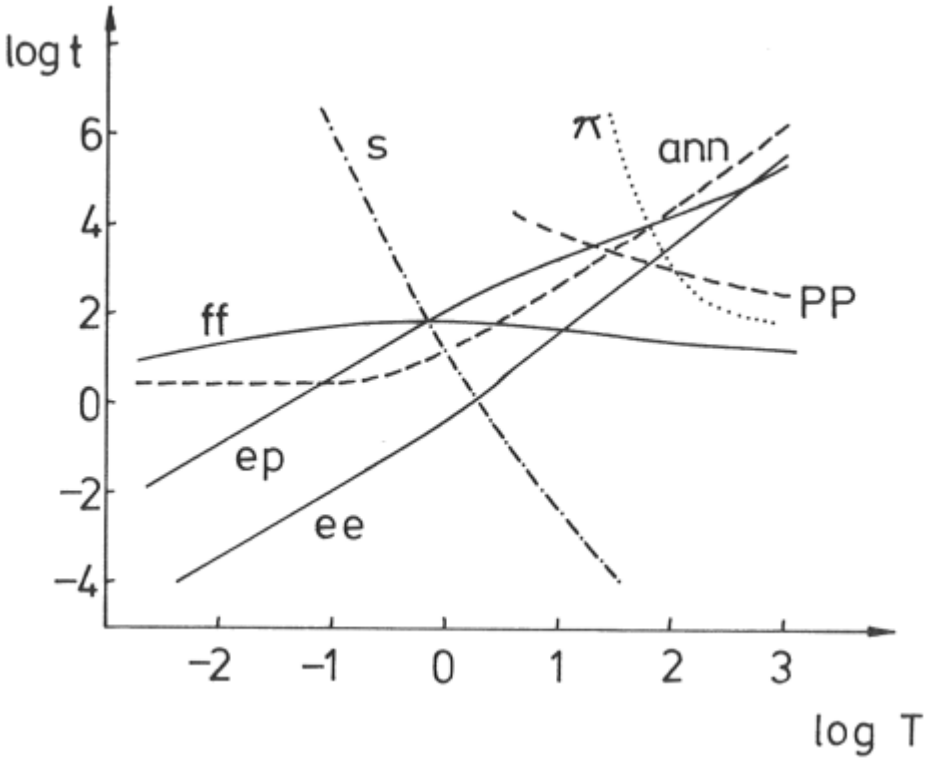

Figure (5.1)

Various timescales; $T_p = T_e$, $z = 0$. **(ee)** electron-electron relaxation **(ep)** electron-proton relaxation **(PP)** particle-particle pair production **(ann)** annihilation **(π)** pion production **(ff)** bremsstrahlung cooling **(s)** self-absorbed synchrotron cooling in an equipartition field

The main conclusion of the work on timescales is that, provided that bremsstrahlung is the dominant electron radiation process, the electrons can have a thermal distribution with temperatures as high as $kT_{*e} \sim 10 m_e c^2$. So it is reasonable to investigate the pair processes in a relativistic thermal plasma in more detail. As has been noted before, the highly non-linear nature of the pair processes means that analytic solutions are not feasible. In the remaining chapters I will describe the development of a computer model of an ultrahot plasma slab which includes most of the processes described above.

6 Numerical Fits to Reaction Rates

As was seen in chapters 3 and 4, the bremsstrahlung, pair production and annihilation cross sections are all available, but are usually expressed as complicated special functions or multidimensional integrals, or both. Efficient computer modelling of these processes requires simple fits to the rates. Here I detail some of the fits to be found in the literature, and some especially calculated for the computer model described in the next chapter.

The processes to be included are Comptonization (which is discussed by Guilbert, 1981b), bremsstrahlung, pair production and annihilation.

6.1 Pair annihilation

The pair annihilation spectrum has been expressed as a single integral by Svensson (1982b), see equation (3.6). He has fitted the integral by

$$I(\zeta) = \frac{3\sqrt{\pi}}{16}\zeta^{3/2}e^{-1/\zeta}C_1(\zeta) \qquad ; \quad \zeta \le 4 \tag{6.1a}$$

$$\frac{3\zeta}{8}\left(\ln 4\zeta - 1 - \gamma_E\right)C_2(\zeta) \quad ; \quad 4 < \zeta \tag{6.1b}$$

where the polynomials C_1 and C_2 are given by his equations (17) and (18). The maximum error of this fit is less than 0.3%.

Zdziarski (1980) has also fitted a function to the spectrum (3.6). This fit includes the Bessel function and exponential, and so is two dimensional. The fit is accurate to 25% for $0.02 < T < 8$.

6.2 Particle-particle pair production

The cross section near threshold is unknown. I have estimated the effect by taking a linear cross section near threshold and matching it with the high energy limit, equation (3.23).

So, taking the electron-proton pair production cross section near threshold to be

$$\sigma_{ep} = A(\gamma - 3) \tag{6.2}$$

gives the production rate

$$R_{ep} = (1 + 2z)\left\langle \sigma_{ep} \right\rangle \tag{6.3a}$$

$$\left\langle \sigma_{ep} \right\rangle = 2AT(4 + 6T + 3T^2)e^{-3/T} \Big/ K_2(1/T) \tag{6.3b}$$

Matching this cross section with the high energy limit at $\gamma_o = 50$, chosen to give a good matching of the slopes, implies that $A = 6.62 \times 10^{-7}$.

The electron-electron cross section is similarly

$$\sigma_{ee} = B(\gamma - 7) \tag{6.4}$$

$\sigma_{\gamma p}(\omega) = \frac{\alpha_f \varepsilon^6}{32}\left[1 + \frac{7}{8}\varepsilon^2 + \frac{483}{640}\varepsilon^4 + \frac{127}{192}\varepsilon^6 + \frac{144\,689}{245\,760}\varepsilon^8 + O(\varepsilon^{10})\right]$ $\simeq \frac{\alpha_f \varepsilon^6}{32}\left(1 + 0.875\varepsilon^2 + 0.755\varepsilon^4 + 0.661\varepsilon^6 + 0.589\varepsilon^8\right)$ (note the very slow convergence)	$2 < \omega < 2.4$, max error = 0.10%
$\sigma_{\gamma p}(\omega) = \left(7.62601 - 8.02178\omega + 2.52502\omega^2 - 0.204658\omega^3\right)\times 10^{-4}$	$2.4 < \omega < 4$, max error = 0.11%
$\sigma_{\gamma p}(\omega) = \frac{7\alpha_f}{6\pi}\left[\ln 2\omega - \frac{109}{42}\right]$ $+\left(473.645 + 241.259\ln 2\omega - 81.1511\ln^2 2\omega + 5.38138\ln^3 2\omega\right)/10^5\omega$	$4 < \omega$, max error = 0.07%

Table (6.1)

Fit to the photon-proton pair production cross section

which gives the production rate, including e^-e^-, e^-e^+ and e^+e^+ contributions, as

$$R_{ee} = \langle\sigma_{ee}\rangle(1+2z)^2/2 \tag{6.5}$$

$$\langle\sigma_{ee}\rangle = 32BT\left[(6+19T^2+6T^4)K_1(4/T) + 2T(7+6T^2)K_0(4/T)\right]/K_2^2(1/T)$$

Matching the cross section at $\gamma_o = 90$ gives $B = 2.90 \times 10^{-7}$.

6.3 Photon-proton pair production

The high and tow temperature formulae of equation (3.24) are only accurate very close to the limits. For example, the error in the threshold approximation is greater than 10% for $\omega = 2.1$. So they are not useful for detailed calculations of reaction rates. I have fitted functions to the whole range of equation (3.23). The fits are given in table (6.1).

The approximation near threshold was found by expanding equation (3.23) in powers of $\varepsilon^2 = 1 - (2/\omega)^2$. The very slow convergence of this power series shows why the low energy limit is such a poor approximation away from threshold.

The approximations in the other regions were found using minimax polynomials. These are polynomials which minimize the maximum error in the fit to the function. They have the "equal error" property in that the maximum error, E, is achieved $n + 2$ (or more) times in the interval, with alternating sign, if the fitted polynomial is of order n. This gives a much better handle on the error than standard least squares methods. See, for example, Ralsten & Rabinowitz (1978).

$\frac{8\pi}{3\alpha_f}\sigma_{\gamma e}(\omega) =$	$\left[5.6+20.4(\omega-4)-10.9(\omega-4)^2-3.6(\omega-4)^3+7.4(\omega-4)^4\right]$ $\times 10^{-3}(\omega-4)^2$	$4 < \omega < 4.6,$
	$0.582814-0.298\,42\,\omega+0.043\,54\,\omega^2-0.001\,297\,7\,\omega^3$	$4.6 < \omega < 6$
	$\frac{3.124\,7-1.339\,7\,\omega+0.146\,12\,\omega^2}{1+0.464\,8\,\omega+0.016\,683\,\omega^2}$	$6 < \omega < 18$
	$(84\ln 2\omega-218)/27$ $+\left(-1.333\ln^3 2\omega+3.863\ln^2 2\omega-11\ln 2\omega+27.9\right)/\omega$	$14 < \omega$

Table (6.2)
Fit to the photon-electron pair production cross section (Haug, 1975)

6.4 Photon-electron pair production

Haug (1981) has fitted simple functions to the photon-electron cross section. For completeness these are given in table (6.2). The reaction rate can be found by averaging this fitted cross section over a Maxwellian electron distribution. Four point Gauss-Laguerre quadrature is sufficient, giving an error of less than 1%.

6.5 Photon-photon pair production

When following photon-photon processes in a computer code it is not the case that the photon distribution is isotropic. Hence Weaver's (1967) result is not applicable. However, if it is assumed that the photons have slab symmetry (i.e. independent of polar angle ϕ) then

$$R_{\gamma\gamma} = 4\pi \int n_1(\mathbf{k}_1)\, n_2(\mathbf{k}_2)\, \omega_1\omega_2\, d\mu_1 d\mu_2 \int_{\omega_-}^{\omega_+} \frac{\omega^3 \sigma_{\gamma\gamma}(\omega)\, d\omega}{\left[(\omega_+^2-\omega^2)(\omega^2-\omega_-^2)\right]^{1/2}} \tag{6.6}$$

where $\omega_\pm^2 = \omega_1\omega_2\left[1-\cos(\theta_1 \pm \theta_2)\right]/2$ and μ = cos θ is the usual polar angle (see appendix 4). The integral over the cross section has poles like $\left|\omega-\omega_\pm\right|^{1/2}$ at the integration limits. This (large) contribution can be subtracted off and evaluated analytically, and the remaining integral can be found to sufficient accuracy (better than 0.5%) using 2 point Gauss-Legendre quadrature.

$$(\gamma^2-1)^{3/2}(\gamma'^2-1)^{1/2}\frac{8\pi\omega}{\alpha_f}\frac{\mathrm{d}\omega}{\mathrm{d}\sigma}=$$

$$4(\gamma^2-1)(\gamma'^2-1)-6\gamma\gamma'(\gamma^2-1+\gamma'^2-1)+3\left\{\gamma'(\gamma'^2-1)+l'\gamma(\gamma^2-1)-ll'(\gamma^2-1)(\gamma'^2-1)\right\}$$
$$+L\left\{\begin{array}{l}8\gamma\gamma'(\gamma^2-1)(\gamma'^2-1)+3\omega^2\left(\gamma^2\gamma'^2+(\gamma^2-1)(\gamma'^2-1)\right)\\ \quad+\frac{3}{2}\omega\left[(l-l')(\gamma^2-1)(\gamma'^2-1)+\gamma\gamma'\left(l(\gamma'^2-1)-l'(\gamma^2-1)+2\omega\right)\right]\end{array}\right\}$$

where

$$l=2\ln\left(\gamma+\sqrt{\gamma^2-1}\right)\Big/\sqrt{\gamma^2-1}$$

$$L=2\ln\left[\left(\gamma\gamma'+\sqrt{\gamma^2-1}\sqrt{\gamma'^2-1}-1\right)\Big/\omega\right]\Big/\sqrt{\gamma^2-1}\sqrt{\gamma'^2-1}$$

$$\gamma'=\gamma-\omega$$

Table (6.3)

Electron-proton bremsstrahlung cross section

6.6 Bremsstrahlung

The cross section for *e-p* bremsstrahlung in the Born approximation ($\alpha_f/\beta \ll 1$) is given by Heitler (1954). In the notation of this thesis the differential cross section in the proton's rest frame is given in table (6.3). Koch & Motz (1959) discuss the Coulomb corrections and hard photon corrections to this expression, but these are negligible when averaging over a thermal electron distribution. The protons are assumed to be cold ($\langle\beta\rangle \ll 1$) and so the transformation of photon energies from the proton to plasma frame is trivial. The thermal emission, differential in photon energy, is then

$$\left\langle \omega\frac{d\sigma}{d\omega}\right\rangle=\int_{1+\omega}^{\infty}\omega\frac{d\sigma}{d\omega}\beta\, n_e(\gamma)d\gamma \tag{6.7}$$

Using 4 point Gauss-Laguerre quadrature results in an error of less than 2% for $T > 0.1$, and less than 1% for $T > 0.4$. The maximum error is in the high energy tail. Gorecki & Kluzniak (1980) give a fit to the spectrum with an error of less than 2% for $T > 0.02$, designed for use on less powerful computers.

The total electron-proton bremsstrahlung emission can be found by integrating equation (6.7) over the photon energy. Svensson (1982b) gives the following fit, which has an accuracy of better than 2% over the whole temperature range:

$$\frac{dE}{dt}=\begin{array}{ll}4\alpha_f\left[\frac{2T}{\pi^3}\right]^{1/2}(1+2z)\left(1+1.781T^{1.34}\right) & ;\quad T<1\\ \frac{9\alpha_f T}{2\pi}\left[\ln(2Te^{-\gamma_E}+0.42)+1.5\right] & ;\quad 1<T\end{array} \tag{6.8}$$

Haug (1975a) gives the multiply differential electron-electron bremsstrahlung cross section. Guilbert has used this to make a numerical fit to the thermal spectrum, for temperatures $0.2 < T < 2$ with an error of less than 5% (see Stepney & Guilbert, 1983). For temperatures above 1 MeV, the ultrarelativistic approximation of Alexanian (1968) is accurate to better than 5%. Below 50 keV the non-relativistic formula (Haug, 1975b) has an error of less than 5% for $\omega/T < 1$.

As far as I know, there are no comparable expressions for the electron-positron bremsstrahlung spectrum. It approaches twice the electron-proton rate in the non-relativistic limit, and twice the electron-electron rate in the ultrarelativistic limit.

7 Computer Modelling of a Relativistic Plasma Slab

7.1 Introduction

Much modelling of X-ray sources has been done by considering the Comptonization of an input flux of soft photons (e.g, cyclotron photons) by a slab of hot plasma. The problem is highly non-linear, and so has been tackled in detail only by computer modelling (see, e.g. Guilbert, 1981). These models treat only Comptonization. Photon number is strictly conserved; there are no sources or sinks internal to the slab. At high temperatures, however, the processes of bremsstrahlung and pair production are important cooling mechanisms in their own right. The additional cooling due to the Comptonization of the internally produced bremsstrahlung photons is catastrophic for some combinations of temperature and optical depth.

Since the particle and photon energies are relativistic, the Fokker-Planck approximation, which assumes small changes in photon energies on scattering, cannot be used. Guilbert (1981a,b) has developed a computational method that correctly treats the relativistic effects (Klein-Nishina corrections to the scattering cross section, fully relativistic electron distribution function, etc.) for temperatures $T_e \lesssim 2$. I have used Guilbert's program to follow the Compton scattering and photon transport, and have extended it by including sources and sinks of photons due to bremsstrahlung, pair production and annihilation. I have used the resulting program to investigate constant temperature states of slabs of various optical depths (chapter 8), and variable temperature plasmas (chapter 9).

The models do not include cyclotron radiation, which adds another free parameter to the system. Since even the zero field case has not been studied in detail, it is unnecessary to introduce further complications at this stage. The program is structured in such a way that it would be relatively simple to add another photons source at a later stage, however.

Bremsstrahlung absorption is not included; it is negligible at the optical depths and photon energies being considered. That is, the plasma is effectively thin.

Double Compton scattering, $e + \gamma \rightarrow e + \gamma' + \gamma''$, is neglected. Lightman & Band (1981) show that bremsstrahlung dominates the double Compton process if the optical depth is less than about 10, which is certainly true in the models discussed here.

Pion production by the protons is also not included. This is unimportant in the equilibrium models, where the protons are effectively cold. In some of the cooling models the protons do start off with temperatures high enough to produce pions. However, even a small deviation from a Maxwellian distribution would be enough to reduce the pion production drastically. It was not thought worthwhile to include a process which might well be spurious.

7.2 Computational Method

The program models one-dimensional radiative transfer in a plasma with slab geometry. The particles' distributions (electrons, positrons, protons) are assumed thermal and isotropic, but not necessarily homogeneous. The electrons and positrons have the same temperature.

A convenient measure of position in the slab is the "proton optical depth", $\tau_p = N_p \sigma_T R = R/ct_p$. This is not the true optical depth to electron scattering since the pair density varies with position in the slab, and the electron scattering cross section varies with temperature. The photon distribution is determined self-consistently, and so photons are binned in energy, angle and position (optical depth). The three dimensional array $N(I,J,K)$ contains the number of photons in the bin with energy $\omega(I)$, angle $\theta(J)$ and position $\tau(K)$. Since the electrons are assumed thermal and isotropic, they are described by one-dimensional arrays; the pair density $z(K)$ and (in the temperature varying models) the temperature $T(K)$. The energy mesh is logarithmic, and the angle and position meshes are linear. Hence the photon distribution function (photons per unit volume of phase space) is

$$\begin{aligned} n_\gamma(\mathbf{k}) &= N(I,J,K) \big/ 2\pi\omega^2 \sin\theta_j \, \Delta\theta_j \, \Delta\omega_j \\ n_\gamma(\omega) &= \sum\nolimits_j N(I,J,K)/\Delta\omega_i \end{aligned} \tag{7.1}$$

In the equilibrium models the resolution of the spatial grid is set by the optical depth. Only one Compton scattering per photon per iteration is considered, so the spatial grid must not be so coarse that it grossly underestimates the effect of multiple scatterings. This requires $\Delta\tau_e \lesssim 1/2$. In cooling models, care must also be taken to ensure that the electron temperature and net photon energy change are not too large per timestep. Since, in this model, $\Delta t = \Delta\tau$, this also sets a limit on the spatial resolution.

Similarly, the number of angle bins must not be so small that all the photons scatter into the same bin. When the photon energies are less than, or of the same order as, the electron energies (as in the case of the internally produced bremsstrahlung and annihilation photons) 8 angle bins are sufficient. More are required if the photon energies are much higher than typical electron energies.

The logarithmic energy grid, $\Delta\omega/\omega \propto T$, ensures adequate resolution at all photon energies. For a temperature $kT_e \sim m_e c^2$, with a range of photon energies 0.5 keV < $h\nu$ < 7 MeV, typically 70 bins are sufficient. Even at lower temperatures, energy bins of a few MeV must still be permitted, to allow for the proper treatment of the hard annihilation photons.

At each timestep the photons are scattered in energy and angle, and transported spatially. The change in photon number and pair density due to each of the various processes is calculated, and the appropriate bins incremented accordingly. For the temperature varying case, the energy balance is calculated.

The pairs are assumed to thermalize instantly, since the thermalization timescale is much shorter than the pair production timescale (see figure 5.1). If the distance travelled by a positron during its lifetime from production to annihilation is less than the size of a spatial bin, diffusion can be neglected, and pairs assumed to stay in the spatial bins where they are created. The number of collisions a positron suffers before it annihilates is

$$N \simeq \frac{N_p \sigma_T \ln\Lambda \langle v \rangle}{N_p (1+z) \langle \sigma_{ann} \rangle \sigma_T c} \tag{7.2}$$

where $\langle \sigma_{ann} \rangle$ is the dimensionless averaged annihilation cross section. The RMS distance the positron travels is then

$$D = \lambda \sqrt{N} / 3 \tag{7.3}$$

where $\lambda = 1 / N_p \sigma_T \ln\Lambda$ is the positron's mean free path, and the factor of 1/3 occurs since we are only interested in motions perpendicular to the plane of the slab. Thus

$$\Delta\tau_D \simeq \frac{1}{3} \sqrt{\frac{\langle \beta \rangle}{\langle \sigma_{ann} \rangle \ln\Lambda (1+z)}} \tag{7.4}$$

So $\Delta\tau_D \simeq 0.2$ for T = 1, z = 0. Since this is less than, or of order of, the typical spatial bin size, pair diffusion will be neglected.

7.2.1 Bremsstrahlung

Electron-proton, electron-positron and electron-electron ($e^{\pm}e^{\pm}$) bremsstrahlung all have to be considered. Since the rate is independent of the photon distribution, the produced photons are just distributed isotropically in each energy bin.

Electron-proton bremsstrahlung is easily included, since the cross section need only be averaged over an electron Maxwellian distribution. 4 point Gauss-Laguerre quadrature gives an error of less than 1% for $T > 0.5$. For electron-electron bremsstrahlung I used Guilbert's numerical fit to the thermally averaged cross section (Stepney & Guilbert, 1983). Thermal electron-positron bremsstrahlung is still unknown at the temperatures of interest. I put it equal to the *e-p* rate for $T \ll 1$, and twice the *e-e* rate for $1 \ll T$, joining smoothly at $T \sim 1$. It is the hard ($\omega \sim 1$) photons that are important. The error produced by this approximation is small provided the pair density is small, since the emission goes like $z(1+z)$.

If the bremsstrahlung emission per unit frequency interval is

$$E(\omega) = (1+2z) E^{ep}(\omega) + \tfrac{1}{2}\left[(1+z)^2 + z^2 \right] E^{ee}(\omega) + z(1+z) E^{+-}(\omega) \tag{7.5}$$

and the total bremsstrahlung emission is

$$E^{tot} = \int_0^\infty E(\omega)\, d\omega$$

then the number of photons emitted into each logarithmic energy bin, per Thomson time, is

$$\Delta N(I) = E(\omega)E^{tot} \Big/ \sum_i \omega_i E(\omega_i) \tag{7.6}$$

This scaling ensures that the total energy emitted is correct. These $\Delta N(I)$ photons are emitted isotropically:

$$\Delta N(I,J) = \Delta N(I)\sin\theta_j \Big/ \sum_j \sin\theta_j \tag{7.7}$$

7.2.2 Pair production

It is the photon-photon pair production which takes all the computing time, since a double sum over both energy and angle bins has to be done each iteration. For a standard grid, this results in $5\times(8\times70)^2/2 = 784\,000$ calculations per iteration. Since some of the photons are below threshold, this number can be reduced by a factor of ~ 10, less at higher temperatures. Using the result for the slab symmetric photon-photon rate (3.6), the change in the photon number is

$$\begin{aligned}\Delta N(I_1,J_1,K) &= \Delta N(I_2,J_2,K) \\ &= -N(I_1,J_1,K)N(I_2,J_2,K)R(I_1,I_2,J_1,J_2)\end{aligned} \tag{7.8}$$

where

$$R(I_1,I_2,J_1,J_2) = \frac{1}{\pi\omega_1\omega_2}\int_{\omega_-}^{\omega_+} \frac{\omega^3\sigma(\omega)\,d\omega}{\left[(\omega_+^2-\omega^2)(\omega^2-\omega_-^2)\right]^{1/2}} \tag{7.9}$$

The associated change in the pair density is

$$\Delta z(K) = \sum_{i_1}\sum_{i_2}\sum_{j_1}\sum_{j_2} N(I_1,J_1,K)N(I_2,J_2,K)R(I_1,I_2,J_1,J_2) \tag{7.10}$$

Since the rate depends only on the angle between the photons and the product of their energies there are certain relationships between the various rates R due to symmetry and to the use of a logarithmic energy mesh:

$$\begin{aligned}R(I_1,I_2,J_1,J_2) &= R(I_1,I_2,J_2,J_1) = R(I_2,I_1,J_1,J_2) \\ &= R(I_1+1,I_2-1,J_1,J_2) \\ &= R(I_1,I_2,JMAX+1-J_1,JMAX+1-J_2)\end{aligned} \tag{7.11}$$

The existence of these relationships means that, instead of $(IMAX\times JMAX)^2/2$ values of the reaction rates (= 156 800 for a typical mesh), only $(2\,IMAX-1)JMAX\,(JMAX+2)/4$ values (= 2780) have to be stored. This makes the computation feasible.

There is no problem with the photon-electron and photon-proton rates, since the cross sections are well known, and only a single sum over energy and angle bins needs to be done each iteration. If $\sigma^{\gamma p}(\omega)$ is the photon-proton cross section and $\left\langle\sigma^{\gamma e}(\omega)\right\rangle$ is the photon-electron cross section averaged over an electron Maxwellian, then

$$\Delta N(I,J,K) = -N(I,J,K)\left[\sigma^{\gamma p}(\omega_i) + \left[1+2z(K)\right]\left\langle\sigma^{\gamma e}(\omega_i)\right\rangle\right] \tag{7.12}$$

$$\Delta z(K) = -\sum_i \sum_j N(I,J,K) \tag{7.13}$$

Particle-particle rates are unknown near threshold. However, these processes are unimportant, since the threshold is much higher than in the other cases. For the sake of completeness I included them by assuming a linear fit to the cross section near threshold. Then

$$\Delta z = (1+2z)\left\langle \sigma^{ep} \right\rangle + \tfrac{1}{2}(1+2z)^2 \left\langle \sigma^{ee} \right\rangle \tag{7.14}$$

7.2.3 Annihilation

Svensson's (1982c) one parameter integral has been fitted with polynomials, (§ 3.1.2), and is used to find the annihilation spectrum. This only requires a single sum each iteration.

Proceeding as for bremsstrahlung, if $E(\omega)$ is the energy emitted in annihilation photons per unit frequency, and E^{tot} is the total annihilation emission, then

$$\Delta N(I,J) = z(1+z)E(\omega_i)E^{tot} \sin\theta_j \Big/ \sum_i \sum_j \omega_i E(\omega_i) \sin\theta_j \tag{7.15}$$

$$\Delta z = -\tfrac{1}{2} \sum_i \sum_j N(I,J) \tag{7.16}$$

7.2.4 Energy balance

In the equilibrium models the temperature is fixed arbitrarily, so no energy balancing needs to be done. In the varying models a new electron temperature needs to be calculated each timestep in each spatial bin. The electrons' total energy changes since they Compton scatter photons, produce pairs and radiate bremsstrahlung. Pair production also means that the number of electrons that share this energy changes.

If the electrons and protons have different temperatures, exchanging energy via Coulomb collisions, then the proton energy balance needs to be calculated separately. The total thermal energy of the electrons, per proton, is

$$E(x) = \left[\frac{K_1(x)}{K_2(x)} + \frac{3}{x} - 1 \right] (1+2z) \tag{7.17}$$

where $x = 1/T$. The new temperature is found by Newton-Raphson iteration

$$x_{p+1} = x_p - \frac{E(x_p) - ETHERM}{dE/dx\big|_{x_p}} \tag{7.18}$$

$$\frac{dE}{dx} = \left\{ \frac{K_1(x)}{K_2(x)} \left[\frac{3}{x} + \frac{K_1(x)}{K_2(x)} \right] - 1 - \frac{3}{x^2} \right\} (1+2z) \tag{7.19}$$

where *ETHERM* is the thermal energy of the electrons after energy balancing has been done. At low temperatures ($x > 15$, $T < 0.067$) the new temperature can be found directly, using

$$ETHERM = \left[\tfrac{3}{2}T + \tfrac{15}{8}T^2\right](1+2z) \qquad (7.20)$$

The new proton temperature is found similarly.

If the electrons and protons are assumed to have the same temperatures always, then $T_p = T_e \lesssim 1$, so $\theta_p = T_p m_e / m_p \ll 1$ and the proton's thermal energy is just $3T/2$. The total thermal energy is found by adding this term to the right hand side of equation (7.17), and then the new temperature is calculated.

7.3 External Sources

As well as the internally produced bremsstrahlung and annihilation photons, the program also allows for external sources. For example, the slab could be illuminated with a flux of soft (cyclotron) photons (Guilbert, 1982). In chapter 9 I will describe the effect of illuminating the slab with a very hard source of photons.

If there are no external sources the solution in the slab is symmetric. Only half the slab needs to be calculated, allowing either a substantial saving in computer time or an increased resolution.

7.4 Other Authors

As the simplest problems concerning relativistic thermal plasmas, i.e. timescales and approximate equilibrium pair densities, are solved, other authors are also turning to computational methods to model the spectra in more detail.

The furthest advanced of these is a program due to Zdziarski (1982, and 1983, private communication). He uses a Monte Carlo program to model annihilation, bremsstrahlung and Comptonization. His model does not assume a balance between pair production and annihilation – z is given as well as T and τ_p. Equilibrium solutions can be found by changing z until, in a given model, the production and annihilation rates are seen to balance.

McKinley & Ramaty (1983, private communication) are developing a Monte Carlo program to model these processes. Their model does not calculate the photon field self-consistently, since the photons that produce pairs are not removed from the field. Also, only the bremsstrahlung photons are used to produce pairs. The differences between their results and mine (described in chapter 8) demonstrate the importance of determining the photon field self-consistently.

Horstman & Cavallo (1983) describe a numerical method to model cosmic fireballs. The situation is different from that described here since in their model a photon spectrum is injected. They model the electron-electron bremsstrahlung and Compton scattering with a Monte Carlo method, and calculate the other rates numerically. Their model has 11 energy bins.

8 Constant Temperature Models

Given a slab of plasma with specified optical depth and temperature, what is the equilibrium pair density?

For an optically thick plasma emitting like a black body the answer follows purely from thermodynamics. Consider the case where there are no background electrons, for simplicity. The density of states in phase space is

$$n(\mathbf{p})\, d^3\mathbf{p} = V\, d^3\mathbf{p} / h^3 \tag{8.1}$$

where each state can contain 2 electrons (spin up and spin down) and the occupation number is that of particles obeying Fermi-Dirac statistics with zero chemical potential:

$$n_o = \frac{1}{\exp(E/kT_*)+1} \tag{8.2}$$

Hence the number of electrons per unit volume is (after some algebra)

$$N_+ = \left[\frac{\alpha_f}{r_e}\right]^3 \frac{1}{\pi^2} \sum_{n=1}^{\infty} (-)^{n+1} \frac{T}{n} K_2\left(\frac{n}{T}\right) \tag{8.3a}$$

The high and low temperature limits are

$$N_+ \sim \left[\frac{\alpha_f}{r_e}\right]^3 \left[\frac{T}{\pi}\right]^{3/2} \frac{e^{-1/T}}{\sqrt{2}} \quad ; \quad T \ll 1 \tag{8.3b}$$

$$N_+ \sim \left[\frac{\alpha_f}{r_e}\right]^3 \frac{3\zeta(3) T^3}{2\pi^2} \quad ; \quad 1 \ll T \tag{8.3c}$$

where $\zeta(3) \simeq 1.2$ is the Riemann zeta function.

In the high temperature limit ($m_e \rightarrow 0$) this is three quarters the black body photon density, the difference being due to the different statistics. In the low temperature limit the pair density is exponentially small, due to the non-zero rest mass of the particles. For T = 1 it corresponds to an enormous pair density of $N_+ \simeq 2\times10^{36}$ m^{-3}. At this temperature the black body flux is 7 × 10^{31} W m^{-2}, or $5 L_{Edd}(M_\odot/M)$ m^{-2}. No steady state astrophysical object emits such a flux; the energy requirements are too great. (For a region just 10 km^2, this corresponds to an emission of $1 M_\odot c^2$ yr^{-1}).

For an optically thin plasma the equilibrium pair density must be calculated by considering the individual particle reactions. Lightman (1982) has coined the term "effectively thin" to describe plasmas that are thin to photon *absorption* but not necessarily to photon *scattering*. I will discuss effectively thin plasmas.

8.1 Qualitative Description

In an optically thin plasma all the photons (produced by bremsstrahlung and annihilation) escape without interaction. The equilibrium pair density is then simply found by balancing the annihilation rate with the pair production rate in particle-particle collisions. This gives the maximum temperature, $T_{max} = 24$, described in § 3.3.2.

As the optical depth increases the photons interact with the matter before escaping, producing pairs and being Comptonized. The nonlinearity of the problem, and the complexity of the reaction rates, means that an analytic solution is not possible. However, by making some very sweeping assumptions, it. is possible to get a qualitative feel for the solutions.

Consider only the processes of photon-photon pair production, bremsstrahlung and annihilation. Then the pair balance equation becomes simply

$$\frac{dz}{dt} = n_\gamma^2 R_{\gamma\gamma} - z(1+z)R_{ann} = 0 \tag{8.4}$$

where $R_{\gamma\gamma}(T)$ is the average pair production rate (averaged over the photon spectrum) and $R_{ann}(T)$ is the average annihilation rate. The photon number, n_γ, is the sum of the annihilation and bremsstrahlung photon numbers, assuming no Comptonization or other modifications to the spectra. (The true spectrum will be modified not only by Compton scattering, but also by the removal of those photons which create pairs, and by energy dependent escape probabilities due to Klein-Nishina corrections). So

$$n_\gamma = n_\gamma(1+\tau_{es}) = (n_A + n_B)\left[1+(1+2z)\tau_p\right] \tag{8.5a}$$

$$n_A = 2z(1+z)R_{ann} \tag{8.5b}$$

$$n_B = (1+2z)R_{ep} + \left[(1+z)^2 + z^2\right]R_{ee} + z(1+z)R_{\pm} \tag{8.5c}$$

where the factor of $1 + \tau_{es}$ is used to describe the photon diffusion out of the source. Substitution of equation (8.5) into (8.4) gives a sixth order polynomial in the pair density z. The equilibrium pair densities are thus the roots of

$$\sum_{i=0}^{6} a_i z^i \tag{8.6}$$

It is clear that all the coefficients except a_1 and a_2 are necessarily positive. The signs of a_1 and a_2 depend on the temperature and optical depth.

When $z = 0$, dz/dt is positive. This is obvious physically, since pairs can be created even if none are present. Mathematically this corresponds to $a_0 > 1$. dz/dt is also positive when z is very large. Physically, this is because the pair production rate is proportional to n_γ^2 and n_γ is proportional to z^3, whilst the annihilation rate is only proportional to z^2. Mathematically this says $a_6 > 0$.

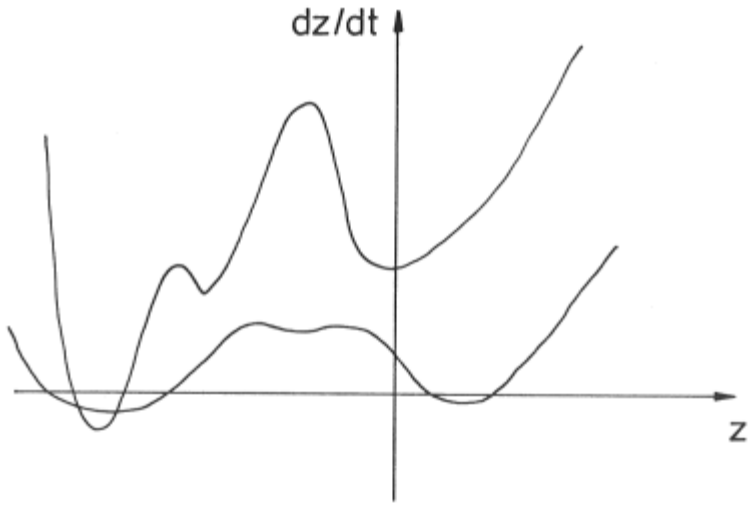

Figure (8.1)

The pair production rate as a function of the pair density, z, showing two or no equilibrium solutions. dz/dt is a 6th order polynomial in z, and so formally has 6 roots. However, there are never more than two roots in the physical ($z > 0$) region. The diagram is schematic, so no values are marked on the axes.

So there must be an even number of equilibrium solutions. The qualitative form of the polynomial pair production rate is shown in figure (8.1). There are in fact either two or no solutions. This conclusion is not changed if the other pair production processes are included. It is, however, different in the case of optically thin pair production, where only particle-particle processes are considered, resulting in a pair balance equation quadratic in z. Since the coefficient of z^2 may have either sign, the solutions are qualitatively different.

So if a plasma starts off with no pairs, dz/dt is positive and pairs are created. There are two possibilities – these extra pairs either increase or decrease the net pair production rate. This is determined by the sign of a_1. Even if a_1 is negative, there may still be no equilibrium solutions. It may be the case that $dż/dz$ reaches zero before dz/dt does. See figure (8.2). It is clear from the figure that the low pair density solution is stable at constant temperature, whilst the high pair density solution is unstable. To find the actual equilibrium pair densities for a given value of the temperature and optical depth, we must calculate the rate coefficients of equations (8.4) and (8.5). These depend not only on the temperature but also on the photon spectrum, consisting of bremsstrahlung and annihilation photons modified by Comptonization, pair production and escape.

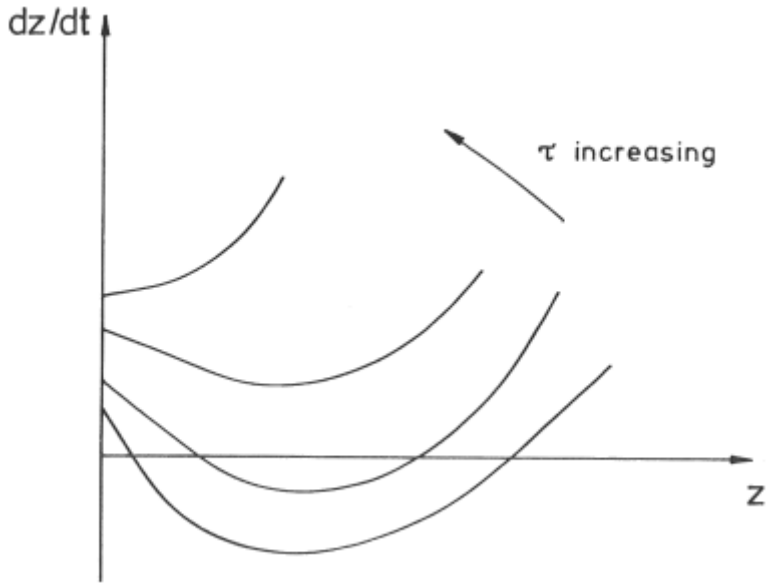

Figure (8.2)

The pair production rate as a function of optical depth, at constant temperature. As τ_p increases, photons are trapped for longer in the plasma, and so can produce more pairs. The annihilation rate is unaffected, so the net pair production rate increases.

The situation is more complicated when the temperature varies, since the pair production rates vary in different ways. For example, $R_{\gamma\gamma}$ decreases at high temperatures, but bremsstrahlung always increases. However, since the annihilation rate always decreases, eventually at high enough temperatures the curve does not cross the *z* axis, and there are no equilibrium solutions.

8.2 Semi-Analytic Results

By extending the above argument to include the other pair production processes and calculating the rate coefficients numerically, Svensson (1982b) has found the equilibrium states of a plasma that is optically thin to Thomson scattering, but not so thin that photon interactions can be neglected. He assumes that the photon field is isotropic and homogeneous, and that it is given by

$$n(\omega) = \left[n_1 n_2 \left\langle \sigma_{brems}(\omega) \right\rangle + n_1' n_2' \left\langle \sigma_{anns}(\omega) \right\rangle \right] (1 + \tau_{es}) \tag{8.7}$$

That is, he assumes the photon distribution is the sum of the photon spectra from the various bremsstrahlung processes, and from annihilation, suitably weighted by the particle densities (also assumed homogeneous). The factor of $1 + \tau_{es}$ is included to take into account the extra time a photon stays in the plasma due to scattering. (Of course, $\tau_{es} < 1$). Since the optical depth is included in this manner, the results are independent of the geometry. He then uses this photon distribution to calculate the pair production rate, balances it against the annihilation rate, and solves for the pair density, *z*.

I have called this method "semi-analytic" since, although the pair balance can be formally written as a polynomial in z, the coefficients are the very complicated rates described in chapter 6. These must be evaluated numerically.

Note that Svensson's method does not calculate the photon field self consistently. It neglects modifications to the distribution function due to the removal of photons which produce pairs, and to the scattering of photons in energy due to Comptonization. These effects are not important provided that the optical depth is low enough that most photons interact at most once before escaping. In this case the rate of pair production is not affected by the assumption though the luminosity will be slightly over-estimated. Neglecting Comptonization is also justified since these internally produced photons, which will produce the pairs, already have energies of the same order as the electrons, so the energy shift per scattering is small. However, there are also internally produced soft bremsstrahlung photons which will be upscattered in energy. The effect at small optical depths (few scatterings) will be to increase the luminosity.

8.3 Numerical Results

For an optical depth of 0.2, less than 2% of the photons scatter more than once before escaping. By the time the optical depth has risen to unity, over one quarter of the photons scatter twice or more. Clearly a more accurate model of the photon field is required in this case. The computer model described in the previous chapter calculates the photon distribution in a self consistent manner, and so is suited for optical depths > 1.

To calculate the equilibrium pair density a model is started with an initial pair density and photon density of zero. It is held at constant electron temperature (i.e. energy balance is not included) and is run until either it converges to an equilibrium solution, or the pair density diverges. The models have spatial structure, and so the equilibrium pair density is a function of position in the slab. I have chosen to characterize the models by their central pair density. The pair density in the outermost bins is typically about half this value. See figure (8.3). The results are given in table (8.1) (central pair density) and table (8.2) (output luminosity). Those for a typical run are shown in figure (8.4). Since bremsstrahlung is an important source of hard photons, models take many Thomson times to converge.

The region of stable solutions is shown in figure (8.5), and is compared with the analytic results of Svensson (1982b). The error bars indicate the density to which the parameter space was explored. The model at the top of an error bar diverged, the one at the bottom converged, and no models were run at intermediate optical depths.

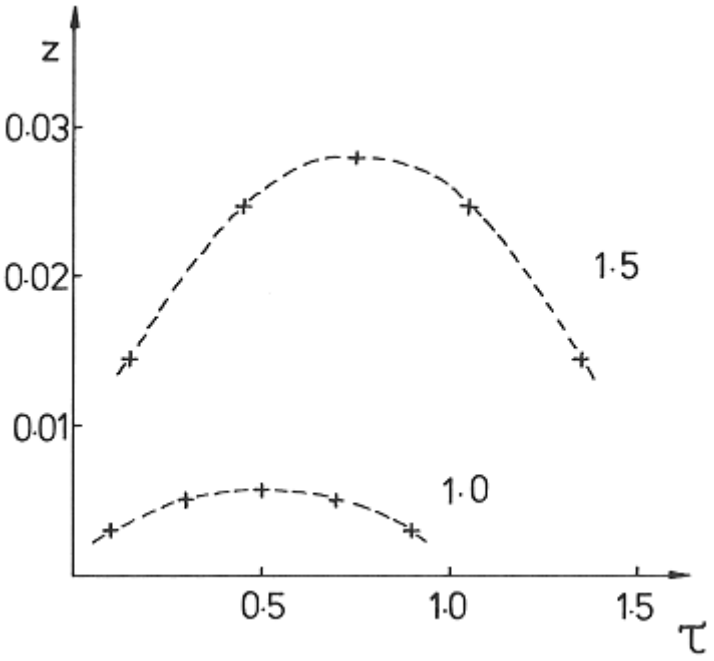

Figure (8.3)

Pair density. Cross section through the slab for $T = 1$, $\tau = 1.0, 1.5$.

The boundary is somewhat lower than the line found by Svensson in his homogeneous models. The reason for this is clear. In the homogeneous models the pairs and photons are spread uniformly throughout the plasma, whilst in the computer model these same pairs and photons are concentrated towards the centre, mimicking a higher temperature or optical depth. Hence 'blowup' occurs sooner. Apart from this, the results from the two different methods are in good agreement. In fact, the methods are complementary. Svensson's semi-analytic approach is fast, but only valid for small optical depths ($\tau \lesssim 1$). The computer model is most accurate at moderate optical depths ($\tau \gtrsim 1$), but requires much more computing time.

These results are replotted in figure (8.6), now showing the equilibrium optical depth as a function of the temperature and central pair density. At constant τ_p, the pair density is a very sensitive function of the temperature. The computer model is unable to find the high pair density branch, which is unstable at constant temperature.

$\tau_p \setminus T$	0.5	0.6	0.7	0.8	0.9	1.0	1.1	1.2	1.3	1.5	1.7
5.0	∞										
4.0	0.090	∞									
3.0	0.019	0.055	∞	∞	∞	∞					
2.0			0.019	0.035	0.064	∞	∞				
1.5					0.018	0.028	0.041	0.088	> 0.13	∞	
1.2									0.04	0.08	∞
1.0						0.0057	0.0082	0.011	0.015	0.022	0.07
0.8								0.0049			
0.7									0.0039		
0.5										0.0018	0.0025

Table (8.1)

Central pair density, *z*.

$\tau_p \setminus T$	0.5	0.6	0.7	0.8	0.9	1.0	1.1	1.2	1.3	1.5	1.7
5.0	∞										
4.0	0.0981	∞									
3.0	0.0639	0.0978	∞	∞	∞	∞					
2.0			0.0822	0.108	0.145	∞	∞				
1.5					0.0992	0.121	0.147	0.20	> 0.26	∞	
1.2									0.16	0.23	∞
1.0						0.0826	0.0972	0.112	0.129	0.162	0.24
0.8								0.0945			
0.7									0.0978		
0.5										0.0988	0.112

Table (8.2)

Output luminosity from one side of slab, units $m_e c^2$ per Thomson time per proton.

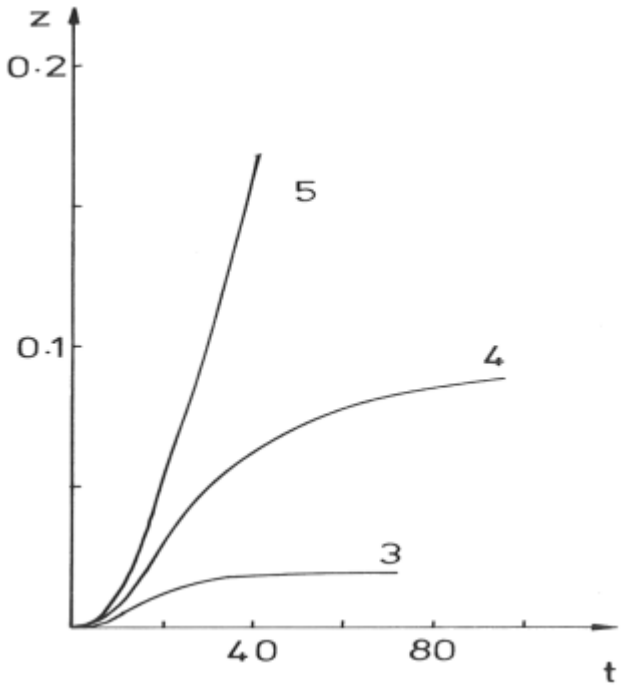

Figure (8.4a)

Central pair density as a function of time for a typical model, $T = 0.5$. The curves are labelled by τ_p. $\tau_p = 3$ reaches its equilibrium value quickly, $\tau_p = 5$ diverges quickly. $\tau_p = 4$ tends slowly to equilibrium.

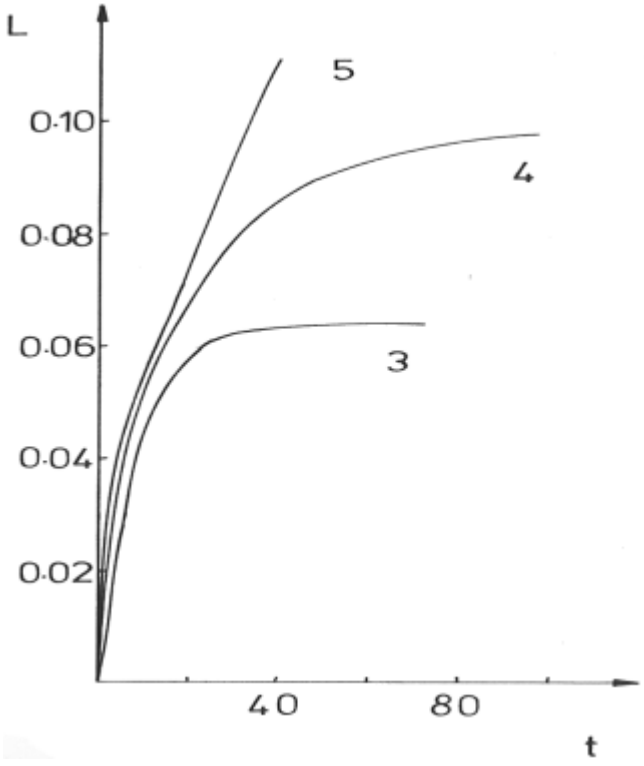

Figure (8.4b)

The emitted luminosity from one side of the slab described in the previous figure. The units are $m_e c^2$ per Thomson time per proton.

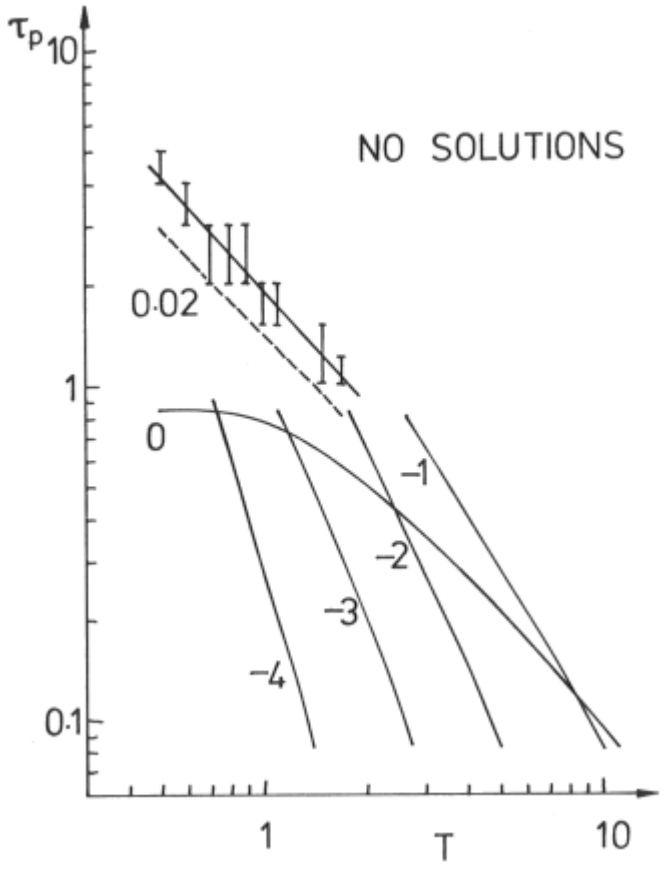

Figure (8.5)

Equilibrium solutions. The solid line passing through the error bars gives the boundary between the region with equilibrium solutions and that which has no equilibrium solutions. The model at the top of an error bar diverged, the one at the bottom converged. The dashed line is a line of constant central pair density, $z = 0.02$. The lines in the lower half of the diagram are Svensson's (1982b) homogeneous solutions, labelled by log z.

The luminosity as a function of temperature is shown in figure (8.7). In Svensson's results the deviations from bremsstrahlung emission with $z = 0$ are due only to the presence of pairs emitting bremsstrahlung, and so emitting more photons. In the computer model the deviations are much larger, even when the pair density is low. This shows the effect of Comptonization – the hot electrons upscatter the photons, and so more energetic photons are emitted. Comptonization has a much larger effect on the luminosity than on the pair density. There are many soft bremsstrahlung photons to upscatter, increasing the luminosity. However, it is not necessary to upscatter them to $\omega \sim 1$ to produce pairs. There are already hard bremsstrahlung and annihilation photons present. Scattering has little effect on these, because for energies above $\omega \sim 1$ the bremsstrahlung spectrum is approximately a Wien law at these temperatures.

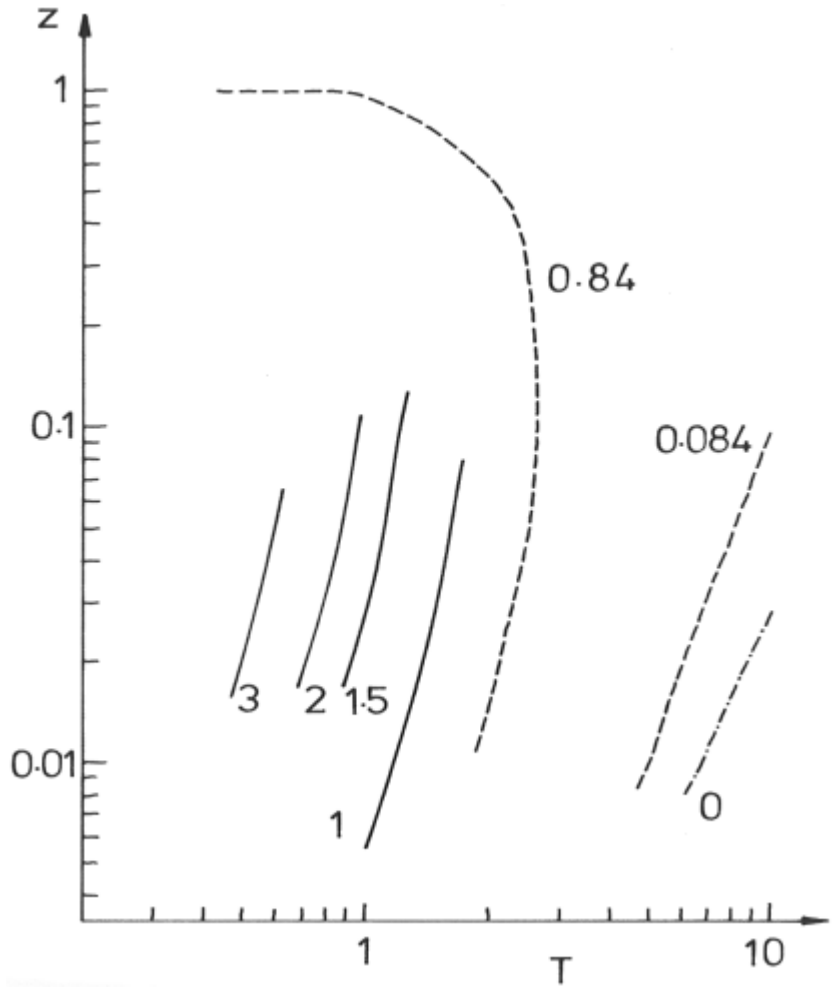

Figure (8.6)

Equilibrium solutions. The central pair density as a function of temperature for various optical depths, τ_p. The dashed lines are Svensson's homogeneous solutions. The dash-dotted line is the zero optical depth limit.

The output spectrum of a typical model (T =1.0, τ_p = 1.5) is show in figure (8.8), along with the relevant optically thin bremsstrahlung and annihilation spectra. The effect of Comptonization on hardening the spectrum is clear. In the case of optically thin bremsstrahlung, the spectral index is $\alpha \simeq -1.2$, while the model has $\alpha \simeq -0.8$.

Steady state, isolated, thermal plasmas do not have the properties of observed γ-ray sources – they have no annihilation lines and their spectra are too hard. The reason for the lack of an annihilation feature is clear. To get a significant density of pairs either a large optical depth, to trap photons, or a high temperature, to produce hard photons, is required. Neither of these conditions will produce a line – photons will either be scattered out of it, or it will be too thermally broadened. The very hard spectrum is due to Comptonization of the already hard internally produced bremsstrahlung spectrum, with a small contribution from the very hard annihilation photons.

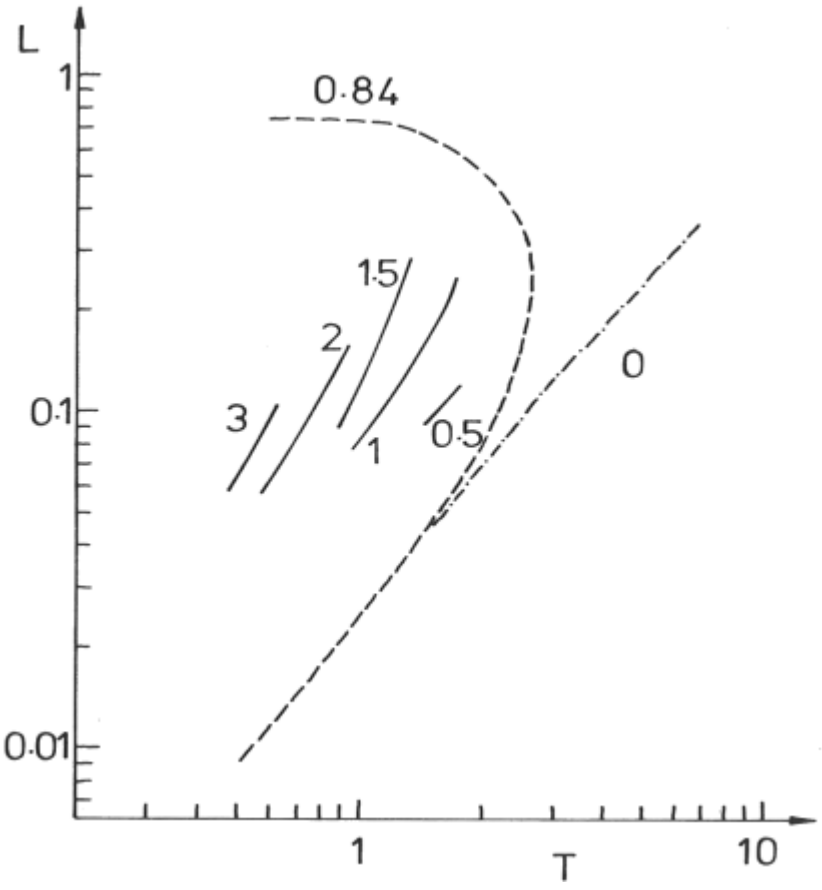

Figure (8.7)

Equilibrium solutions; cooling rate per unit volume. The dash-dotted line is bremsstrahlung from a $z = 0$ plasma. The dashed line is Svensson's (1982b) $\tau_p = 0.84$ result. The deviation from the bremsstrahlung line is due purely to the non-zero pair density, since his model neglects Comptonization.

The solid lines are the computer model results, labelled by τ_p. Now the deviations are mainly due to Comptonization of the soft bremsstrahlung photons, since the pair densities are quite low ($z < 0.1$).

To produce more realistic spectra at least one of the assumptions – steady, state, isolated, thermal – must be relaxed. In the next chapter I will discuss time varying (cooling) plasmas, and externally heated plasmas. Except for the brief discussion in the next section, the thermal assumption will not be relaxed here. To do so would either require an ad hoc specification of the electron distribution, or a massive increase in computational effort to calculate the distribution self-consistently.

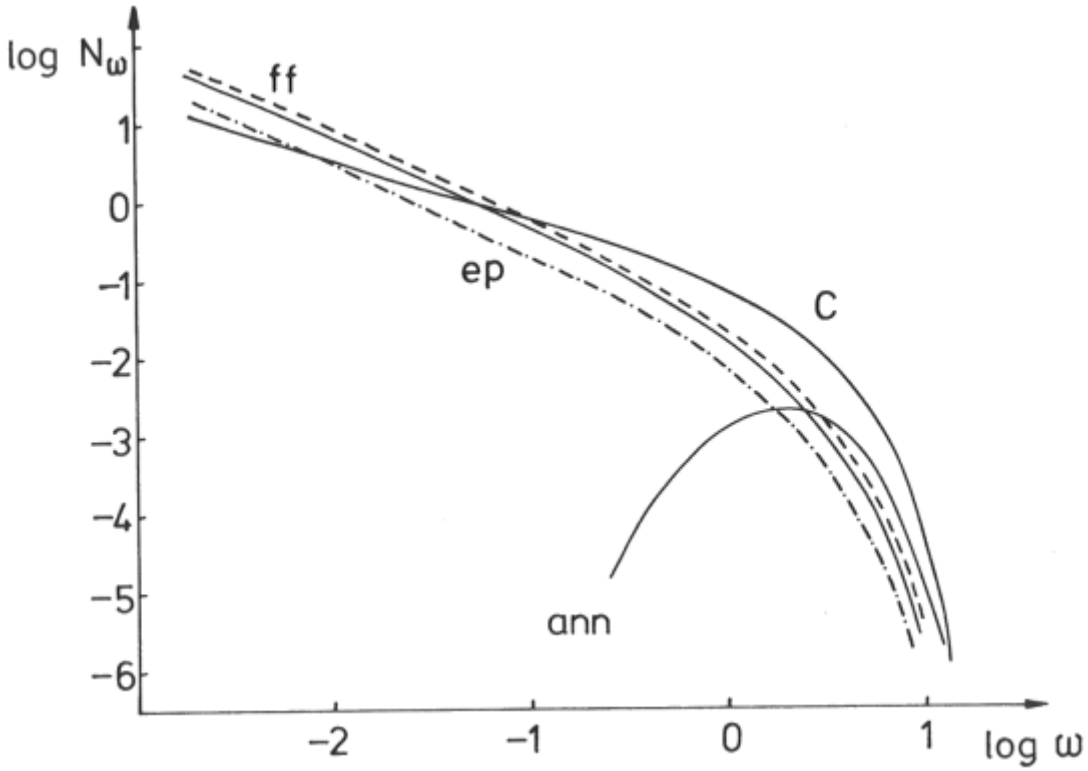

Figure (8.8a)

The output photon spectrum from a slab with T = 1.0, τ_p = 1.5. Such a slab has a central pair density $z \simeq 0.03$. For comparison some optically thin (uncomptonized) radiation spectra are shown. **(C)** Comptonized spectrum **(ff)** bremsstrahlung spectrum (the dashed line has z = 0.1) **(ep)** electron-proton bremsstrahlung **(ann)** annihilation spectrum, z = 0.03.

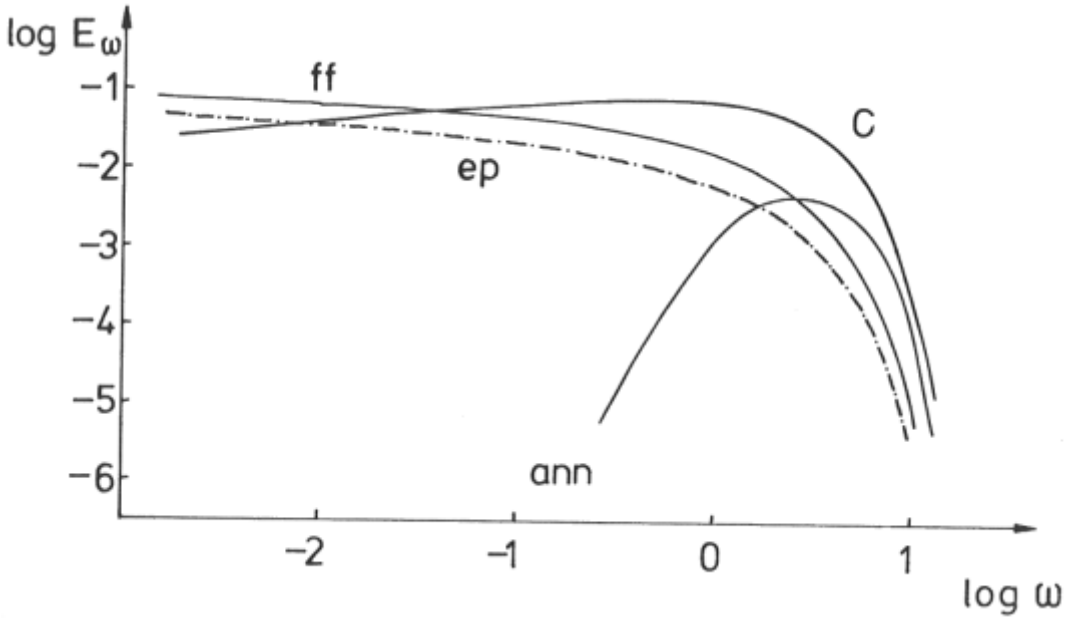

Figure (8.8b)

The output energy spectrum for the model described in figure (8.8a).

8.4 Effect of Truncating the Electron Distribution

What happens if the electron distribution is not Maxwellian?

In principle, it is simple to change the assumed electron distribution in the program – just the rates involving electrons have to be modified. In practice it is not so easy.

Consider the annihilation spectrum. When the electron distribution is Maxwellian, detailed balance considerations allow a simple expression for the spectrum, a single integral, to be found (Svensson, 1982c). When the electron distribution is non-Maxwellian, the resulting spectrum is given as a double integral over the distribution functions and has a complicated integrand (Svensson, 1982a). The computation of the spectrum is now messy.

Electron-electron bremsstrahlung is even worse. The calculation of the fit in the case of Maxwellian distributions (Stepney & Guilbert, 1983) took many hours of computer time. Fits to arbitrary distributions are unfeasible.

A simple qualitative answer can be given, however. The electrons produce the hard photons, via bremsstrahlung and annihilation, and these produce the pairs. At the temperatures considered here most of the pair processes are occurring near threshold, so removing the electrons in the high energy tail mimics a lower temperature. Thus the effect of truncating the distribution will be to move the line separating the stable and unstable regions to the right.

9 Temperature Varying Models

Physically, the unstable region represents catastrophic cooling due to pair production. If a real plasma were to have a temperature and proton optical depth corresponding to this region, it would produce copious pairs, thus rapidly decreasing its temperature (and increasing its true optical depth). It would thus move to the left in figure (8.5), into the stable region, and the pairs would start to annihilate. This behaviour is demonstrated by the cooling models.

A small extension to the program allows variable temperature plasmas to be modelled. Now energy balance must be considered. The change in electron energy due to any heating and cooling is found each iteration, and the new electron temperature is calculated. This version of the program runs at about half the speed of the constant temperature case, since certain temperature dependent rates (particularly the Compton scattering) have to be recalculated each iteration.

Two sorts of temperature variation can be modelled. If the slab is subjected to some steady heating (for example, a flux of hard photons, or some sort of turbulent heating of the protons) then the temperature will vary throughout the slab, but will be time-independent. On the other hand, if the slab is heated impulsively, the temperature will vary with time (as well as spatially) as the slab cools.

9.1 Steady Heating

Two cases will be considered here, steady heating of the protons, and heating of the electrons by an external flux of hard photons.

9.1.1 Steady proton heating

Consider some form of steady mechanical heating of the protons, for example turbulent heating in shocks. The precise details of the mechanism are not important, provided energy is given to the protons at a constant rate, the protons heat the electrons via Coulomb collisions, and the electrons radiate.

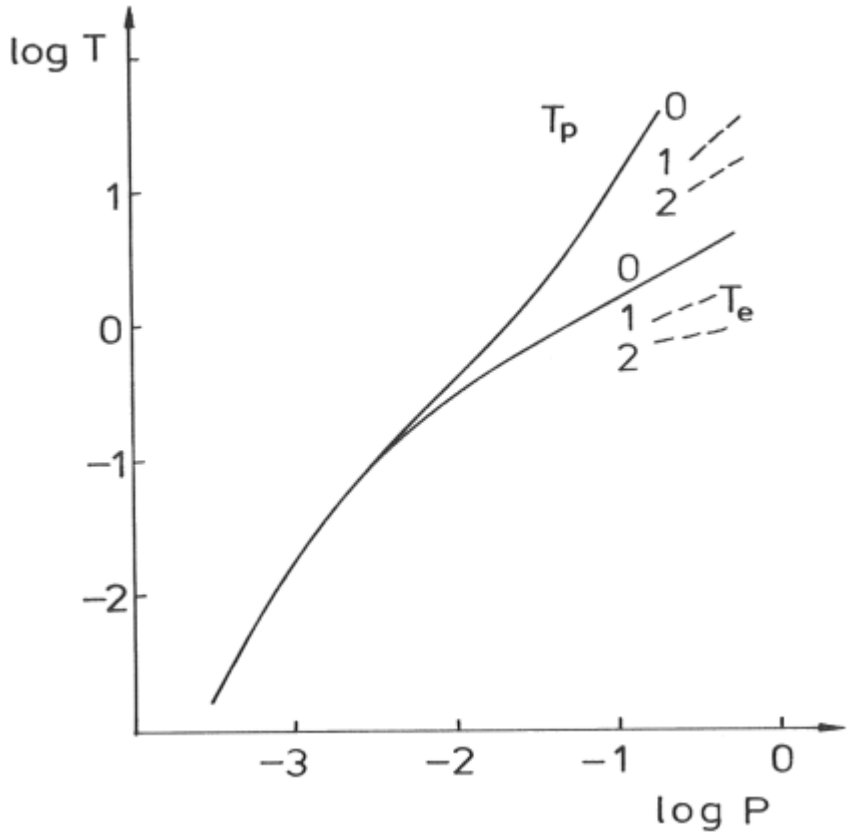

Figure (9.1)

Equilibrium proton and electron temperatures for a steady proton heating of $P\ m_e c^2$ per proton per Thomson time, assuming energy exchange by Coulomb collisions. The curves are labelled with the optical depth, τ_p.

In the steady state these three rates – input, heating and radiation – are the same. Consider first the zero optical depth limit, and no pairs. Then the only radiation is via bremsstrahlung. Since the electrons' bremsstrahlung rate balances the input, and since the total bremsstrahlung emission is a monotonically increasing function of the temperature, higher proton heating rates give higher electron temperatures. The Coulomb heating of the electrons by the protons must also balance the input. This heating gets *less* efficient at higher temperatures. So the difference between the electron and proton temperatures must increase faster than the electron temperature. See figure (9.1).

When pairs are present the electrons can radiate more (per proton), since there are more of them. So their temperature need not be so high in order to balance P_{in}. Thus the proton temperature will be much lower.

The results for various P_{in} and τ_p are also shown in figure (9.1). The corresponding pair densities do not differ much from the equilibrium models at constant temperature (rather than constant heating), although there is a range of temperature throughout the slab. They thus serve to demonstrate the correctness of the energy balancing in the program.

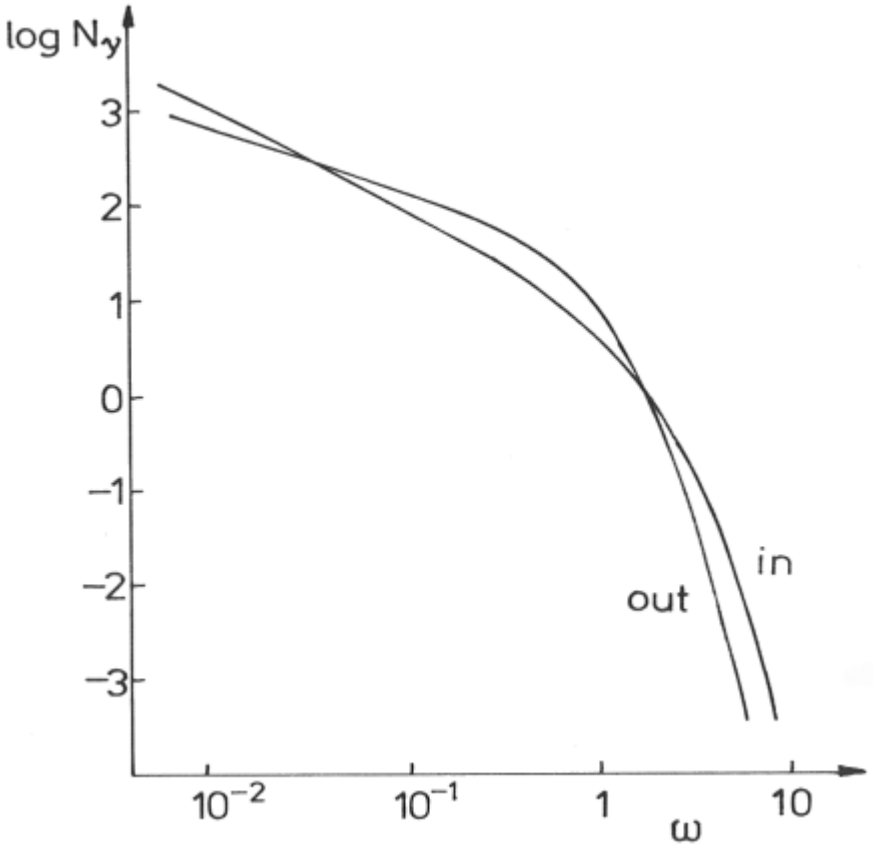

Figure (9.2a)

Photon spectra for a source with input $N_\gamma \propto \omega^{-1} e^{-\omega_o}$ at the centre of the slab.

9.1.2 Steady electron heating

As well as mechanical heating, a plasma could also be heated by shining hard photons onto it. These photons will Compton heat the electrons and produce pairs. Two viewpoints are possible. One can either consider the heating effect of the photons on the electrons, or consider the effect of the electrons on reprocessing the input spectrum. The latter approach is probably more interesting.

Guilbert, Fabian & Rees (1983) discuss a plasma with $\tau_p \ll 1$ which has an internally produced non-thermal radiation spectrum extending to $\omega \gg 1$. The hard photons produce ultrarelativistic pairs which quickly cool, maybe producing more pairs in the process. The authors show that, if the source is optically thick to pair production, $\tau_{\gamma\gamma} > 1$, then the resulting pairs will make it optically thick to scattering, $\tau_{es} > 1$. Thus the internally produced spectrum will be significantly modified.

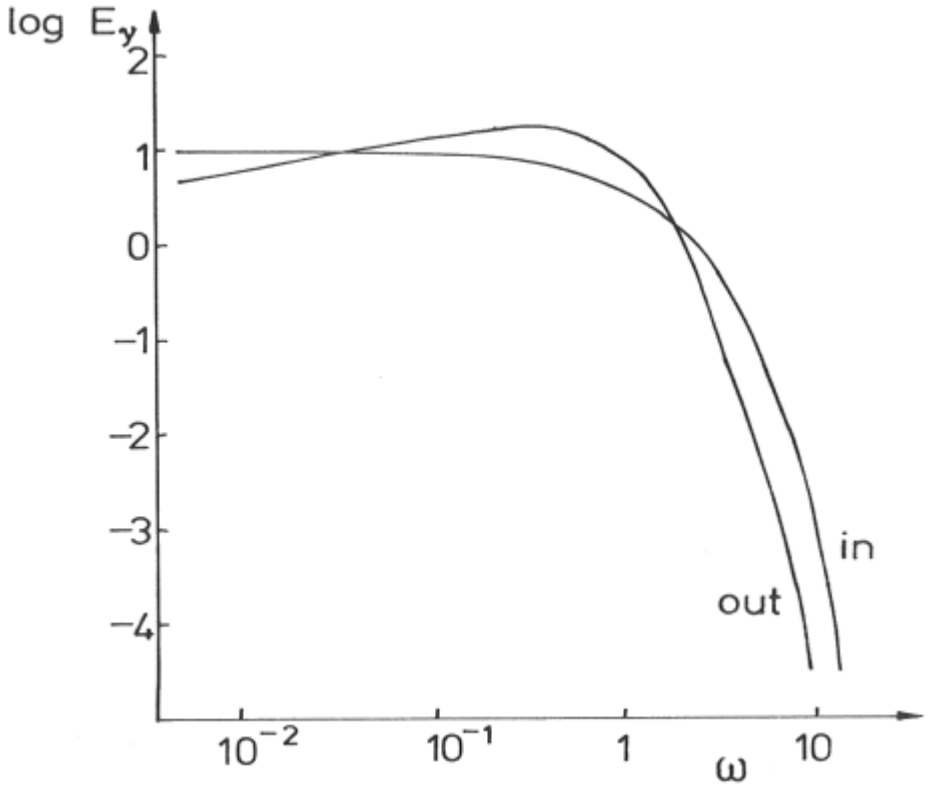

Figure (9.2b)

Energy spectra corresponding to the previous figure.

The computer program cannot investigate this precise problem – it cannot deal with non-thermal electron distributions – but it can address a qualitatively similar problem. If the input spectrum extends up to $\omega \sim 1$, rather than $\omega \gg 1$, then the pairs produced will only be mildly relativistic, and no cascade process will occur as they cool. The modification to such a spectrum can be found.

An isotropic source with photon spectrum $N_\gamma \propto \omega^{-1} e^{-\omega/T_o}$ was introduced at the centre of a slab with optical depth $\tau_p < 1$, and the slab was allowed to come to equilibrium. The resulting spectrum, for $T_o = 1$ and $\tau_p = 0.6$, is shown in figure (9.2). As predicted by Guilbert, Fabian & Rees, the high energy tail has been eaten away, and a bump of Comptonized photons has been produced. The final temperature of the slab was $T \sim 0.2$, and the optical depth has risen to $\tau_{es} \sim 3$,

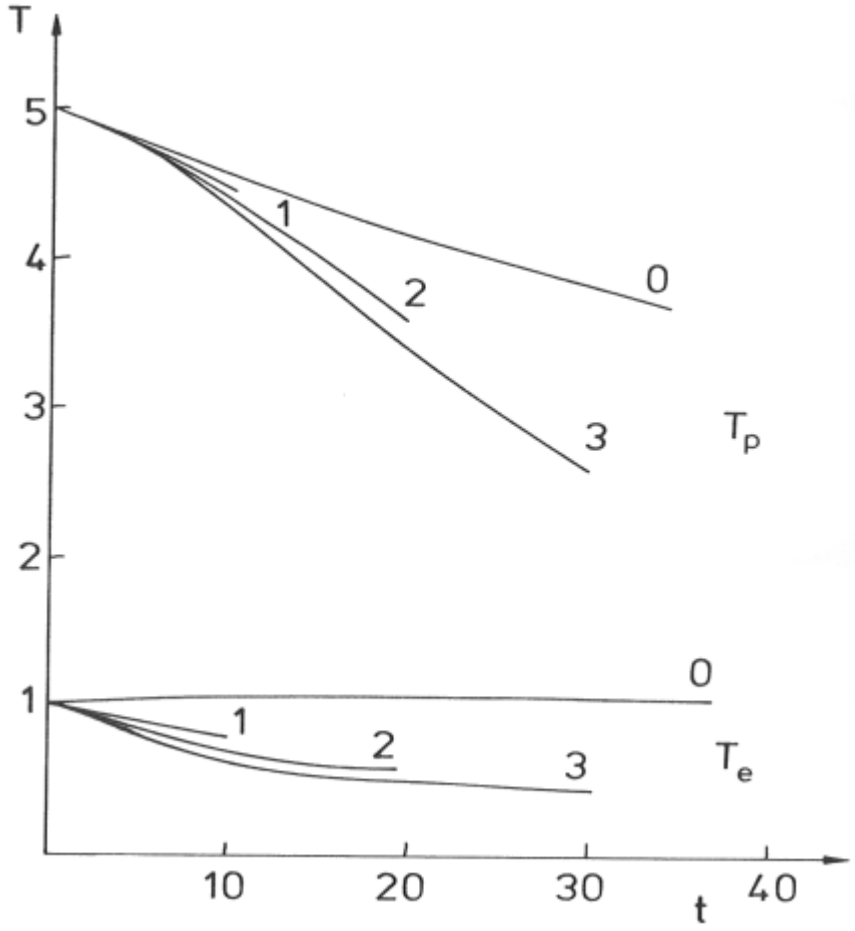

Figure (9.3)

Central temperatures of cooling slabs with $T_{e0} = 1$, $T_{p0} = 5$. The curves are labelled with the optical depths, τ_p

9.2 Impulsive Heating

If the protons start off at a higher temperature than the electrons (for example, by being shock heated) then it is possible that they can transfer their thermal energy to the electrons faster than the electrons can cool. In that case it might be possible to hold the electrons in the 'unstable' region of the constant temperature models long enough for an appreciable pair density to build up. For an optical depth of 2, any temperature greater than 1 is in the unstable region. For $\tau = 3$, all temperatures above 0.7 are unstable.

Two limits to the electron heating by the protons can be considered. Either the heating is purely Coulomb, so $T_p > T_e$, or it is effectively 'instant', in which case $T_p = T_e$ always. Here only the former case is considered.

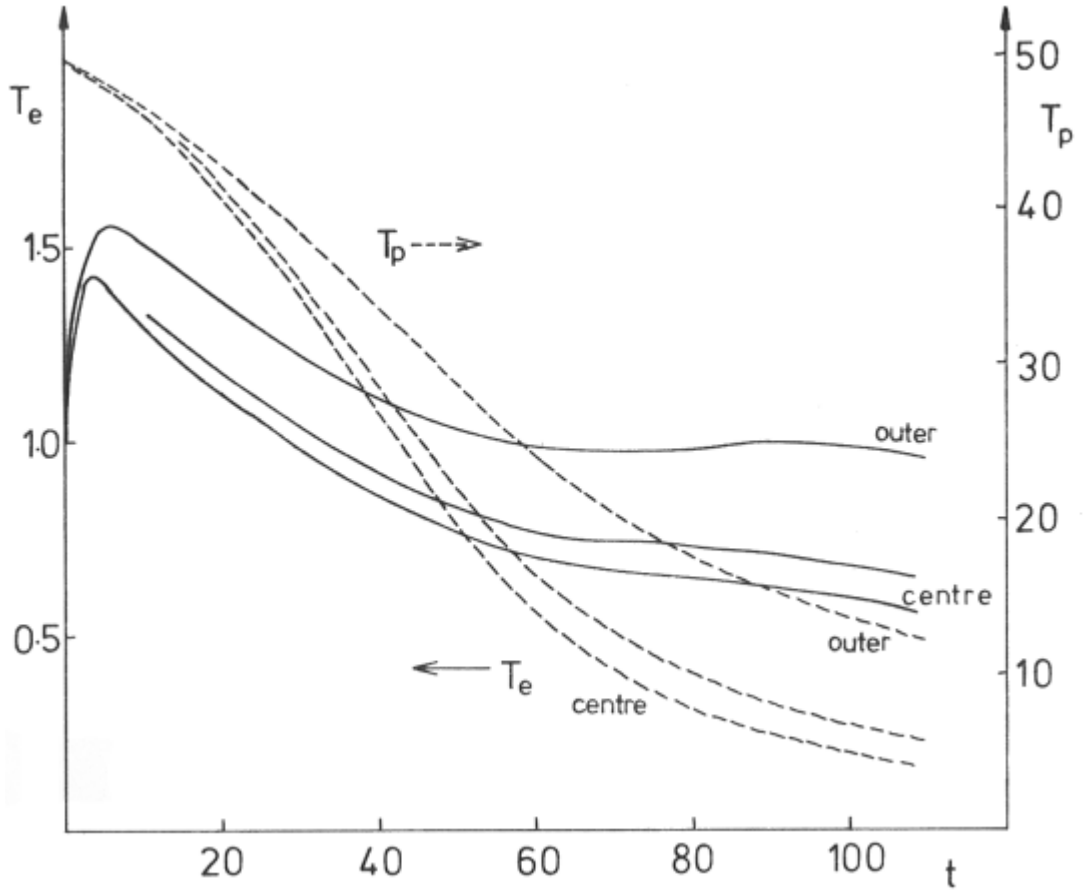

Figure (9.4a)

Temperatures in a cooling slab with $T_{e0} = 1$, $T_{p0} = 50$ and $\tau_p = 2$. (Note the different scales for T_e and T_p)

These cooling models now have three parameters: the initial temperatures T_{e0} and T_{p0}, and the optical depth τ_p. The initial photon density and pair density are taken as zero, for simplicity. The models are then allowed to cool. The results for $T_{e0} = 1$, $T_{p0} = 5$, are shown in figure (9.3), and for $T_{p0} = 50$ in figure (9.4). The curves are labelled by the optical depth, τ_p. That labelled '0' represents the limit of zero optical depth, where the only electron cooling is due to bremsstrahlung.

For the case $T_{p0} = 5$, the electrons do not stay in the unstable region, they cool too quickly. Increasing the optical depth (i.e. decreasing T_{crit}) only increases the cooling due to Comptonization.

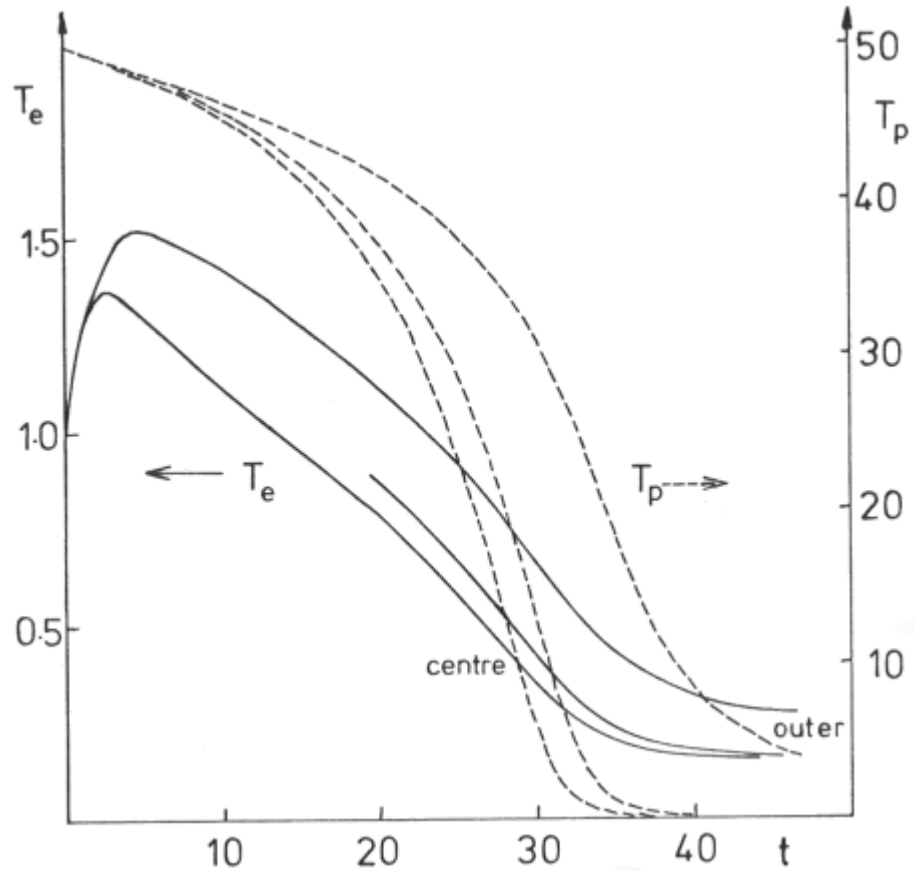

Figure (9.4b)

As the previous figure, but with $\tau_p = 3$.

For $T_{p0} = 50$, however, the electrons remain hot enough long enough for a significant number of pairs to be produced. These models stay in the 'unstable' region for 20 – 30 Thomson times. The pair density goes on increasing for about 10 Thomson times after the temperature has dropped below the critical value, since the slab has hard photons trapped in it. Eventually, though, the pairs start to annihilate. The pair densities as a function of time are shown in figure (9.5). After annihilation starts the electron temperatures stay steady for a while. This is due to heating by the hard annihilation photons.

These slabs have their lowest temperature and highest pair density in the centre, since this is where the cooling is greatest. See figure (9.6). The photon density is highest, giving more pair production and more electron cooling by Comptonization. The protons also cool faster in the higher pair density, since the coupling is increased: the cooling $dT_p/dt \propto 1+2z$.

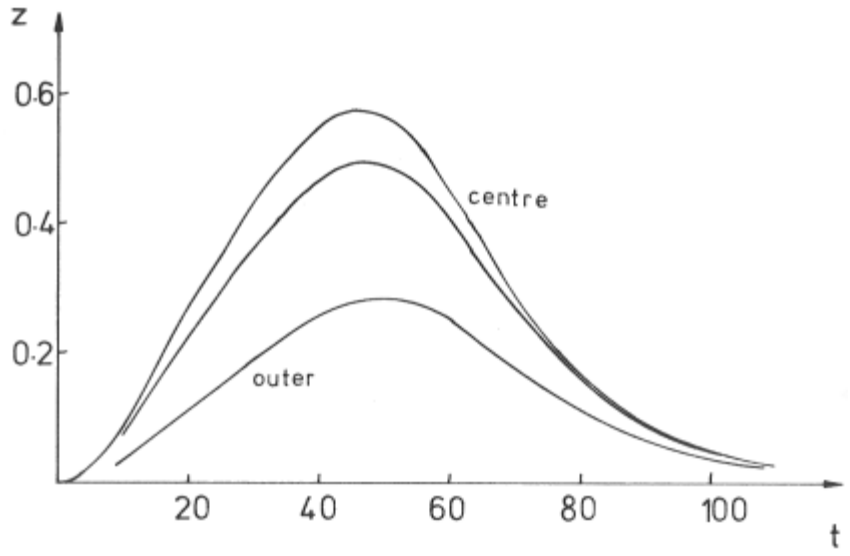

Figure (9.5a)

Pair densities in a cooling slab with $T_{e0} = 1$, $T_{p0} = 50$ and $\tau_p = 2$.

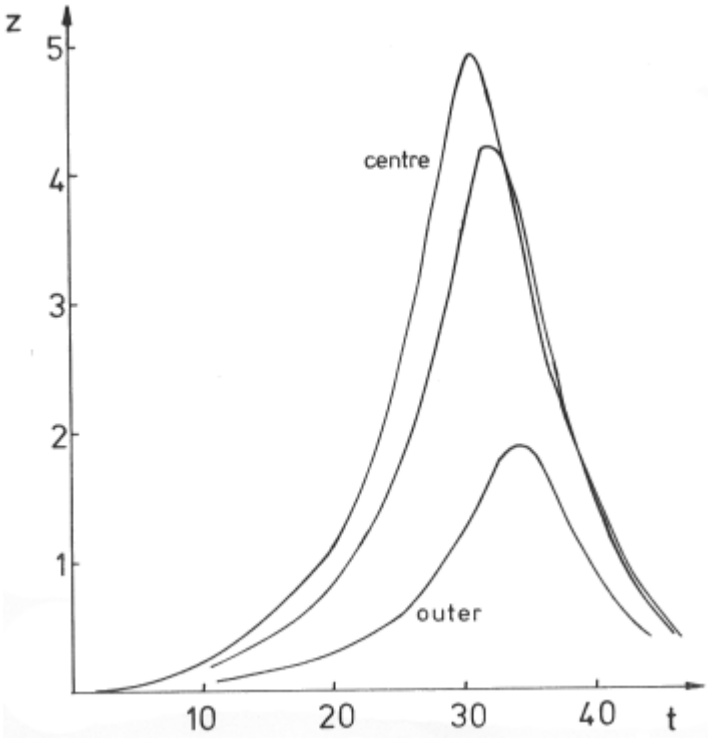

Figure (9.5b)

As the previous figure, but with $\tau_p = 3$.

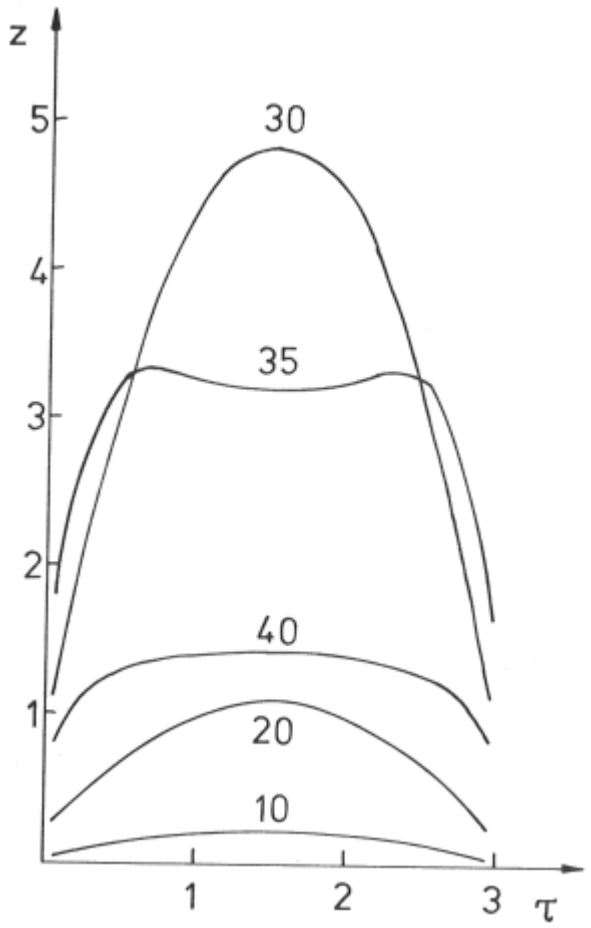

Figure (9.6)

Pair densities through the $\tau_p = 3$ slab, at different times.

Since the maximum pair density is reached well after the plasma has left the 'unstable' region, the pairs annihilate at a relatively low temperature, $T_{ann} \sim 0.2 - 0.4$. Thus there is a chance of seeing an annihilation feature in the spectrum. The instantaneous spectra at the moment of maximum pair density in the outer bin are shown in figure (9.7). The energy spectrum has a very prominent annihilation line, less noticeable in the photon spectrum. The time averaged spectrum (from the initial time to the time of maximum pair density) also has a line. The feature is not as prominent, but is still visible. These spectra are also much harder than any observed spectra, since they consist of Comptonized bremsstrahlung and annihilation photons, with no soft component.

It is encouraging, however, that it is possible to produce an annihilation feature with such a simple model: a cooling slab with no input.

–ooOoo–

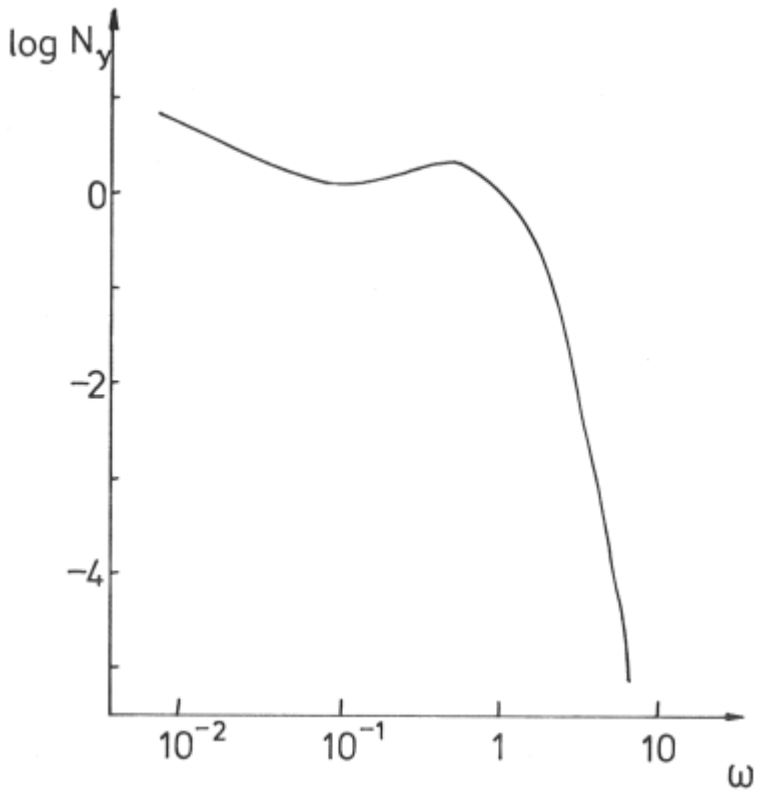

Figure (9.7a)

Photon spectrum of the τ_p = 3 slab after 36 Thomson times (the time of maximum pair density in the outer bin).

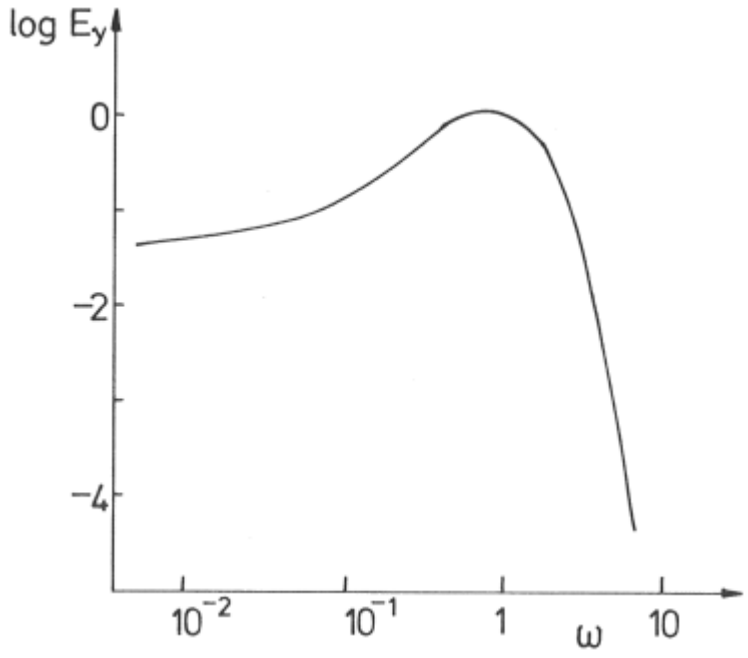

Figure (9.7b)

Energy spectrum after 36 Thomson times.

References

Abramowitz, M. & Stegun, I.A. (1964) Handbook of Mathematical Functions. Dover.

Alexanian, M. (1968) Phys.Rev. **165** 253. "Photon bremsstrahlung from an extreme-relativistic electron gas"

Baier, V. N., Fadin, V.S. & Khoze V.A. (1967) Sov.Phys.-J.E.T.P. **24** 760. "Photon bremsstrahlung in collisions of high-energy electrons"

Baier, V. N., Fadin, V. S. & Khoze V.A. (1968) Sov.Phys.-J.E.T.P. **26** 1238. "Total bremsstrahlung spectrum of ultra relativistic electrons"

Bisnovatyi-Kogan, G.S. & Blinnikov, S.I. (1977) A. & A. 59 111. "Disk accretion onto a black hole at subcritical luminosity"

Bisnovatyi-Kogan, G. S., Zel'dovich, Ya.B. & Syunyaev, R.A. (1971) Sov.Astron.-A.J. **15** 17. "Physical processes in low-density relativistic plasma"

Blatt, AM. & Weisskopf, V.F. (1952) *Theoretical Nuclear Physics*. Wiley.

Budnev, V.M., Ginzburg, I.F., Meledin, G.V. & Serbo, V.G. (1975) Phys.Rep. **C15** 181. "The two-photon particle production mechanism. Physical problems. Applications. Equivalent photon approximation"

Cavallo, G. & Rees, M.J. (1978) M.N.R.A.S. **183** 359. "A qualitative study of cosmic fireballs and γ-ray bursts"

Daugherty, J.K. & Harding, A. (1983) NASA Technical Memorandum 84935. "Pair production in superstrong magnetic fields"

Eilek, AA. & Kafatos, M. (1983) Ap.J. **271** 804. "The high energy spectrum of hot accretion discs"

Erdélyi, A., Magnus, W., Oberhettinger, F. & Triconi, F.G. (1953) *Higher Transcendental Functions*. McGraw-Hill.

Felten, J. E. & Rees, M.J. (1972) A. & A. **17** 226. "Continuum radiative transfer in a hot plasma, with application to Scorpius X-1"

Frankel, N.E., Hines, K.C. & Dewar, R.L. (1979) Phys.Rev.A **20** 2120. "Energy loss due to binary collisions in a relativistic plasma"

Górecki, A. & Kluźniak, W. (1981) Acta Astronomica **31** 457. "Bremsstrahlung spectra at relativistic temperatures"

Gould, R. J. (1980) Ap.J. **238** 1026. "Thermal bremsstrahlung from high-temperature plasmas"

Gould, R. J. (1981) Phys.Fluids **24** 102. "Kinetic theory of relativistic plasmas"

Gould, R. J. (1982a) Ap.J. **254** 755. "Processes in relativistic plasmas"

Gould, R. J. (1982b) Ap.J. **269** 879. "Effects of nuclear forces on ion thermalization in high-temperature plasmas"

Guilbert, P.W. (1981a) M.N.R.A.S. **197** 451. "Numerical solutions of time dependent Compton scattering problems by means of an integral equation"

Guilbert, P.W. (1981b) Ph.D. Thesis (Cambridge).

Guilbert, P.W, Fabian, A.C. & Rees, MA. (1983) Preprint. "Spectral and variability constraints on compact sources"

Guilbert, P.W., Fabian, A. C. & Ross, R.R. (1982) M.N.R.A.S. **199** 763. "Time dependent X-ray spectra of Compton cooled plasmas"

Haug, E. (1975a) Z.Naturforsch. **30a** 1099. "Bremsstrahlung and pair production in the field of free electrons"

Haug, E. (1975b) Z.Naturforsch. **30a** 1546. "Electron-electron bremsstrahlung in a hot plasma"

Haug, E. (1981) Z.Naturforsch. **36a** 413. "Simple analytic expressions for the total cross section for γ-e pair production"

Heitler, W. (1954) *The Quantum Theory of Radiation*, 3rd edn. Oxford Clarendon Press.

Horstman, H.M. & Cavallo, G. (1983) A. & A. **122** 119. "The energy spectrum of cosmic fireballs"

Illarionov, A.F. & Syunyaev, R.A. (1972) Sov.Astron.-A.J. **16** 45. "Compton scattering by thermal electrons in X-ray sources"

Jauch, J.M. & Rohrlich, F. (1980) *The Theory of Photons and Electrons*, 2nd edn. Springer.

Jost, R., Luttinger, J.M. & Slotnick, M. (1950) Phys.Rev. **80** 189. "Distribution of recoil nucleus in pair production by photons"

Koch, H.W. & Motz, J.W. (1959) Rev.Mod.Phys. **31** 920. "Bremsstrahlung cross-section formulas and related data"

Kolykhalov, P. I. & Syunyaev, R.A. (1979) Sov.Astron.-A.J. **23** 189. "Gamma emission during spherically symmetric accretion onto black holes in binary stellar systems"

Landau, L. D. & Lifshitz, E.M. (1971) *Relativistic Quantum Theory*. Pergamon.

Landau, L. D. & Lifshitz, E.M. (1975) *The Classical Theory of Fields*, 4th edn. Pergamon.

Leventhal, M., MacCullam, C. J. & Stang, P. D. (1978) Ap.J. **225** L11. "Detection of 511 keV positron annihilation radiation from the galactic centre direction"

Liang, E. P. (1982) Nature **299** 321. "Emission mechanism and source distances of gamma ray bursts"

Liang, E. P., Jernigan, T.E. & Rodrigues, R. (1983) Ap.J. **271** 766. "Analysis of the Konus catalog of γ-ray bursts with the thermal synchrotron model"

Liang, E. P. T. & Price, R.H. (1977) Ap.J. **218** 247. "Accretion disk coronae and Cygnus X-1"

Lightman, A. P. (1982) Ap.J. **253** 842. "Relativistic thermal plasmas: pair processes and equilibria"

Lightman, A. P. & Band, D. L. (1981) Ap.J. **251** 713. "Relativistic thermal plasmas: radiation mechanisms"

Masters, A.R. (1978) Ph.D. Thesis (Illinois)

Mazets, E.P., Golenetskii, S.V., Apteker, R.L., Gur'yan, Yu.A. & Il'inskii, V. N. (1981a) Nature **290** 378. "Cyclotron and annihilation lines in γ-ray bursts"

Mazets, E.P. et al. (1981b) Ap.SpOci. **80** 3. "Catalog of cosmic gamma-ray bursts from the KONUS experimental data"

Nolan, P. L. & Matteson, AL. (1983) Ap.J. **265** 389. "A feature in the X-ray spectrum of Cygnus X-1: a possible positron annihilation line"

Particle Data Group (1980) Rev.Mod.Phys. **52**. "Review of particle properties"

Perkins, D.H. (1972) *Introduction to High Energy Physics*. Addison-Wesley.

Ralston, A. & Rabinowitz, P. (1978) *A First Course in Numerical Analysis*. McGrawHill Kogakusha.

Ramaty, R., Lingenfelter, R.E. & Bussard, R.W. (1981) Ap.Sp.Sci. **75** 193. "Synchrotron cooling and annihilation of an e^+-e^- plasma: the radiation mechanism for the 5 March, 1979 transient"

Ramaty, R. & Mészáros, P. (1981) Ap.J. **250** 384. "Annihilation radiation from a hot e^+-e^- plasma"

Rybicki, G.B. & Lightman, A. P. (1979) *Radiative Processes in Astrophysics*. Wiley.

Schiff, L.I. (1968) *Quantum Mechanics*, 3rd edn. McGraw-Hill.

Shapiro, S.L., Lightman, A. P. & Eardley, D.M. (1976) Ap.J. **204** 187. "A two temperature accretion disk model for Cygnus X-1: structure and spectrum"

Spitzer, L. (1956) *Physics of Fully Ionised Gases*. Wiley.

Stepney, S. & Guilbert, P.W. (1983) M.N.R.A.S., **204** 1269. "Numerical fits to important rates in high temperature astrophysical plasmas"

Stickforth, J. (1961) Z.Physik. **164** 1. "Zur Theorie der Bremsstrahlung in Plasmen hoher Temperatur"

Stoeger, W.R. (1977) A. & A. **61** 659 and (1979) A. & A. **78** 124. "Photon pair production in astrophysical transrelativistic plasmas" and erratum

Svensson, R. (1982a) Ap.J. **258** 321. "The pair annihilation process in relativistic plasmas"

Svensson, R. (1982b) Ap.J. **258** 335. "Electron-positron pair equilibria in relativistic plasmas"

Svensson, R. (1982c) preprint. "The thermal pair annihilation spectrum: a detailed balance approach"

Weaver, T.A. (1976) Phys.Rev.A **13** 1563. "Reaction rates in a relativistic plasma"

Whittaker, E.T. & Watson, G. N. (1927) *A Course of Modern Analysis*, 4th edn. Cambridge University Press.

Zdziarski, A.A. (1980) Acta Astronomica **30** 371. "Annihilation spectrum of relativistic plasma"

Zdziarski, A. A. (1982) European Workshop on Very Hot Astrophysical Plasmas, Nice, 1982. "Effect of Compton scattering on the pair annihilation and bremsstrahlung spectra"

A1. Transformation of Scattering Angles

We need to transform angles from the rest frame (unprimed) of the target particle to the CM (primed) frame. Let the CM scattering angle be θ', and the scattering half-angle be α'. The relative velocity and γ-factor are β and γ respectively. If the target particle is B and the incident particle is A, then $\mu \equiv M_A/M_B = 1$ for electron-electron ($e^{\pm}e^{(\pm)}$) scattering, and $\mu = 1/1836 \ll 1$ for electron-proton scattering.

The transformation velocity V is

$$V = \frac{\gamma\beta M_A}{M_B + \gamma M_A} = \frac{\gamma\beta\mu}{1+\gamma\mu} \tag{A1.1}$$

So $1 - V\beta = 1/\gamma$ and $\beta - V = \beta(1+\gamma\mu)$. Transforming $p_A^{\mu} = \gamma M_A(1, \boldsymbol{\beta})$ to the CM gives

$$p_A'^{\mu} = \gamma M_A \Gamma(1 - V\beta,\ \beta - V,\ 0,\ 0) = M_A \Gamma\left[1,\ \frac{\gamma\beta}{1+\gamma\mu},\ 0,\ 0\right] \tag{A1.2}$$

where $\Gamma^2 = 1/(1-V^2) = (1+\gamma\mu)/(1+2\gamma\mu+\mu^2)$. Since there is no energy exchange in the CM frame, after scattering

$$p_{A2}'^{\mu} = \Gamma M_A\left[1,\ \frac{\gamma M\beta\cos\theta'}{1+\gamma\mu},\ \frac{\gamma M\beta\sin\theta'}{1+\gamma\mu},\ 0\right] \tag{A1.3}$$

Transforming back to the rest frame gives

$$p_{A2}^{\mu} = \Gamma M_A\left[\Gamma\left(1 + \frac{V\gamma\beta\cos\theta'}{1+\gamma\mu}\right), \Gamma\left(\frac{\gamma\beta\cos\theta'}{1+\gamma\mu} + V\right), \frac{\gamma\beta\sin\theta'}{1+\gamma\mu}, 0\right] \tag{A1.4}$$

Substituting for V and Γ, and using

$$\cos^2\theta = p_{A2x}^2 \Big/ \left(p_{A2x}^2 + p_{A2y}^2\right) \tag{A1.5}$$

gives

$$\begin{aligned}\cos^2\theta &= \frac{\left[(1+\gamma\mu)\cos\theta' + \mu(\gamma+\mu)\right]^2}{\left[(1+\gamma\mu)\cos\theta' + \mu(\gamma+\mu)\right]^2 + (1+2\gamma\mu+\mu)^2\sin^2\theta'} \\ &= \frac{\left[\gamma\mu(1+\cos\theta') + \mu^2 + \cos\theta'\right]^2}{\left[\gamma\mu(1+\cos\theta') + \mu^2 + 1\right]^2 - \mu^2(1-\cos\theta')^2}\end{aligned} \tag{A1.6}$$

So for the case of electron-proton scattering, $\mu \ll 1$

$$\cos\theta = \frac{(1+\cos\theta')\gamma\mu + \cos\theta'}{(1+\cos\theta')\gamma\mu + 1} = \frac{(\gamma\mu+1)2\cos^2\alpha' - 1}{2\gamma\mu\cos^2\alpha' + 1} \tag{A1.7}$$

$$\sin^2\alpha = \sin^2\alpha' / (2\gamma\mu\cos^2\alpha' + 1) \tag{A1.8}$$

$$\frac{d\Omega}{\sin^4\alpha} = (1+2\gamma\mu)\frac{d\Omega'}{\sin^4\alpha'} \tag{A1.9}$$

For electron-electron scattering, $\mu = 1$. Then

$$\cos^2\theta = \frac{(\gamma+1)(1+\cos\theta')}{(\gamma-1)\cos\theta'+\gamma+3} = \frac{(1+\gamma)\cos^2\alpha'}{1+\sin^2\alpha'+\gamma\cos^2\alpha'} \tag{A1.10}$$

$$\frac{d\Omega}{\cos^3\theta} = \frac{2\,d\Omega'}{(\gamma+1)(1+\cos\theta')^2} = \frac{d\Omega'}{2(\gamma+1)\cos^4\alpha'} \tag{A1.11}$$

$$\frac{d\Omega}{\sin^4\alpha} = \frac{4\,d\Omega'}{\sin^4\alpha'} \quad ; \quad \beta \ll 1,\ \alpha' \ll 1 \tag{A1.12}$$

A2. Properties of Modified Bessel Functions

Some of the more frequently used properties of the modified Bessel functions of the second kind, K_ν, are summarised here for reference. These relations are used in, for example, the derivation of the reaction rate and energy exchange rate in chapter 2, and to find the high and low temperature limits of the rates in chapters 3 & 4. The argument z is often of the form n/T, where n is some small integer and T is the temperature. For more obscure properties see, e.g., Abramowitz & Stegun, 1964, § 9.

Integral representation:

$$K_\nu(z) = \left(\frac{z}{2}\right)^\nu \frac{\sqrt{\pi}}{\Gamma(\nu+\frac{1}{2})} \int_0^\infty e^{-z\cosh t} \sinh^{2\nu} t \; dt \tag{A2.1}$$

$$= \int_0^\infty e^{-z\cosh t} \cosh(\nu t) dt \tag{A2.2}$$

$$= \left(\frac{z}{2}\right)^\nu \frac{\sqrt{\pi}}{\Gamma(\nu+\frac{1}{2})} \int_0^\infty (t^2-1)^{\nu-1/2} e^{-zt} \; dt \tag{A2.3}$$

Small argument limit, $z \ll 1$ (high temperature limit):

$$\begin{aligned} K_0(z) &= -\left(\ln\frac{z}{2} + \gamma_E\right) + O(z^2) \\ K_1(z) &= \frac{1}{z} + \frac{z}{2}\left(\ln\frac{z}{2} + \gamma_E - \frac{1}{2}\right) + O(z^3) \\ K_2(z) &= \frac{2}{z^2} - \frac{1}{2} - \frac{z^2}{8}\left(\ln\frac{z}{2} + \gamma_E - \frac{3}{4}\right) + O(z^4) \end{aligned} \tag{A2.4}$$

Large argument limit, $z \gg 1$ (low temperature limit):

$$K_\nu(z) = \sqrt{\frac{\pi}{2z}} e^{-z}\left[1 + \frac{\mu-1}{8z} + \frac{(\mu-1)(\mu-9)}{2!(8z)^2} + \cdots\right] \tag{A2.5}$$

where $\mu = 4\nu^2$

Recurrence relations:

$$\begin{aligned} K_{\nu+1}(z) &= \frac{2\nu}{z} K_\nu + K_{\nu-1} \\ K_3 &= \left(\frac{8}{z^2} + 1\right) K_1 + \frac{4}{z} K_0 \\ K_2 &= \frac{2}{z} K_1 + K_0 \end{aligned} \tag{A2.6}$$

$$
\begin{aligned}
K_\nu' &= -K_{\nu-1} - \frac{\nu}{z} K_\nu \\
K_0' &= -K_1 \\
K_1' &= -K_0 - \frac{1}{z} K_1 \\
K_2' &= -K_1 - \frac{2}{z} K_2
\end{aligned}
\tag{A2.7}
$$

A3. The Integrals $I_1(N)$ and $I_2(N)$

We wish to evaluate

$$I_1(n) \equiv \int_0^\infty x^{\nu-1} \ln^n x \, e^{-x} dx \tag{A3.1}$$

The integral representation of the gamma function is

$$\Gamma(\nu) = \int_0^\infty x^{\nu-1} e^{-x} dx \tag{A3.2}$$

Differentiating with respect to ν yields

$$I_1(n) = \frac{d^n \Gamma(\nu)}{d\nu^n} \equiv \Gamma^{(n)}(\nu) \tag{A3.3}$$

This differentiation under the integral sign is valid because both integrals are convergent, and the integrand of (A2.1) is a continuous function of both x and ν (Whittaker & Watson, 1927)

So using the relationship between the polygamma functions and the Reiman zeta function (Abramowitz & Stegun, 1964)

$$\Gamma'(\nu) = \psi(\nu)\Gamma(\nu)$$
$$\psi^{(n)} = (-1)^{n+1}\Gamma(n+1)\zeta(n+1,\nu)$$

where, for integral m

$$\zeta(s,m) = \zeta(s) - \sum_{k=1}^{\infty} 1/k^s$$

gives

$$\begin{aligned}
\int x^2 e^{-x} dx &= \Gamma(3) = 2 \\
\int x^2 \ln x \, e^{-x} dx &= \Gamma(3)\psi(3) = 1.8456 \\
\int x^2 \ln^2 x \, e^{-x} dx &= \Gamma(3)\left[\psi(3) + \zeta(2,3)\right] = 2.493 \\
\int x^2 \ln^3 x \, e^{-x} dx &= \Gamma(3)\left[\psi^2(3) + 3\psi(3)\zeta(2,3) - 2\zeta(3,3)\right] = 3.450
\end{aligned} \tag{A3.4}$$

Similarly we can evaluate

$$I_2(n) \equiv \int_0^\infty x^\nu \ln^n x \, K_1(x) \, dx \tag{A3.5}$$

Abramowitz & Stegun (1964) give

$$I_2(0) \equiv \int_0^\infty x^\nu K_1(x) \, dx = \nu \, 2^{\nu-2} \Gamma^2(\nu/2) \tag{A3.6}$$

Proceeding as above, with

$$
\begin{aligned}
I_2(n) &= \frac{d^n I_2(0)}{d\nu^n} \\
&= I_2(0)\left[\psi(\nu/2) + \ln 2 + 1/\nu\right]
\end{aligned}
\tag{A3.7}
$$

gives

$$
\begin{aligned}
\int x^4 K_1(x)\,dx &= 16 \\
\int x^4 \ln x\, K_1(x)\,dx &= 16\left[\psi(2) + \ln 2 + \tfrac{1}{4}\right] = 21.855 \\
\int x^4 \ln^2 x\, K_1(x)\,dx &= 16\left\{\left[\psi(2) + \ln 2 + \tfrac{1}{4}\right]^2 + \tfrac{1}{2}\zeta(2,2) - \tfrac{1}{16}\right\} = 34.01 \\
\int x^4 \ln^3 x\, K_1(x)\,dx &= 16\left\{\begin{array}{l}\left[\psi(2) + \ln 2 + \tfrac{1}{4}\right]^3 \\ +3\left[\psi(2) + \ln 2 + \tfrac{1}{4}\right]\left[\tfrac{1}{2}\zeta(2,2) - \tfrac{1}{16}\right] \\ -\tfrac{1}{2}\zeta(3,2) + \tfrac{2}{4^3}\end{array}\right\} = 56.71
\end{aligned}
\tag{A3.8}
$$

A4. Photon-Photon Rates for Non-Isotropic Distribution Functions

For a general photon distribution, $dn_\gamma(\mathbf{k}) = n(\mathbf{k})\,\omega^2 d\omega\, d\mu\, d\phi$, the reaction rate is given by

$$R_{\gamma\gamma} = \int \tfrac{1}{2}\sigma(\omega)(1-\mu)n_1(\mathbf{k}_1)n_2(\mathbf{k}_2)\,\omega_1^2 d\omega_1\, d\mu_1\, d\phi_1\, \omega_2^2 d\omega_2\, d\mu_2\, d\phi_2 \tag{A4.1}$$

where $\sigma(\omega)$ is the cross section in terms of ω, the centre of momentum energy, and μ = cos θ is the cosine of the angle between the photon directions. Changing variables from ϕ_2 to $\phi = \phi_2 - \phi_1$ we have (by geometry)

$$\begin{aligned} \cos\phi &= \frac{\mu - \cos\theta_1 \cos\theta_2}{\sin\theta_1 \sin\theta_2} \\ d\phi &= \frac{-d\mu_2}{\sin\theta_1 \sin\theta_2 \sin\phi} \end{aligned} \tag{A4.2}$$

The limits of the μ integration are given by | cos ϕ | $\leq$ 1, hence

$$\cos(\theta_1 + \theta_2) \leq \mu \leq \cos(\theta_1 - \theta_2) \tag{A4.3}$$

If the distribution functions are independent of polar angles ϕ_1 and ϕ_2 then the ϕ_1 integration is trivial, and

$$\begin{aligned} R_{\gamma\gamma} = \pi \int \sigma(\omega)(1-\mu) & n_1(\omega_1,\mu_1)n_2(\omega_2,\mu_2)\omega_1^2 d\omega_1\, d\mu_1\, \omega_2^2 d\omega_2\, d\mu_2 \\ & \times \int_{\mu=\cos(\theta_1+\theta_2)}^{\mu=\cos(\theta_1-\theta_2)} \frac{d\mu}{\sin\theta_1 \sin\theta_2 \sin\phi} \end{aligned} \tag{A4.4}$$

Now change variables from μ to ω, using $2\omega^2 = \omega_1\omega_2(1-\mu)$. The integration limits become $\omega_\pm^2 = \omega_1\omega_2\left[1 - \cos(\theta_1 \pm \theta_2)\right]/2$.

Then $\sin\theta_1 \sin\theta_2 \sin\phi = 2\left[(\omega_+^2 - \omega^2)(\omega^2 - \omega_-^2)\right]^{1/2} / \omega_1\omega_2$ and so

$$R_{\gamma\gamma} = 4\pi \int n_1(\omega_1,\mu_1)n_2(\omega_2,\mu_2)\omega_1\, d\mu_1\, \omega_2\, d\mu_2 \int_{\omega_-}^{\omega_+} \frac{\omega^3 \sigma_{\gamma\gamma}(\omega)\, d\omega}{\left[(\omega_+^2 - \omega^2)(\omega^2 - \omega_-^2)\right]^{1/2}} \tag{A4.5}$$

The major contribution to the ω integral comes from the limits, which behave like $1/|\omega - \omega_\pm|^{1/2}$. This contribution can be subtracted off analytically, and the remaining small portion can be evaluated numerically.